STOCHASTIC DYNAMICS IN SPATIALLY EXTENDED PHYSICAL AND BIOLOGICAL SYSTEMS

BY

FARSHID JAFARPOUR

DISSERTATION

Submitted in partial fulfillment of the requirements
for the degree of Doctor of Philosophy in Physics
in the Graduate College of the
University of Illinois at Urbana-Champaign, 2016

Urbana, Illinois

Doctoral Committee:

Professor Karin Dahmen, Chair
Professor Nigel Goldenfeld, Director of Research
Professor Michael Stone
Assistant Professor Thomas Kuhlman

Abstract

In this thesis, I discuss three different problems of stochastic nature in spatially extended systems: (1) a noise induced mechanism for the emergence of biological homochirality in early life self-replicators, (2) the amplification effect of nonnormality on stochastic Turing patterns in reaction diffusion systems, and (3) the velocity statistics of edge dislocations in plastic deformation of crystalline material.

In Part I, I present a new model for the origin of homochirality, the observed single-handedness of biological amino acids and sugars, in prebiotic self-replicator. Homochirality has long been attributed to autocatalysis, a frequently assumed precursor for self-replication. However, the stability of homochiral states in deterministic autocatalytic systems relies on cross inhibition of the two chiral states, an unlikely scenario for early life self-replicators. Here, I present a theory for a stochastic individual-level model of autocatalysis due to early life self-replicators. Without chiral inhibition, the racemic state is the global attractor of the deterministic dynamics, but intrinsic multiplicative noise stabilizes the homochiral states, in both well-mixed and spatially-extended systems. I conclude that autocatalysis is a viable mechanism for homochirality, without imposing additional nonlinearities such as chiral inhibition.

In Part II, I study the amplification effect of nonnormality on the steady state amplitude of fluctuation-induced Turing patterns. The phenomenon occurs generally in Turing-like pattern forming systems such as reaction-diffusion systems, does not require a large separation of diffusion constant, and yields pattern whose amplitude can be orders of magnitude larger than the fluctuations that cause the patterns. The analytical treatment shows that

patterns are amplified due to an interplay between noise, non-orthogonality of eigenvectors of the linear stability matrix, and a separation of time scales, all built-in feature of stochastic pattern forming systems. I conclude that many examples of biological pattern formations are nonnormal stochastic patterns.

In Part III, I study the dynamics of edge dislocations with parallel Burgers vectors, moving in the same slip plane, by mapping the problem onto Dyson's model of a two-dimensional Coulomb gas confined in one dimension. I show that the tail distribution of the velocity of dislocations is power-law in form, as a consequence of the pair interaction of nearest neighbors in one dimension. In two dimensions, I show the presence of a pairing phase transition in a system of interacting dislocations with parallel Burgers vectors. The scaling exponent of the velocity distribution at effective temperatures well below this pairing transition temperature can be derived from the nearest-neighbor interaction, while near the transition temperature, the distribution deviates from the form predicted by the nearest-neighbor interaction, suggesting the presence of collective effects.

Acknowledgments

The person who deserves the most to be acknowledged here is my advisor Nigel Goldenfeld. He has been supportive over the years of me pursuing my own interests and ideas, and also providing new insights and ideas whenever I needed them. He has been kind and supportive through out my graduate school and has spent countless hours with me discussing my projects. There are few advisors who place the education and interests of their graduate students above their own; Nigel is one them. Thank you Nigel, I was lucky to have you as my advisor.

The students and postdocs in Nigel's group have made my graduate career far more interesting and fruitful. I would like to thank all the current and former members of the group, Luiza Angheluta, Tommaso Biancalani, Michael Martini, Vikyath Rao, Hong-Yan Shih, Chi Xue, Maksim Sipos, Purba Chatterjee, Nicholas Chia, Michael Assaf, Patricio Jeraldo, Zhenyu Wang, Minhui Zhu, and Tsung-Lin Hsieh. In particular, I was very fortunate to have worked with our two postdocs, Luiza and Tommaso whome I consider my mentors and friends. I am thankful to Luiza for very enthusiastically walking me through my first project in graduate school, and Tommaso from whom I learned a great deal about stochastic processes. They were also my collaborators in the projects presented in this thesis. I am thankful to Elbert Branscomb, Georgios Tsekenis, and Professors Lee DeVille and Seppe Kuehn for great discussions, and to Nicholas Guttenberg at ELSI for hosting my visit and introducing me to the field of machine learning and neural networks.

I would like to thank some of the professors who deserve special acknowledgment for either their wonderful inspiring courses and passion for teaching or for their kind and caring

mentorship throughout my academic career. In reverse chronological order, professors: Mike Stone for his wonderful math methods courses at UIUC, Stephen Reynolds for his awesome classical mechanics courses and his mentorship at NCSU, Laura Taylor for her beautifully taught environmental economics class and for helping me to choose my career path at NCSU, Marry Bridget Kustusch for her wonderful and passionately taught modern physics class at NCSU, Gholam Reza Karimi for introducing me to my first research experience and his mentorship at ShirazU, Nasir Mehranbod for the extra time and effort that he put into several chemical engineering classes at ShirazU, and Mahdi Jahanmiri for his introductory physics course that sparked my interest in physics for the first time at ShirzU.

I would like to specially thank my family, my mother Gowhar, my father Khosrow, and my sister Mahshid for their unconditional love and support. My thanks to physics friends in UIUC in no particular order: Akbar Jaefari, Rezvan Shahoei, Zack Dell, Barbara Stekas, Brandon Langley, Carolyn Kan, Benjamin Esham, Tanya Perolva, Mohammad Sahrapour, and many others for the journey we shared and the wonderful memories. Finally, I would like to thank Emily Schlafly. She helped me with all my writings for my prelim paper, my job applications, and my papers, and listened to all my practice talks, despite not having any background in physics.

Some of the work presented in this thesis was partially supported by the National Aeronautics and Space Administration through the NASA Astrobiology Institute under Cooperative Agreement No. NNA13AA91A issued through the Science Mission Directorate. In particular, I was supported by the NASA Astribiology Institute for Universal Biology. I would like to thank this Institute for supporting such ambitious and unusual problems as the emergence of homochirality: without NASA's intent to support high risk and unconventional research, my work would have been more difficult. I would also like to thank them for supporting work that did not make it into this thesis; if it had been successful, there would have been an additional chapter describing the dynamics of self-referential systems.

Table of Contents

Chapter 1

Introduction

In studies of statistically large systems of interacting agents, the detailed modeling of every individual is often replaced by a probabilistic approach in which the exact state of the system is uncertain. In this approach, the lack of knowledge about the individual degrees of freedom imposes a seemingly random force on the variables of interest. There can be different sources of these stochastic forces: the lack of information about the number and interactions of individuals in the system leads to what is known as *intrinsic noise*. The noise produced by the probabilistic treatment of collision of molecules in chemical reactions is an example of intrinsic noise. In contrast, *extrinsic noise* is produced by the probabilistic treatment of the interaction of the system with the external environment. Noise could also be produced from physical sources such as sound vibrations, collective motion of defects in plastic deformation, or by spatial or environmental heterogeneity.

The effects of these random forces can be conveniently circumvented in classical statistical mechanics due to the fact that the distributions of various extensive thermodynamical variables approach a narrow Gaussian around their mean in large systems, where the width of the distribution is proportional to the square root of the system size (or the inverse of the square root of the system size for intensive variables), and therefore, they can be approximated by their expected values. In systems with quenched randomness representing frozen spatial heterogeneity, the Gibbs distribution is modified by the disorder and methods such as the replica method need to be used to handle the quenched, out of equilibrium spatial disorder. In pure systems that are far from equilibrium, global average variables are rarely of interest, since they no longer can be used as full descriptions for the state of a large system.

The further a system from equilibrium, the smaller is the coarse graining system size around each point in space, and therefore, the larger the effect of the stochasticity. Moreover, systems far from equilibrium do not obey Boltzmann statistics, and therefore, the distributions of thermodynamical variables may not even peak around their average values, resulting in a complete disagreement between the stochastic and deterministic dynamics.

In this thesis, I introduce three different problems of stochastic nature. In Part I, I propose a model for the origin of homochirality in biological systems. In this model, multiplicative intrinsic noise induces extra stable points in the stochastic dynamics that are not the fixed points of the deterministic dynamics. In Part II, I study how the effect of noise on the steady state noise-induced pattern-forming behavior of a system can be greatly amplified by the transient dynamics, thus making it more likely that such effects can be observed experimentally. In Part III, I study the effect of physical noise produced by the avalanche dynamics in plastic deformations on the velocity statistics of edge dislocations, by mapping the problem to Dyson's model of nuclear energy levels, itself related to the two-dimensional Coulomb gas [1]. I show that the stochastic dynamics of dislocations can explain the power-law distribution of their velocities.

In the remainder of this introduction, I briefly explain the problems I have addressed in this thesis, and I summarize my contributions to the collaborations that entailed.

1.1 Noise-Induced Mechanism for the Origin of Biological Homochirality

The origin of biological homochirality, the single handedness of virtually all amino acids incorporated in proteins and all sugars in the backbones of DNA and RNA molecules, has been one of the mostly debated topics since its discovery by Louis Pasteur in 1848. There are those who argue that homochirality must have preceeded the first chemical systems undergoing Darwinian evolution, and there are those who believe homochirality is a consequence

of life, not a prerequisite. There are even those who go as far as saying that homochirality is a consequence of underlying asymmetries from the laws of physics, invoking complicated astrophysical scenarios for the origin of chiral organic molecules or even the violation of parity from the weak interactions! In fact, such explanations that are based on physical asymmetries can only predict an enantiomeric excess of one handedness over another, and not the 100% effect observed in nature.

Kinetic instability of the racemic mixture of chiral molecules in particular sets of autocatalytic reactions involving a mutually antagonistic relationship between two enantiomeres of a chiral molecule gives rise to a huge class of spontaneous symmetry breaking mechanisms invoked to explain homochirality. Although autocatalysis is an expected prerequisite for early life self-replicators, the mutually antagonistic relationship between the two chiral molecules may not have an obvious biological justification depending on when we place the origin of homochirality with respect to the origin of life.

In Chapter 2, I give a complete introduction to this topic and the theories to date. This sets the stage for Chapter 3, where I remove the mutually antagonistic relationship form the set of autocatalytic chemical reaction, replacing it by linear decay and production reactions of chiral molecules. In this new model, I will show that when the autocatalysis (modeling the self-replication) is the dominant production mechanism for early life self-replicators, even though the only deterministic dynamical attractor of the reactions kinetics is a racemic solution, the homochiral states are stabilized by the intrinsic noise from autocatalysis.

Since, this mechanism for homochirality depends on intrinsic noise, it is important to determine how robust it is with respect to spatial inhomogeneities. In Chapter 4, first, I show that when a well-mixed system described by this model is perturbed by diffusion of chiral molecules of perhaps opposite chirality from neighboring well-mixed systems, the system maintains its homochirality. Then, I will show that in a continuous one-dimensional model, the reactions at different points in space synchronize their final homochiral state, showing that this noise-induced mechanism for the origin of homochirality is robust with respect to the spatial extension.

1.2 Nonnormality of Stochastic Spatial Patterns in Reaction Diffusion Systems

One of the most fundamental problems in ecology and developmental biology is the emergence of spatial and temporal patterns from an initially homogeneous state. Previous work from our group showed that in contrast to earlier work based on Turing's classic calculation of diffusive instabilities, demographic stochasticity provides a mechanism for pattern formation that does not require exquisite fine-tuning of the parameters in the model, especially the ratio of the diffusion coefficients of the morphogens. However, the amplitude of the fluctuation-induced patterns far from the fine-tuned parameter regime as estimated by current mathematical techniques [2] is expected to be small, casting a shadow on the prospect of ever confirming the prediction of spatially extended patterns due to demographic fluctuations. We show that the current mathematical analyses miss an important amplifying effect due to *nonnormality*, a generic and necessary feature of pattern-forming systems. My work shows that stochastic patterns are in fact observable and likely to be ubiquitous in systems characterized by demographic stochasticity.

In Chapter 5, I review the concept of nonnormality (a property of matrices with nonorthogonal eigenvectors) in dynamical systems, and show that it leads to a transient growth of perturbations near a stable fixed point. Then I discusses how this transient growth has a lasting effect on the final state of stochastic dynamical systems. I derive a natural measure of nonnoramality in terms of the angle between the eigenvectors and the separation of the time scales associated with the eigenvalues. This measure quantifies the amplification effect of nonnormality on the steady state amplitude of stochastic variables. In Chapter 6, I review the Turing mechanism for spatial instability in reaction diffusion systems, and how the fine tuning problem of Turing mechanisms is solved by introducing fluctuations. I show why stochastic patterns are presumed to have small amplitude, making them hard to

be experimentally observed. Then, I show that all the stochastic patterns are nonnormal, and therefore, their amplitude is much larger than expected purely from naive eigenvalue analysis. The amplification that I calculate means that stochastic pattern forming systems exit the linear regime much quicker than would otherwise have been the case, allowing the instabilities to grow and ultimately interact through nonlinearities.

In Chapter 7, I study the patterns that emerge in the stochastic extension of a model whose deterministic behavior was previously examined by Ridolfi et al. [3], and show that (1) the range of parameters in which the system exhibits steady state patterns is drastically expanded by the demographic noise, and (2) the nonnormality amplifies the amplitude of the stochastic patterns by orders of magnitude.

1.3 Velocity Statistics of Edge Dislocations in Plastic Deformation of Crystalline Material

At mesoscopic scales, crystalline materials under stress exhibit intermittent behavior through plastic slip avalanches that follow power-law statistics [4, 5, 6, 7, 8, 9, 10, 11, 12, 13]. The origin of intermittency in plastic strain rate is attributed to the collective dynamics of defects such as dislocations. Reference [5] shows that the experimentally measured $E^{-3/2}$ distribution of the acoustic energy, E, of these avalanches is associated with the power-law distribution of velocity of dislocations with the exponent -2.5 which is independent of the value of the external stress.

In this project, I propose a model to study the velocity distribution of edge dislocations by mapping the problem to Dyson's two-dimensional Coulomb gas confined to one dimension [1]. This work has already appeared in print [14]. In this model we show that a power-law probability distribution, $P(v)$, of the velocity of edge dislocations is not necessarily due to a collective effect arising from avalanche dynamics, non-equilibrium critical points, or self-organized criticality as was previously claimed [15, 16, 8, 5, 17, 13, 11, 18]. In a one-

dimensional model, I show that the velocity distribution of dislocations has a temperature-dependent power-law. This power-law distribution can be derived by considering only the nearest-neighbor interactions of dislocations, and therefore, is not a consequence of collective interactions; it is only a consequence of the logarithmic interaction potential between the one-dimensional edge dislocation.

In two dimensions, there exists a transition between a state at which the nearest neighbors are bound to each other and a state where they can escape from each other's attractive force. This transition takes place at an effective temperature where the effective thermal energy becomes equal to the pairwise interaction potential. For temperatures significantly smaller than this transition temperature, the probability density function of the velocities of dislocations agrees with the scaling v^{-2} found from the nearest-neighbor analysis, while for temperatures close to or larger than this transition temperature, the probability density function follows a power-law with an exponent steeper than -2 suggesting that the high velocity events are dominated by collective effects due to the interaction of more than two dislocations. This exponent is very weakly temperature dependent and has the value -2.4 at the transition temperature.

1.4 List of Publications

The work presented in this thesis is an expanded version of the following papers published or under preparation:

- F. Jafarpour, T. Biancalani, N. Goldenfeld. *Noise-Induced Mechanism for Biological Homochiralinnty of Early Life Self-replicators.* Phys. Rev. Lett. 115.15 (2015) [19]

- F. Jafarpour, L. Angheluta, N. Goldenfeld. *Velocity Statistics for Interacting Edge Dislocations in One Dimension from Dyson's Coulomb Gas Model.* Phys. Rev. E. 88.4 (2013) [14]

- F. Jafarpour, T. Biancalani, N. Goldenfeld. *Stochastic Patterns with Unexpectedly Large Amplitudes.* (under preparation)
- F. Jafarpour, T. Biancalani, N. Goldenfeld. *Spatially Extended Noise-Induced Mechanism for the Origin of Biological Homochiralinnty.* (under preparation)

1.5 My Contribution

The work in this thesis was developed in close conceptual collaboration and, in some instances, detailed technical input from my advisor Nigel Goldenfeld. It also involved my close interactions with the postdocs in our group. It has led to two publications and two papers in preparation. In this section, I briefly summarize my contribution to these collaborations.

In the work on homochirality, I proposed the set of reactions in Chapter 3 and derived the stochastic differential equation for its time evolution; this equation was previously solved by Tommaso Biancalani and is related to the Wright-Fisher model of evolutionary biology. I performed all the simulations for well-mixed, two-patch and one-dimensional models. The derivation of the stochastic differential equation for the spatial extension was done by me. I performed the perturbation theory calculations for the two-patch model which was developed by Tommaso and me. The analysis of the one-dimensional model was done by me.

In the work on nonnomrality of spatial patterns, I derived the steady state solution to the complex valued linear Fokker-Planck equation and found the expression for the amplification. I showed that all pattern forming systems are far from normal. I derived the stochastic differential equations for the spatial extension of the model by Ridolfi, and carried out the stability analysis of the uniform solution, calculated the phase diagram, and performed the simulations.

In the work on plasticity, I performed the simulations on both one-dimensional and quasi-two-dimensional models. I proposed the quasi-two-dimensional model, while all the analytic

calculations were done in close collaboration with Luiza Angheluta.

All the numerical simulations shown in this thesis were performed by me. All the figures and plots presented here were generated by me. Most of the material in the appendices is common knowledge in the field and is included for completeness and to assist future students in the group. The exception is the row reduction in Appendix A.2, and Appendices A.6, A.7, and B.3 that are my own work.

Part I

Noise-Induced Origin of Homochirality in Prebiotic Self-Replicators

Chapter 2

Introduction to Homochirality

One of the very few universal features of biological systems is homochirality: virtually all naturally occurring amino acid are left-handed (L-chiral) while all sugars are right-handed (D-chiral) [20, 21]. Although such unexpected broken symmetries are well-known in physics, complete biological homochirality still defies explanation.

In this chapter, I will give an introduction to the basic concepts related to chirality and biological homochirality. I review spontaneous and explicit symmetry breaking theories of homochirality. The main focus of this work is on spontaneous symmetry breaking mechanisms. All of the previous spontaneous symmetry breaking models of homochirality have the same basic mechanism [22] as that of the seminal model by C. F. Frank [23], which is reviewed in Section 2.3. Frank has shown that in a population of self-replicating (autocatalytic) chiral molecules that are mutually antagonistic, the racemic solution is unstable. While autocatalysis is expected in a model of prebiotic chemistry, the mutual antagonistic relationship has no obvious biological justification.

In Chapter 3, I will replace the reaction modeling the mutual antagonistic relationship by linear decay and growth reactions and show that even though the racemic solution is the global attractor of the deterministic dynamics, when the intrinsic stochasticity of the self-replication process is taken into the account, the system transitions to homochirality. This transition takes place when the efficiency of self-replication exceeds a threshold. The relationship between the transition to homochirality in this model and the origin of life is discussed in Section 3.3. In Section 3.4, I discuss the nonequilibrium aspects of our model and the principle of detailed balance.

The effect of spatial inhomogeneity and diffusion is discussed in Chapter 4, where I show that a system of diffusively coupled otherwise independent replicas of this model synchronize their final homochiral states. Moreover, in a continuous one-dimensional spatial extension of this model, even for infinite system size, the system reaches a uniformly homochiral final state at pure autocatalytic limit, where self-replication is the only production mechanism of the chiral molecules.

2.1 Chirality

In 1848, Louis Pasteur discovered that a certain salt of synthetic tartaric acid (known at the time as racemic[1] acid) produces two distinct types of crystals known as "+" and "−" forms, which are mirror images of one another. Pasteur showed that if we shine linearly polarized light through solutions made by each one of these two types of crystals, they rotate the angle of polarization of light in opposite directions. He concluded that the racemic acid was made of two kinds of molecules with opposite optical activity, and the asymmetry of the crystals was related to an asymmetry at the molecular level [24]. A clear explanation did not emerge until 1874, when J. H. van't Hoff and J. A. Le Bel independently discovered that organic molecules with a carbon atom connecting to four different groups are not mirror symmetric, and as a result, the groups can be placed around the carbon atom in two different left-handed and right-handed order, two configurations that are mirror images of one another [25, 26]. Such molecules that are not superimposable on their mirror image are called chiral (Greek for hand), and the atom surrounded by four different groups is known as the chiral center of the molecule.

There are at least three different conventions to determine which one of the two optical isomers (also known as *enantiomers*) should be called left-handed, and which one should be

[1]The word racemic is Latin for 'bunch of grapes,' and at the time, it was used to refer to synthetic tartaric acid, since tartaric acid is naturally found in grapes. However, the tartaric acid found in grape does not produce the two distinct crystals, since it is produced biologically and is homochiral. The word racemic is nowadays used to mean a fifty-fifty mixture of two chiral molecules, which could be misleading knowing the etymology of the word. Thanks to Prof. Michael Stone for pointing this out in my preliminary exam.

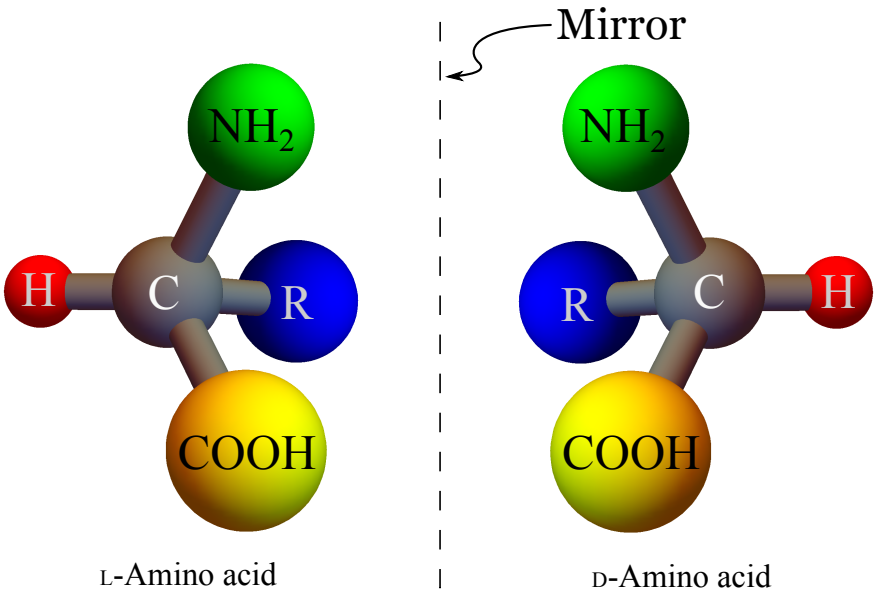

Figure 2.1: Ball and stick model of a generic α-amino acid and its mirror image. α-amino acids are organic compounds with a chiral carbon connected to an amino group ($-NH_2$), a carboxylic acid group ($-COOH$), a hydrogen atom ($-H$), and a side chain ($-R$) that varies depending on the particular amino acid. The L/D chirality of amino acids is determined by the CORN rule: an amino acid is L−chiral (D−chiral) if by wrapping your left hand (right hand) fingers around the direction of CORN ($-CO$, $-R$, and $-N$ groups in order) your thumb points toward the direction of the hydrogen atom.

called right-handed:

1. The $(+)/(-)$ classification that is based on the optical activity is important for historical reasons, but it is not very useful for our purpose, as there is no way to determine the optical activity just by looking at the structure of the molecule. Moreover, the optical activity of the chiral solutions could also depend on the properties of the solvent.

2. More commonly used in chemistry is the R/S (referring to *Rectus* and *Sinister*) nomenclature, where the ordering of the groups on the chiral centers is chosen based on the atomic numbers, and can be easily determined by looking at the three dimensional structure of the molecule. However, atomic number is not always the most biologically relevant criteria, and as it turns out, the R/S classification does not keep the ordering of the functional groups consistent across, *e.g.* all amino acids.

3. The D/L (named after *Dexter* and *Laevus* Latin for right and left) convention (also known as Fisher-Rosanoff convention) is chosen for a molecule if it can be theoretically

derived from R/S-glyceraldehyde without changing the configuration of the chiral center [27]. This seemingly arbitrary convention happens to be the one that keeps the order of similar functional groups in biological molecules consistent and makes it possible to compare the chirality of different molecules with similar groups such as different amino acids (see Fig. (2.1)).

It is important to note that there is no fixed relation between the three conventions, as a right-handed molecule in one convention can be left-handed in the other.

Parity is a symmetry of laws of physics (with the exception of weak interaction). In particular, two enantiomeres of a chiral molecule have identical physical, chemical, and thermodynamical properties. Therefore, chemical reactions producing chiral molecules from achiral molecules, by symmetry, are expected to produce solutions of fifty percent right-handed, and fifty percent left-handed molecules. Such solutions are called racemic. In contrast, a solution of all left-handed or all right-handed molecules is called homochiral or enantiopure. During the emergence of life, many chiral molecules were formed from simpler achiral molecules existed in early atmosphere or the ocean. As a result, one would expect the modern life to consist of equal number of left-handed and right-handed enantiomers of each chiral molecule. However, virtually all amino acids and sugars found in nature are homochiral. This homochirality is uniform across all amino acids, all organisms, and all ecosystems. In Section 2.2, I will discuss the origin of homochirality as a symmetry-breaking problem.

2.2 Biological Homochirality: A Symmetry Breaking Problem

Amino acids are building blocks of proteins and their chirality plays an important role in the structure and the function of proteins in living cells. Most of us know sugars as molecules used to store chemical energy, but more importantly, sugars play a key role in the structure of RNA and DNA molecules. The famous double helix structure of DNA is a result of the chirality of the sugar molecules in its backbone. Despite the diversity of proteins and

their functions virtually all chiral biological amino acids[2] are L-chiral[3], while all sugars are D-chiral.

Homochirality is particularly surprising, when considering the fact that all the physical, chemical, and thermodynamical properties of the two enantiomeres of a chiral molecule are identical. This is due to the symmetry of laws of electromagnetism under reflection. When life was emerging on the planet, chiral molecules were formed from simpler achiral molecules that existed in early atmosphere and the ocean. Since, the initial state was symmetric (solution of achiral molecules), and the laws of physics are symmetric, one would expect a symmetric final state, that is a biosphere made of a racemic solution of chiral molecules. A phenomenon in which the initial state and the corresponding laws of physics are symmetric with respect to a particular transformation, but the final state of the system violates that symmetry, is called a symmetry-breaking. There are two resolution to a symmetry breaking problem: (1) Explicit symmetry breaking is when the laws of physics are only approximately symmetric, or there is an asymmetric perturbation to the system. (2) In contrast, spontaneous symmetry breaking happens when the governing laws are perfectly symmetric, and as a result, the symmetric state is a final solution, but it may be an unstable solution. In this case, even the slightest perturbation to the system moves the system far away from the symmetric state.

There have been some attempt to explain homochirality through explicit symmetry breaking mechanisms. For example, if life was formed from chiral organic molecules that were produced under a steady radiation of circularly polarized light, the asymmetric interaction of different enantiomeres of chiral molecules with the light over hundreds of millions of years could lead to a significant enantiomeric excess [31]. These theories are partly motivated by reports of observation of slight L-enantiomeric excess of some of amino acids found in

[2]From the 23 proteinogenic amino-acids found in life, Glycine is the only achiral amino acid.

[3]There are some D-amino acids in biological system (*e.g.* D-aspartate is a regulator of adult neurogenesis[28]) and are generated by enzymes that are specialized in the inversion of the stereochemistry (of the corresponding L-amino acids) known as *racemases* and *epimerases*. These amino acids cannot participate in proteins structures through ribosomal synthesis but can take part in structure of peptides (*e.g.* D-phenylalanine in the antibiotic Tyrocidine[29]) through either posttranslational conversion of L- to D-amino acids or the activity of nonribosomal peptide synthetases. For a review of the role of D-amino acids, see for example Ref. [30]

Murchison meteorite [32, 33, 34]. Another prominent example relates to the parity violation in weak interaction. Unlike electromagnetic interaction, the weak interaction grossly violates the mirror symmetry [35]. Even though weak interaction has a negligible effect at molecular scales, it has been argued that it can cause an asymmetry affecting the rate of production of two enantiomeres in a manner that over billions of years could lead to an observable level of enantiomeric imbalance [36, 37].

A common weakness of explicit symmetry breaking mechanisms is that the homochirality achieved is only partial: These mechanisms lead to an imbalance between the concentrations of the two enantimeres, but do not result in complete homochirality. As a result, there is a common misunderstanding in the field that the origin of homochirality requires two steps: (1) an explicit symmetry breaking mechanism to break the symmetry in the initial condition, followed by (2) a mechanism to amplify the initial asymmetry. However, if there is a mechanism amplifying the initial asymmetry, the symmetric solution is unstable, and over time the system decays to one of the two homochiral states, even with a symmetric initial condition; this is spontaneous symmetry breaking.

The first model of spontaneous symmetry breaking for homochirality was proposed by C. F. Frank in 1953 [23]. There have been many other models of homochirality since Franks model, but the underlying mechanism for spontaneous symmetry breaking in all of these models is the same as the mechanism by Frank [22]. Frank's model is reviewed in detail in Section 2.3.

2.3 Frank's Model of Homochirality

Every physicist knows the year 1905 as one of the most important years in the history of modern physics; 1953 is the 1905 of biology and the origin of life. The seminal paper on the structure of DNA by Watson and Crick [38] published in 1953 opened the world of biology to understanding of genetics and the genetic code. In the same year, Stanley Miller

working in the laboratory of Harold Urey, published the results of the first abiotic synthesis of amino acids in what he thought to be the conditions of primitive earth [39]. Another very important, but perhaps less well-known publication in 1953, was the first spontaneous symmetry-breaking theory of homochirality by Charles Frank suggesting that homochirality could be a consequence of chemical autocatalysis [23], a frequently presumed mechanism associated with the emergence of early life self-replicators.

Frank introduced a model in which the D and L enantiomers of a chiral molecule are autocatalytically produced from an achiral molecule A in reactions

$$A + \mathrm{D} \xrightarrow{k_a} 2\mathrm{D}, \qquad A + \mathrm{L} \xrightarrow{k_a} 2\mathrm{L}, \tag{2.1}$$

and are consumed in a chiral inhibition reaction[4],

$$\mathrm{D} + \mathrm{L} \xrightarrow{k_i} 2A. \tag{2.2}$$

The state of this system can be described by the chiral order parameter ω defined as

$$\omega = \frac{[\mathrm{D}] - [\mathrm{L}]}{[\mathrm{D}] + [\mathrm{L}]}, \tag{2.3}$$

where [D] and [L] are the concentrations of D and L. The order parameter ω is zero at the racemic state, and ± 1 at the homochiral states. In order to determine the time evolution of the order parameter ω, we can use the law of mass action to set the rates of reactions (2.1) and (2.2) proportional to the products of the concentrations of the corresponding reactants. The result is the following set of mean field equations for the rate of change of concentrations

[4] In the original model by Frank, the concentration of the molecules A was kept constant to reduce the degrees of freedom by one, and the chiral inhibition was introduced by the reaction $\mathrm{D} + \mathrm{L} \to \varnothing$. This model leads to indefinite growth of D or L molecules and does not have a well-defined steady state. To resolve this problem, we let the concentration of A molecules be variable and replaced this reaction by $\mathrm{D} + \mathrm{L} \to 2A$ which conserves the total number of molecules. This conservation law reduces the number of degrees of freedom by one again. The mechanism to homochirality in the modified model is the same as the original model by Frank, since the order parameter in both models obeys Eq. (2.6).

of A, D, and L:

$$\begin{aligned}
\frac{d[A]}{dt} &= 2k_i\,[\mathrm{D}]\,[\mathrm{L}] - k_a\,[A]\,([\mathrm{D}]+[\mathrm{L}]) \\
\frac{d[\mathrm{D}]}{dt} &= k_a\,[A]\,[\mathrm{D}] - k_i\,[\mathrm{L}]\,[\mathrm{D}] \\
\frac{d[\mathrm{L}]}{dt} &= k_a\,[A]\,[\mathrm{L}] - k_i\,[\mathrm{D}]\,[\mathrm{L}].
\end{aligned} \tag{2.4}$$

The rate of change of ω can be derived by a the chain rule resulting in the mean field equation of motion:

$$\frac{d\omega}{dt} = \frac{1}{2}k_i\,([\mathrm{D}]+[\mathrm{L}])\,\omega\left(1-\omega^2\right). \tag{2.5}$$

Equation (2.5) has three deterministic fixed points; the racemic state, $\omega = 0$, is an unstable fixed point, and the two homochiral states, $\omega = \pm 1$ are stable fixed points. Starting from almost everywhere in the D-L plane, the system converges to one of the homochiral fixed points (Fig. (2.2a)).

In the context of biological homochirality, extensions of Frank's idea have essentially taken two directions. On the one hand, the discovery of a synthetic chemical system of amino alcohols that amplifies an initial excess of one of the chiral states [40] has motivated several autocatalysis-based models (see [22] and references therein). On the other hand, ribozyme-driven catalyst experiments [41] have inspired theories based on polymerization and chiral inhibition that minimize [42, 43, 44] or do not include at all [45, 46] autocatalysis. In contrast, a recent experimental realization of RNA replication using a novel ribozyme shows such efficient autocatalytic behavior that chiral inhibition does not arise [47]. Further extensions accounting for both intrinsic noise [22, 48] and diffusion [49, 50, 51, 52] build further upon Frank's work.

Regardless of the specific model details, all these models share the three-fixed-points paradigm of Frank's model, namely that the time evolution of the chiral order parameter ω is given by a deterministic equation of the form [22]

$$\frac{d\omega}{dt} = f(t)\,\omega\left(1-\omega^2\right), \tag{2.6}$$

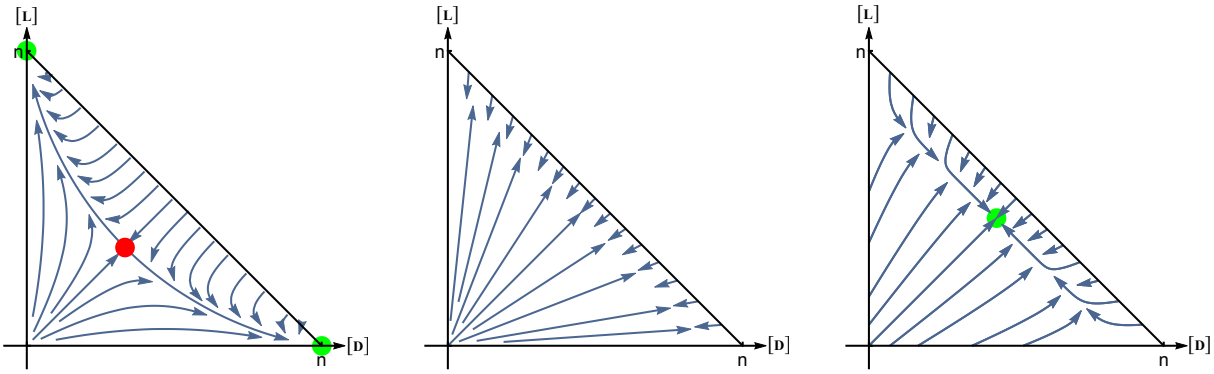

(a) $A + \text{D} \to 2\text{D}$, $A + \text{L} \to 2\text{L}$, $\text{D} + \text{L} \to 2A$

(b) $A + \text{D} \to 2\text{D}$, $A + \text{L} \to 2\text{L}$, $\text{D} \to A$, $\text{L} \to A$

(c) $A + \text{D} \to 2\text{D}$, $A + \text{L} \to 2\text{L}$, $\text{D} \rightleftharpoons A$, $\text{L} \rightleftharpoons A$

Figure 2.2: (Color online) (a) Phase portrait of Frank's model: the racemic state is an unstable fixed point (red dot), while the homochiral states are stable fixed points (green dots). (b) If chiral inhibition is replaced by linear decay reaction, the ratio of D and L molecules stays constant. (c) Adding even the slightest amount of non-autocatalytic production of D and L molecules makes the racemic state (green dot) the global attractor of the dynamics.

where the function $f(t)$ is model-dependent. The sole exception to this three-fixed-points model in a variation of Frank's model is the work of Lente [53], where purely stochastic chiral symmetry breaking occurs, although chiral symmetry breaking is only partial, with $\omega \neq 0$ but $|\omega| < 1$. In all models obeying Eq. (2.6), the homochiral states arise from a nonlinearity which is not a property of simple autocatalysis, but, for instance in the original Frank's model, is due to chiral inhibition. To clarify this, one can repeat the analysis of the rate equations for a variation of Frank's model in which the chiral inhibition reaction (2.2) is replaced by independent linear decay reactions

$$\text{D} \xrightarrow{k_d} A, \qquad \text{L} \xrightarrow{k_d} A. \tag{2.7}$$

Figure (2.2b) shows that in this modified model, the homochiraity is lost, and the ratio of D and L molecules stay constant over time. The situation is even worse: if the reactions (2.7) are even slightly reversible,

$$\text{D} \underset{k_n}{\overset{k_d}{\rightleftharpoons}} A, \qquad \text{L} \underset{k_n}{\overset{k_d}{\rightleftharpoons}} A, \tag{2.8}$$

the racemic solution becomes the global attractor of the deterministic dynamics (see Fig. (2.2c)). Even starting from a homochiral solution, such system eventually converges to racemic so-

lution.

In Section 3, I will show that despite the fact that the stability analysis of rate equations shows that the modified Frank's model without chiral inhibition approaches a racemic steady state, when the intrinsic noise from the autocatalytic reactions is taken into account, the system can transition to homochirality under certain conditions.

Chapter 3

Noise-Induced Origin of Homochirality in Prebiotic Self-Replicators

In this chapter, I will show that efficient early-life self-replicators can exhibit universal homochirality, through a stochastic treatment of Frank's model *without* requiring nonlinearities such as chiral inhibition. In our stochastic treatment, the homochiral states arise not as fixed points of deterministic dynamics, but instead are states where the effects of chemical number fluctuations (i.e. the multiplicative noise [54]) are minimized. The mathematical mechanism proposed here [55, 56, 57, 58] is intrinsically different from that of the class of models summarized by Eq. (2.6). I conclude that autocatalysis alone can in principle account for universal homochirality in biological systems far from equilibrium, when autocatalysis is the strongly dominant mechanism for the production of chiral molecules.

It may be helpful for the audience not familiar with the stochastic treatment of chemical reactions to clarify in what sense chemical reactions are stochastic, and when the stochasticity matters. In reaction kinetics, the rate of reactions are calculated using the law of mass action. The law of mass action states that the rate of a reaction is proportional to the product of the concentrations of its reactants, and the proportionality constant is defined as the reaction rate. An intuitive explanation of this law is following: A chemical reaction takes place when its reactants collide with enough energy to overcome the activation energy of the reaction. The probability of the collision of these reactants is proportional to the product of their concentration, and therefore, the expected value of the number of such collisions per unit time is also proportional to the product of the concentrations of the reactants. This is the law of mass action, and it is in an intrinsically mean field approximation.

Near equilibrium, a system of large number of interacting chemicals follows Boltzmann

statistics and can be approximated by its expected value. This approximation is possible because the distribution of various quantities converge to the a narrow Gaussians around their mean. This is the reason that, in calculating rates of reactions, the expected value of number of collisions is used instead of the actual probability distribution of the number of collisions per unit time.

However, this property is not generalizable to systems that are maintained far from equilibrium. For such systems, instead of using the law of mass action as the expected value of the number of reactions per unit time, it is more helpful to interpret the law of mass action as the probability per unit time of occurrence of a chemical reaction. Also, instead of the rate equations for the rate of change of the expected value of the concentrations of the reactants and the products, we can write the *master equation* for the rate of change of the probability of the system having certain concentrations of reactants and products. A step by step treatment of the master equation is given in Section 3.2 (audience not interested in the technical aspects of stochastic processes can skip this section). An intuitive explanation of the mechanism for the symmetry breaking and its relationship with the origin of life follows in Section 3.3.

Our proposed reactions (reactions (3.1)) are chosen as an effective minimal model in which the transition to homochirality via a noise-induced symmetry breaking in the absence of chiral inhibition can be observed. Of course, the actual set of reactions that took place during the emergence of life leading to the symmetry breaking may involve more chemical species and more intermediate steps. In particular, the steady state of our reaction set will be a nonequilibrium steady state implying that self-replication process has to be driven by an external source of energy. This could mean that self-replication may be coupled to other set of reactions, in the same way that some energy consuming reactions in biological cells are driven by ATP hydrolysis. A more detailed analysis of the thermodynamical aspects of our model and other variations are discussed in Section 3.4.

3.1 Description of the Model

Motivated in part by the experimental demonstration of autocatalysis without chiral inhibition [47], we propose the reaction scheme below, which is equivalent to a modification of a model by Lente [53] with the additional process representing the recycling of enantiomers:

$$\begin{aligned} A + \mathrm{D} &\xrightarrow{k_a} 2\mathrm{D}, & A + \mathrm{L} &\xrightarrow{k_a} 2\mathrm{L}, \\ A &\underset{k_d}{\overset{k_n}{\rightleftharpoons}} \mathrm{D}, & A &\underset{k_d}{\overset{k_n}{\rightleftharpoons}} \mathrm{L} \end{aligned} \tag{3.1}$$

Compared to Frank's model, the chiral inhibition is replaced by reversible linear decay reactions which model both recycling and non-autocatalytic production. The rate constants are denoted by k, with the subscript serving to identify the particular reaction (subscript $_a$ for autocatalysis, $_d$ for decay, and $_n$ for nonautocatalytic production). The only deterministic fixed point of this model is the racemic state (see Fig. (2.2c)). This model can be interpreted as a model of the evolution of early life where primitive chiral self-replicators can be produced randomly through non-autocatalytic processes at very low rates; the self-replication is modeled by autocatalysis while the decay reaction is a model for the death process.

It is important to note that for the nonautocatalytic reaction to occur at a very small rate compared to the decay rate, the self-replication process should be an energy consuming reaction (as is the case in biological systems). Hence, in order to maintain an irreversible self-replication, system has to be driven by an external source of energy. This steady inflow of the energy keeps the steady state of the system far from equilibrium. The source of this driving energy is not included in our model. For more details on the thermodynamics of this model see Section 3.4.

Section 3.2 details the derivation of an exactly solvable stochastic differential equation for the time evolution of chiral order parameter ω from reactions (3.1), which shows that in the regime where autocatalysis is the dominant reaction, the functional form of the multiplicative intrinsic noise from autocatalytic reactions stabilizes the homochiral states. Readers not interested in the derivation the stochastic differential equation for ω can skip Section 3.2

and go directly to Section 3.3 where the main results are discussed.

3.2 Master Equation, Fokker-Planck Equation, and Langevin Equation

Chemical reactions are inherently stochastic, as they rely on stochastic collision of molecules with sufficient energy to overcome the activation energy. The goal of this section is to derive a master equation for the rate of change of probability of the system being at a state defined by the concentration of A, D, and L molecules and a stochastic differential equation for the rate of change of the chirality order parameter ω.

Consider reactions (3.1) taking place in a well-mixed system of volume V with total number of molecules N. The state of the system is defined by the concentration vector $(a, d, l) \equiv (x_1, x_2, x_3) \equiv \vec{x}$ of the molecules A, D, and L respectively. We define the transition rate $T(\vec{y}|\vec{x})$ as the probability per unit time per unit volume of the system transitioning to the state $\vec{y}$, given the initial state $\vec{x}$. From the reaction set reaction (3.1), there are four types of transitions characterized by the four rows of the stoichiometry matrix $\boldsymbol{S}$

$$\boldsymbol{S} = \begin{pmatrix} -1 & 1 & 0 \\ -1 & 0 & 1 \\ 1 & -1 & 0 \\ 1 & 0 & -1 \end{pmatrix}, \tag{3.2}$$

corresponding to the reactions that consume A, and produce D or L respectively and the ones that consume D or L and produce A respectively. The columns of $\boldsymbol{S}$ correspond to the species A, D, and L respectively, and the negative or positive signs refer to consumption or production. From the law of mass action, the transition rates corresponding to different

types of transitions are given by

$$\begin{aligned} T(\vec{x}+\epsilon\vec{s}_1|\vec{x}) &= (k_n + k_a d)a, \quad T(\vec{x}+\epsilon\vec{s}_3|\vec{x}) = k_d d, \\ T(\vec{x}+\epsilon\vec{s}_2|\vec{x}) &= (k_n + k_a l)a, \quad T(\vec{x}+\epsilon\vec{s}_4|\vec{x}) = k_d l, \end{aligned} \tag{3.3}$$

where the vector $\vec{s}_i$ (with $i = 1, \ldots, 4$) is i-th row of the stoichiometry matrix $\boldsymbol{S}$, $\epsilon = 1/V$ is one over the volume of the system, $\epsilon\vec{s}_i$'s are the changes in the concentration vector $\vec{x}$ due to a reaction of type i.

Now, the rate of change of the probability of the system being at a state $\vec{x}$ at time t, $P(\vec{x}, t)$, is given by the sum of the probability of the system being at some state $\vec{y}$ times the probability per unit time of transitioning from $\vec{y}$ to $\vec{x}$ minus the probability of the system being already at state $\vec{x}$ times the probability per unit time of transitioning out of $\vec{x}$ to some other state $\vec{y}$.

$$\frac{\partial P(\vec{x}, t)}{\partial t} = V \sum_{\vec{y}} \left(T(\vec{x}|\vec{y})P(\vec{y}, t) - T(\vec{y}|\vec{x})P(\vec{x}, t) \right). \tag{3.4}$$

Equation (3.4) is called the master equation [59], and it describes the time evolution of probability of the system at a state defined by discrete concentration values. The master equation is the most accurate description of the individual level model and can be simulated exactly using the Gillespie algorithm [60]. In the master equation for the reaction set reaction (3.1), most of the transition rates are zero, except the allowed transitions specified by Eq. (3.3). Substituting the allowed transitions from Eq. (3.3) in Eq. (3.4), we obtain

$$\frac{\partial P(\vec{x}, t)}{\partial t} = V \sum_{i=1}^{4} \left(T(\vec{x}|\vec{x} - \epsilon\vec{s}_i)P(\vec{x} - \epsilon\vec{s}_i, t) - T(\vec{x} + \epsilon\vec{s}_i|\vec{x})P(\vec{x}, t) \right). \tag{3.5}$$

The next step is to take the continuous limit of Eq. (3.4) at large total number of molecules $N \gg 1$ to derive a partial differential equation for the time evolution of the probability density of finding the system a state defined by continuous concentration variables. This equation in known as the *Fokker-Planck equation.* We begin by defining the functions F_i's

as

$$F_i(\vec{x},t) = T(\vec{x}|\vec{x}+\epsilon\vec{s}_i)P(\vec{x},t), \tag{3.6}$$

so that the master equation can be written as:

$$\frac{\partial P(\vec{x},t)}{\partial t} = \sum_{i=1}^{4} \frac{F_i(\vec{x}-\epsilon\vec{s}_i,t) - F_i(\vec{x},t)}{\epsilon}. \tag{3.7}$$

The right-hand side of the master equation can be expanded in ϵ,

$$\frac{\partial P(\vec{x},t)}{\partial t} = -\sum_{i,j} S_{i,j}\frac{\partial F_i}{\partial x_j} + \frac{\epsilon}{2}\sum_{i,j,k} S_{i,j}S_{i,k}\frac{\partial^2 F_i}{\partial x_j \partial x_k} - \frac{\epsilon}{6}\sum_{i,j,k,l} S_{i,j}S_{i,k}S_{i,l}\frac{\partial^3 F_i}{\partial x_j \partial x_k \partial x_l} + \dots. \tag{3.8}$$

If $P(\vec{x},t)$ is analytic in ϵ, before truncation, Eq. (3.8) is exact and does not require ϵ to be small. For $N \gg 1$, by central limit theorem, the fluctuations are Gaussian, and therefore, the probability density function $P(\vec{x},t)$ has to obey a second order Fokker-Planck equation. At this limit, even if ϵ is not small, we can truncate the series to second order, and after evaluating the corresponding partial derivatives, we obtain the following Fokker-Planck equation for the time evolution of $P(\vec{x},t)$:

$$\frac{\partial P}{\partial t} \approx -\sum_{j=1}^{3}\frac{\partial\left(H_j P\right)}{\partial x_j} + \frac{1}{2}\sum_{j,k=1}^{3}\frac{\partial^2\left(B_{jk}P\right)}{\partial x_j \partial x_k}, \tag{3.9}$$

where the drift vector $\vec{H}$ with component H_j is given by

$$\vec{H} = \sum_i T(\vec{x}+\epsilon\vec{s}_i)|\vec{x})\vec{s}_i = \begin{pmatrix} k_d(d+l) - a(2k_n + k_a(d+l)) \\ -k_d d + a(k_n + k_a d) \\ -k_d l + a(k_n + k_a l) \end{pmatrix}.$$

The symmetric diffusion matrix $\boldsymbol{B}$ is given by

$$\begin{aligned}\boldsymbol{B} &= \epsilon \sum_i T(\vec{x}+\epsilon\vec{s}_i)|\vec{x})\vec{s}_i \otimes \vec{s}_i \\ &= \epsilon \begin{pmatrix} k_d(d+l)+a(2k_n+k_a(d+l)) & -k_d d - a(k_n+k_a d) & -k_d l - a(k_n+k_a l) \\ -k_d d - a(k_n+k_a d) & k_d d + a(k_n+k_a d) & 0 \\ -k_d l - a(k_n+k_a l) & 0 & k_d l + a(k_n+k_a l) \end{pmatrix},\end{aligned} \tag{3.10}$$

where the symbol $\otimes$ indicates the Kronecker product.

Equation (3.9) describes the time evolution of the probability density of the concentration vector $\vec{x}$ in the continuous model, and all further approximations and simplifications can be done directly on this equation. However, it is more insightful to keep track of the stochastic dynamics of the concentration variables. The following is the set of stochastic differential equations (defined in the Itō sense, see Appendix A.1 for more details on Itō vs. Stratonovich) corresponding to a probability density function obeying Eq. (3.9) [54].

$$\frac{d\vec{x}}{dt} = \vec{H}(\vec{x}) + \vec{\xi}(t), \tag{3.11}$$

where ξ_i's, the components of $\vec{\xi}(t)$, are zero mean Gaussian noise functions with correlation

$$\langle \xi_i(t)\xi_j(t')\rangle = B_{i,j}\delta(t-t'). \tag{3.12}$$

To rewrite Eq. (3.11) in terms of uncorrelated Gaussian noise functions, we seek to decompose the matrix $\boldsymbol{B}$ to $\boldsymbol{B} = \boldsymbol{G}\boldsymbol{G}^{\mathsf{T}}$. This decomposition is not unique and multiple choices for $\boldsymbol{G}$ exist [61]. It is easy to check that the following 3×2 matrix satisfies the decomposition:

$$\boldsymbol{G} = \sqrt{\epsilon} \begin{pmatrix} \sqrt{a\,(k_a d + k_n) + k_d d} & \sqrt{a(k_a l + k_n) + k_d l} \\ -\sqrt{a\,(k_a d + k_n) + k_d d} & 0 \\ 0 & -\sqrt{a(k_a l + k_n) + k_d l} \end{pmatrix}. \tag{3.13}$$

For more details on how such decompositions are found, see Appendix A.2. Now, for a two dimensional zero mean Gaussian white noise $\vec{\eta}(t)$ with correlation

$$\langle \eta_j(t)\eta_k(t')\rangle = \delta_{j,k}\delta(t-t'), \tag{3.14}$$

the correlated noise $\vec{\xi}(t)$ can be rewritten as $\vec{\xi}(t) = \boldsymbol{G}\vec{\eta}(t)$ (see Appendix A.2). Now, Eq. (3.11) can be written in terms of $\vec{\eta}$ as

$$\frac{d\vec{x}}{dt} = \vec{H}(\vec{x}) + \boldsymbol{G}(\vec{x})\vec{\eta}(t). \tag{3.15}$$

Note that since the Fokker-Planck equation (3.9) only depends on $\boldsymbol{B}$ and not the particular choice of its decomposition $\boldsymbol{G}$, the probability density function of $\vec{x}$ and its time evolution do not depend on $\boldsymbol{G}$ either [61].

To obtain a stochastic differential equation for the time evolution of the chirality order parameter ω, we perform the following change of variables in Eq. (3.15):

$$\begin{pmatrix} a \\ d \\ l \end{pmatrix} \rightarrow \begin{pmatrix} n \\ r \\ \omega \end{pmatrix} = \begin{pmatrix} a+d+l \\ d+l \\ (d-l)/(d+l) \end{pmatrix} \tag{3.16}$$

Using Itō's lemma (see Appendix A.3) we can obtain an equation for the time evolution of the new state vector $\vec{y} = (n, r, \omega)$.

In general, it is not easy to solve for the joint probability density of coupled stochastic differential equations (SDE), but for a single variable first order SDE the steady state distribution is always exactly solvable. Therefore, we seek to reduce the number of degrees of freedom in the problem using the following two facts:

1. The reaction scheme reaction (3.1) conserves the total number of molecules, meaning that the total concentration $n = a + d + l$ is constant.

2. Simulations show that the concentration $r = d + l$ settles to a Gaussian distribution

around its fixed point value r^*, allowing us to substitute $r(t) \to r^*$. Therefore, the dynamics at long time occurs only in the chiral order parameter ω.

In the new variables, we find that $\dot{n} = 0$ and, by taking the positive solution of $\dot{r} = 0$, that is

$$r^* = \frac{\sqrt{(k_a n - k_d - 2k_n)^2 + 8k_a k_n n} + k_a n - k_d - 2k_n}{2k_a}, \tag{3.17}$$

we substitute $r \to r^*$ in the equation for ω, and use the rule for summing Gaussian variables (i.e. $a\eta_1 + b\eta_2 = \sqrt{a^2 + b^2}\eta$; where a and b are generic functions [54]) to express the stochastic part of the equation using a single noise variable. Expressing the result in terms of the total number of molecules $N = Vn$, for $N \gg 1$, we arrive at the following stochastic differential equation for the chirality order parameter ω:

$$\frac{d\omega}{dt} = -\frac{2k_n k_d V}{N k_a}\omega + \sqrt{\frac{2k_d}{N}(1-\omega^2)}\eta(t), \tag{3.18}$$

where $\eta(t)$ is Gaussian white noise with zero mean and unit variance. The time evolution of the probability density function of ω is described by the corresponding Fokker-Planck equation of Eq. (3.18) given by

$$\frac{\partial P(\omega,t)}{\partial t} = \frac{\partial}{\partial \omega}\left(\frac{2k_n k_d V}{N k_a}\omega P(\omega,t)\right) + \frac{1}{2}\frac{\partial^2}{\partial \omega^2}\left(\frac{2k_d}{N}(1-\omega^2)P(\omega,t)\right). \tag{3.19}$$

This is an exactly solvable partial differential equation with time dependent solution given in [62]. The steady state solution of Eq. (3.19) is given by (see Appendix A.4)

$$P_s(\omega) = \mathcal{N}\left(1-\omega^2\right)^{\alpha-1}, \quad \text{with} \quad \alpha = \frac{k_n V}{k_a}, \tag{3.20}$$

with the normalization constant

$$\mathcal{N} = \left(\int_{-1}^{+1}\left(1-\omega^2\right)^{\alpha-1} \mathrm{d}\omega\right)^{-1} = \frac{\Gamma\left(\alpha+\frac{1}{2}\right)}{\sqrt{\pi}\,\Gamma(\alpha)}. \tag{3.21}$$

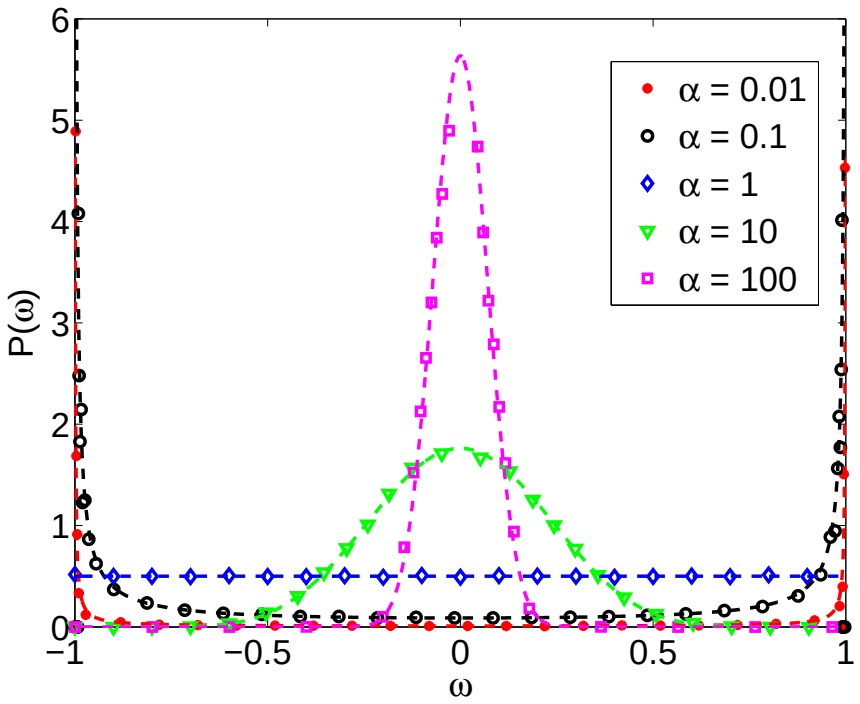

Figure 3.1: (Color online) Comparison between the stationary distribution, Eq. (3.20), (dashed lines) and Gillespie simulations of reactions reaction (3.1) (markers), for different values of α. Simulation parameters: $N = 10^3$, $k_a = k_n = k_d = 1$.

Equation (3.20) is compared in Fig. (3.1) against exact Gillespie simulations [60] of reactions (3.1). For $\alpha = \alpha_c = 1$, ω is uniformly distributed. For $\alpha \gg \alpha_c$, where the non-autocatalytic production is the dominant production reaction, $P_s(\omega)$ is peaked around the racemic state, $\omega = 0$. For $\alpha \ll \alpha_c$, where autocatalysis is dominant, $P_s(\omega)$ is sharply peaked around the homochiral states, $\omega = \pm 1$. The simulations were performed for $N = 1000$, where the analytic theory is expected to be accurate; for much smaller values of N, the theory is qualitatively correct, but very small quantitative deviations are observable compared to the simulations.

The importance of this treatment is not only in the analytical results for the probability density function of ω, but also the intuitive picture that Eq. (3.18) provides to understand the mechanism through which autocatalysis leads to homochirality. We will discuss an intuitive interpretation of Eq. (3.18) and the behavior of its solution Eq. (3.20) in the Section 3.3 along with the relationship of this model with the origin of life.

3.3 Transition to Homochirality and Origin of Life

In Section 3.2, we saw that for the reactions (3.1), in a well-mixed system of volume V and total number of molecules N, the time evolution of the chiral order parameter ω obeys the stochastic differential equation

$$\frac{d\omega}{dt} = -\frac{2k_n k_d V}{N k_a}\omega + \sqrt{\frac{2k_d}{N}(1-\omega^2)}\eta(t), \tag{3.22}$$

where $\eta(t)$ is a normalized Gaussian white noise with zero mean defined in the Itō sense [54]. The deterministic part of Eq. (3.22)

$$\frac{d\omega}{dt} = -\frac{2k_n k_d V}{N k_a}\omega, \tag{3.23}$$

which could alternatively be derived by reaction kinetic analysis (see Section 2.3), has one stable fixed point at the racemic state, consistent with the phase portrait in Fig. (2.2c). The multiplicative noise in Eq. (3.22) vanishes at homochiral states, and admits its maximum at the racemic state. In order to determine which one of the two terms is dominant, one can define the dimensionless parameter α as the ratio of the two constants $2k_n k_d V/Nk_a$ and $2k_d/N$, that is

$$\alpha = \frac{k_n V}{k_a}. \tag{3.24}$$

Note that the steady state solution of Eq. (3.22), given in Eq. (3.20), only depends on α. When $\alpha \gg 1$, the deterministic part of the Eq. (3.22) is dominant, and therefore, we expect a racemic solution. That is indeed the case, and the steady state probability density of ω is peaked around zero for large α (see Fig. (3.1)). However, for $\alpha \ll 1$, where autocatalysis is the dominant production mechanism, the amplitude of the noise term in Eq. (3.22) is much larger than the amplitude of the corresponding deterministic term. Since the noise is maximum at the racemic state, the variable ω stochastically walks away from the racemic state over time and ends up at homochiral states where the noise term vanishes.

To understand this result physically, note that the source of the multiplicative noise is the

intrinsic stochasticity of the autocatalytic reactions. While, on average, the two autocatalytic reactions do not change the variable ω (see Fig. (2.2b)), each time one of the reactions takes place, the value of ω changes by a very small discrete amount. As a result, over time the value of ω drifts away from its initial value. Since the amplitude of the noise term is maximum at racemic state and zero at homochiral states, this drift stops at one of the homochiral states.

The absence of the noise from autocatalysis at homochiral states can be understood by recognizing that at homochiral states, the molecules with only one of two chiral states D and L are present, hence only the autocatalytic reaction associated with that chiral state has a non-zero rate. This reaction produces molecules of the same chirality, keeping the system at the same homochiral state without affecting the value of ω, and therefore, the variable ω does not experience a drift away from the homochiral states due the autocatalytic reactions.

Note that the stationary distribution of ω in Eq. (3.20) is only dependent on α and is independent of the decay reaction rate, k_d. The only role of this reaction is to prevent the A molecules from being completely consumed, thus providing a well-defined non-equilibrium steady state independent of the initial conditions.

The parameter α is proportional to the ratio of the non-autocatalytic production rate, k_n, to the self-replication rate, k_a. In the evolution of early life, when self-replication was a primitive function, k_a would be small and the value of α would therefore be large. As life evolved, the self-replicators would evolve to become more efficient at self-replication, and would be less likely to be produced spontaneously through non-self-replicating mechanisms. As a result the value of k_a would increase, while k_n decrease, and α would become very small. Therefore, in our model, we expect that life started in a racemic state, and it transitioned to homochirality after self-replication became efficient (i.e. when $\alpha \ll 1$). It is a necessary weakness of the present state of understanding that we do not have a dynamical description of $\alpha(t)$, so in this sense, our theory is incomplete.

It is important to note that all of the previous mechanisms suggested for homochirality rely on assumptions that cannot be easily confirmed to hold during the emergence of life. However, even if all of such mechanisms fail during the origin of life, our mechanism guar-

antees the emergence of homochirality, since it only relies on self-replication and death, two processes that are inseparable from any living system.

3.4 Pigs *Can* Fly: Violation of Detailed Balance is a Necessary Condition for Homochirality

Our model violates the principle of microscopic reversibility, and in this section, I wish to comment on this fact and explore its physical origin. The violation of microscopic reversibility follows because our model explicitly violates the principle of detailed balance, as is required for an externally driven minimal model far from equilibrium. Here, I review some thermodynamical aspects of our model, which I believe have important implications for understanding the origin of life. Before, starting to analyze the model, I would like to review the history of criticisms to minimal models for homochirality that violate microscopic reversibility.

The story dates back to 2009, when Donna Blackmond published an essay titled: *"If pigs could fly" chemistry: a tutorial on the principle of microscopic reversibility* [63]. In this essay, she criticizes several kinetic models of homochirality similar to Frank's model with the type of recycling that exists in our model. She argues that these kinetic models are written with arbitrary reactions constants without a regard for whether reactions with these constants are thermodynamically feasible or not. The crux of the argument boils down to the following: *the principle of microscopic reversibility* states that at equilibrium, the rate of the forward reaction and the reverse reaction are equal for all reactions. For systems involving recycling, or more generally cyclic reactions, this principle puts a constraint on the relationship of the rate constants of the set of reactions that share their pool of reactants

and products. For example, consider the cyclic reaction set

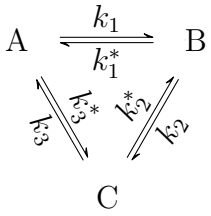

(3.25)

At equilibrium, the rate of forward and backward reactions are the same for each reaction, giving rise to the following relationships:

$$k_1[A] = k_1^*[B], \qquad k_2[B] = k_2^*[C], \qquad k_3[C] = k_3^*[A]. \tag{3.26}$$

Eliminating the concentrations $[A]$, $[B]$, and $[C]$, we have

$$\frac{k_1}{k_1^*}\frac{k_2}{k_2^*}\frac{k_3}{k_3^*} = 1. \tag{3.27}$$

This relationship was discovered by Wegscheider in 1901 [64]. It implies that, at equilibrium, the six reaction rates cannot be chosen independently. In particular, one cannot have a set of cyclic irreversible reactions, that is for nonzero k_1, k_2, and k_3, we cannot set k_1^*, k_2^*, and k_3^* simultaneously to zero, at equilibrium. Of course, once an equilibrium solution exists, these constant should obey Wegscheider's conditions, even far from equilibrium, because after all, reaction constants are constants, *i.e.* independent of the extent of reactions. In other words, Wegscheider's condition is the condition for the existence of an equilibrium solution. The principle of microscopic reversibility is a consequence of detailed balance, which is obeyed by equilibrium systems. If a model has an equilibrium solution, one can derive the rate constants from the free energy differences. However, in a cyclic reaction set, not all the free energy differences are independent. As a result, for a model to have an equilibrium solution, its rate constants have to obey a constraint, and that is Wegscheider's condition.

What does it all have to do with homochirality? There is a similar situation in the model defined by reactions (3.1) because of the recycling and irreversibility of the autocatalytic

reactions. Note that the linear and the autocatalytic reactions have the same reactants and products, therefore, doing the same analysis on reactions

$$A + \text{D} \underset{k_a^*}{\overset{k_a}{\rightleftharpoons}} 2\text{D}, \qquad A \underset{k_d}{\overset{k_n}{\rightleftharpoons}} \text{D}, \tag{3.28}$$

results in the following condition at equilibrium

$$k_a[A][\text{D}] = k_a^*[\text{D}]^2, \qquad k_n[A] = k_d[\text{D}], \tag{3.29}$$

which implies

$$\frac{k_a}{k_a^*} = \frac{k_n}{k_d}. \tag{3.30}$$

This suggests that for this model to have an equilibrium solution, it cannot have an irreversible autocatalysis and recycling simultaneously (*i.e.* k_a^* cannot be zero for a nonzero k_d).

This is a potential source of criticism against this model. After all, one might say, every set of chemical reactions should have an equilibrium. No, it should not: every *closed* set of chemical reactions should have an equilibrium. I have made this clear that the stationary solution of my model is a nonequilibrium steady state, and therefore, it has to be a driven system with an external source of energy or disequilibrium. In fact, as I will show in this section, any system modeling a prebiotic chemistry, and more importantly any model attempting to achieve complete homochirality has to be a driven model. Like Frank and most other workers in this field, we chose not to include the external source of energy in our model for several reasons: (1) it is unnecessary and not the main point of the exercise; (2) it forces us to make specific and detailed choices about chemical processes that have no experimental support in an early life context; (3) it obscures the basic mechanisms leading to homochirality.

Before I show why it is necessary for model to be driven by an external source of energy, in order to give rise to a homochiral steady state, let me show a couple of different ways one

can implement such energy sources, keeping the autocatalysis irreversible.

The reaction set (3.1) was set up with the idea in mind that self-replication (modeled by the autocatalytic reactions) has exclusive access to an external source of energy, as is the case in all biological systems, and therefore the effective "reaction constants" (which are dependent on the amount of energy to which the replicator has access) can be tuned independently of the other non-autocatalytic reactions. This can be shown by adding extra molecular species representing the source of energy. For example, modern organisms couple the hydrolysis reaction of adenosine triphosphate (ATP) that produces adenosine diphosphate (ADP) and a phosphate (P) to their autocatalytic cylces in their cell, using the free energy difference to drive the cycles [65]. Consider the following set of reactions

$$\begin{aligned} A + \text{D} + ATP &\xrightarrow{k_s} 2\text{D} + ADP + P \\ A + \text{L} + ATP &\xrightarrow{k_s} 2\text{L} + ADP + P \\ A &\underset{k_d}{\overset{k_n}{\rightleftharpoons}} \text{D} \\ A &\underset{k_d}{\overset{k_n}{\rightleftharpoons}} \text{L} \end{aligned} \tag{3.31}$$

It is easy to see how all of these reaction rates are independent of each other. Now keeping the concentration of ATP constant (by providing a constant supply of ATP), the self-replication reactions can be written in the compact form

$$A + \text{D} \xrightarrow{k_s[ATP]} 2\text{D}, \qquad A + \text{L} \xrightarrow{k_s[ATP]} 2\text{L} \tag{3.32}$$

ignoring the inactive compounds, ADP and P. Now we can simply define an *effective* reaction rate $k_a = k_s[ATP]$, recovering reactions (3.1). This reaction rate, as promised, is tunable independently of the other reaction constants; it depends on the availability of the energy source.

Another potential solution to this problem is to change the set of proposed reactions to

$$\begin{aligned} A + \text{D} &\xrightarrow{k_a} 2\text{D}, \qquad \text{D} \underset{k_n}{\overset{k_d}{\rightleftharpoons}} B \\ A + \text{L} &\xrightarrow{k_a} 2\text{L}, \qquad \text{L} \underset{k_n}{\overset{k_d}{\rightleftharpoons}} B. \end{aligned} \tag{3.33}$$

In this model, D and L enantiomeres are autocatalytically produced from a less stable achiral molecule A, and decay to a more stable achiral molecule B. Now, all we need to do to drive the reactions to a nonequilibrium steady state is to provide a constant supply of A and continuously remove B from the system. The free energy difference between A and B will provide the driving force. Unlike the previous solution, this is a different model with slightly different kinetics. However, it does result in a homochiral steady state through exactly the same noise-induced mechanism described in this chapter. This attests to the fact that our mechanism only depends on self-replication and decay, and the details of the chemical reactions implementing these processes are irrelevant. There are other ways to model the source of driving energy in the system; see, for example Ref. [66] for a resolution of a similar problem in another model of homochirality.

A steady process of self-replication requires a constant supply of energy, and therefore, an open-system. This is true of all biological systems today, and so has to have been true during the emergence of life. In general the source of energy for self-replication could be a constant supply of high free energy molecules, steady flow of photons from sunlight, voltage difference across an alkaline hydrothermal vent in the bottom of the ocean, or any perhaps unknown kind of interesting chemistry that led to the emergence of life. These cases may all look like "exceptional cases" compared to typical test tube experiments done in the lab, but it would be hard to imagine a scenario for the origin of life that does not involve an external driving force.

The fact that biological systems are driven is not the only reasoning behind open driven models for homochirality. In fact there are thermodynamical constraints on the type of model that could lead to complete homochirality. Perhaps the most straightforward argument for

open driven models of homochirality with recycling is the following: it is a well known fact that amino acids spontaneously racemize over the time scale of years to millennia depending on temperature and PH [67, 68, 69]. Note that this is a very short time scale compared with the geological time scale associated with the origin of life. Any mechanism for homochirality that does not continuously recycle the product will end up with a racemic equilibrium mixture of amino acids. Of course a continuous recycling and production through a separate mechanism requires a steady supply of external driving force leading to a nonequilibrium steady state.

This argument goes deeper than amino acids: there is no closed system with a completely homochiral equilibrium. Suppose, that the equilibrium state of a system is homochiral for at least one type of the chiral molecules in the system. Let us make a replica of the system and replace half of those chiral molecules with their mirror images. This transformation does not change the internal energy, U, of the system, since both of the chiral molecules have the same internal energy. It does not change the pressure or the volume of the system either, since all the physical properties of the two chiral molecules are identical by symmetry. However, the entropy of the racemic replica is larger than that of the homochiral system. Therefore, the Gibbs free energy, $G = U + pV - TS$, of the racemic mixture is lower than that of homochiral mixture, and the homochiral solution cannot be the equilibrium solution of the system; over long time, such a homochiral solution will racemize. Only a continuously driven mechanism can keep such a system in a homochiral state over long time, and that state will be a nonequilibrium steady state.

Chapter 4

Noise-Induced Homochirality in Spatially Extended Systems

Consider your favorite origin of life scenario. For example, imagine life started through autocatalytic reactions in Alkaline hydrothermal vents in the bottom of the ocean [70] (this is just an example, and what follows does not depend on the details of the origin of life scenario). Now, whatever symmetry-breaking mechanism we propose for the origin of homochirality in this prebiotic world should be robust in the following sense: First, consider two nearby hydrothermal vents. In the absent of diffusion, over time, each one becomes homochiral through some symmetry-breaking mechanism. This homochirality should be robust with respect to the perturbation caused by (*e.g.*) molecules of opposite chirality diffusing from the other vent. Second, over time the particular choice of homochirality should be synchronized over all of the sources of production of these chiral molecules.

In this chapter, I will show that the noise-induced homochirlaity mechanism suggested in Chapter 3 is robust with respect to these two criteria. In Section 4.1, I define the spatial extension of our model as a set of well-mixed reaction patches diffusively coupled to their neighbors. The Fokker-Planck equation for two diffusively coupled patches is derived in Section 4.2, followed by a perturbation theory analysis in Section 4.3, showing the first robustness criteria for our model holds when autocatalysis is the dominant production mechanism. In Section 4.4, we study the one dimensional spatial extension of the model in the continuum limit, where we see that the correlation length for the chiral order parameter diverges as the nonautocatalytic reaction rates approaches zero. Moreover, I show simulation results for a one-dimensional system of diffusively coupled patches at pure autocatalytic limit, where the patches synchronize their final homochiral state. This indicates that the

pure autocatalytic limit of our model is robust with respect to the second robustness criteria.

4.1 Description of the spatially extended model

Consider the following spatial extension [71] of the model described in Chapter 3: let reactions (3.1) take place in a set of M well-mixed patches of volume V, while molecules can diffuse between neighboring patches with diffusion rate δ. The set of neighbors of each patch i, $i = 1, \ldots, M$, is denoted by $\langle i \rangle$ (e.g., for a linear chain, $\langle i \rangle = \{i-1, i+1\}$) and molecules of species A, D, and L in patch i by A_i, D_i, and L_i respectively. In summary, the following set of reactions defines the spatial model:

$$\begin{aligned} &A_i \underset{k_d}{\overset{k_n}{\rightleftharpoons}} \mathrm{D}_i, \quad A_i \underset{k_d}{\overset{k_n}{\rightleftharpoons}} \mathrm{L}_i, \qquad i = 1, \ldots, M \\ &A_i + \mathrm{D}_i \xrightarrow{k_a} 2\mathrm{D}_i, \qquad A_i + \mathrm{L}_i \xrightarrow{k_a} 2\mathrm{L}_i \\ &\mathrm{D}_i \overset{\delta}{\rightleftharpoons} \mathrm{D}_j, \qquad \mathrm{L}_i \overset{\delta}{\rightleftharpoons} \mathrm{L}_j, \qquad j \in \langle i \rangle. \end{aligned} \tag{4.1}$$

A similar analytical treatment to that of Section 3.2 results in the following set of coupled stochastic differential equations for the time evolution of the chiral order parameter ω_i, of each patch i (I will show a step by step derivation of the special case $M = 2$ in Section 4.2):

$$\frac{d\omega_i}{dt} = -\frac{2k_n k_d V}{N k_a}\omega_i + \delta \sum_{j \in \langle i \rangle} (\omega_j - \omega_i) + \sqrt{\frac{2k_d}{N}(1-\omega_i^2)}\eta_i(t) + \sqrt{\frac{\delta}{N}}\xi_i(\vec{\omega}, t), \tag{4.2}$$

where now N represents the average number of molecules per patch, η_i's are independent normalized Gaussian white noises, ξ_i's are zero mean Gaussian noise with correlator

$$\langle \xi_i(t)\xi_j(t') \rangle = \left(2 \sum_{k \in \langle i \rangle} (1 - \omega_i \omega_k)\, \delta_{i,j} + \left(\omega_i^2 + \omega_j^2 - 2\right) \chi_{\langle i \rangle}(j) \right) \delta(t - t'), \tag{4.3}$$

and $\chi_{\langle i \rangle}(j)$ is equal to one if $j \in \langle i \rangle$ and zero otherwise.

4.2 Two-Patch Model: Fokker-Planck Equation

Let us analyze the homochirality in each patch of the spatial extension of our model described by reactions (4.1) with $M = 2$. We can follow the procedure explained in Section 3.2 to obtain a Fokker-Planck equation for the time evolution of the probability density of the system being at a state with concentrations a_1, d_1, l_1, a_2, d_2, and l_2. Again we can reduce the number of variables using the following facts (i) the total concentration $n_t = n_1 + n_2 = a_1 + d_1 + l_1 + a_2 + d_2 + l_2$ is conserved; (ii) simulation shows that in long time, the variables $r_1 = d_1 + l_1$, $r_2 = d_2 + l_2$, and $\Delta = n_1 - n_2$ settle to Gaussian distributions around their fixed point values $r_1 = r_2 = r^*$ and $\Delta = 0$. We do the following change of variables

$$\begin{pmatrix} a_1 \\ d_1 \\ l_1 \\ a_2 \\ d_2 \\ l_2 \end{pmatrix} \rightarrow \begin{pmatrix} n_t \\ \Delta \\ r_1 \\ r_2 \\ \omega_1 \\ \omega_2 \end{pmatrix} = \begin{pmatrix} a_1 + d_1 + l_1 + a_2 + d_2 + l_2 \\ a_1 + d_1 + l_1 - a_2 - d_2 - l_2 \\ d_1 + l_1 \\ d_2 + l_2 \\ (d_1 - l_1)/(d_1 + l_1) \\ (d_2 - l_2)/(d_2 + l_2) \end{pmatrix} \tag{4.4}$$

using Itō's formula. Now the dynamics only occurs only in $\vec{\omega} = (\omega_1, \omega_2)$. For large average number of molecules per patch $N \gg 1$, the resulting Fokker-Planck equation for the time evolution of the joint probability density function of ω_1 and ω_2, $Q(\vec{\omega}, t)$, reads

$$\frac{\partial Q}{\partial t} = -\sum_{i=1}^{2} \frac{\partial \left((\boldsymbol{L}\vec{\omega})_i \, Q \right)}{\partial \omega_i} + \frac{1}{2} \sum_{i,j=1}^{2} \frac{\partial^2 \left(U_{ij} Q \right)}{\partial \omega_i \partial \omega_j}. \tag{4.5}$$

Note that the above sums are now over the patches, and not over species as in Eq. (3.9). The Jacobian matrix $\boldsymbol{L}$ is given by

$$\boldsymbol{L} = -\frac{2k_d k_n V}{N k_a} \begin{pmatrix} 1 & 0 \\ 0 & 1 \end{pmatrix} + \delta \begin{pmatrix} -1 & 1 \\ 1 & -1 \end{pmatrix}, \tag{4.6}$$

and the diffusion matrix $\boldsymbol{U}$ by

$$\boldsymbol{U} = \frac{2k_d}{N}\begin{pmatrix} 1-\omega_1^2 & 0 \\ 0 & 1-\omega_2^2 \end{pmatrix} + \frac{\delta}{N}\begin{pmatrix} 2(1-\omega_1\omega_2) & \omega_1^2+\omega_2^2-2 \\ \omega_1^2+\omega_2^2-2 & 2(1-\omega_1\omega_2). \end{pmatrix}. \tag{4.7}$$

This Fokker-Planck equation describes the time evolution of the probability density of stochastic variables obeying the spacial case, $M = 2$, of Eq. (4.2).

4.3 Two-Patch Model: Homochirality

Does a system described by reactions (3.1) stay homochiral when diffusively coupled to similar systems? To answer this question, we need to analyze the homochirality in each patch of the spatial extension of our model described by reactions (4.1) with $M = 2$. In Section 4.2, I showed that the joint probability density of chiral order parameters of two diffusively coupled patches obeys Eq. (4.5). probability density function of the chiral order parameter of a single patch, $Q_s(\omega)$ is defined by

$$Q_s(\omega) = \int_{-1}^{+1} Q_s(\omega,\omega_2)d\omega_2 = \int_{-1}^{+1} Q_s(\omega_1,\omega)d\omega_1, \tag{4.8}$$

where $Q_s(\omega_1,\omega_2)$ is the stationary solution of Eq. (4.5). We first analyze the condition for each patch reaching homochirality using perturbation theory, in the case of slow diffusion. For $\delta \sim k_d/N$ or smaller, we can treat the diffusion deterministically by ignoring the last term in Eq. (4.7). To solve for $Q_s(\omega)$, we begin by rewriting Eq. (4.5) as a continuity equation,

$$\partial_t Q + \nabla \cdot \vec{J} = 0, \tag{4.9}$$

which defines the probability current $\vec{J}$ as [54]

$$\vec{J} = \boldsymbol{L}\vec{\omega}\, Q - \frac{1}{2}\nabla \cdot (\boldsymbol{U}Q)\,. \tag{4.10}$$

By the conservation of probability, at steady state, the total probability flux $\vec{J}_s$ through each vertical section of ω_1-ω_2 plane must be zero. That is

$$\begin{aligned}\int_{-1}^{+1} J_{s,1}\mathrm{d}\omega_2 &= \int_{-1}^{+1}\left((\boldsymbol{L}\vec{\omega})_1 Q_s - \frac{1}{2}\partial_{\omega_1}(U_{11}Q_s)\right)\mathrm{d}\omega_2 \\ &= Q_s(\omega_1)\omega_1\left(\frac{2k_d}{N}(1-\alpha)-\delta\right) - \frac{k_d}{N}(1-\omega_1^2)\frac{dQ_s}{d\omega_1} + \delta\int_{-1}^{+1}\omega_2 Q_s(\omega_1,\omega_2)\mathrm{d}\omega_2 = 0.\end{aligned} \tag{4.11}$$

The last integral can be evaluated using Bayes' theorem

$$\delta\int_{-1}^{+1}\omega_2 Q_s(\omega_1,\omega_2)\mathrm{d}\omega_2 = \delta\int_{-1}^{+1}\omega_2 Q_s(\omega_2|\omega_1)Q_s(\omega_1)\mathrm{d}\omega_2 = \delta\, Q_s(\omega_1)\langle\omega_2\rangle_{\omega_1} = \mathcal{O}(\delta^2), \tag{4.12}$$

which is of order δ^2 for small δ, since, $\langle\omega_2\rangle_{\omega_1}$ (the expected value of ω_2 given ω_1) vanishes at zero δ, and therefore, of order δ for small δ. In this regime, Eq. (4.11) provide us with a differential equation for $Q_s(\omega)$ with the solution

$$Q_s(\omega) = \mathcal{Z}(1-\omega^2)^{\alpha+\frac{\delta N}{2k_d}-1}, \tag{4.13}$$

where the normalization constant $\mathcal{Z}$ is given by

$$\mathcal{Z} = \frac{\Gamma\left(\alpha+\frac{\delta N}{2k_d}+\frac{1}{2}\right)}{\sqrt{\pi}\,\Gamma(\alpha+\frac{\delta N}{2k_d})}. \tag{4.14}$$

This result shows that the critical α below which each patch becomes homochiral, up to the first order correction in δ, is given by

$$\alpha_c \approx 1 - \delta\frac{N}{2k_d}, \quad \text{for } \delta \approx 0. \tag{4.15}$$

We can now turn to the case of high diffusion. Recall that the patches are defined as the maximum volume around a point in space in which the system can be considered well-mixed. This can be interpreted as the maximum volume in which diffusion dominates over the other

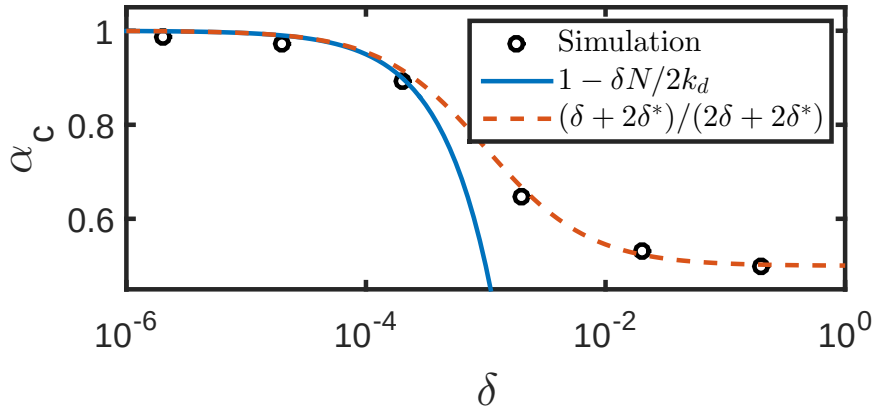

Figure 4.1: (Color online) Parameter α_c^{patch} in the two-patch system as a function of the diffusion rate δ. Gillespie simulations (markers) are compared against Eq. (4.15) (solid blue line) and Eq. (4.17) (dashed red line). Simulation parameters as in Fig. (3.1).

terms acting on the variable of interest (in this case ω). From Eq. (4.2), this condition is fulfilled for $\delta \sim 2k_d\alpha/N$. In the vicinity of the transition α is of order unity, therefore the condition becomes $\delta \sim k_d/N$. For $\delta \gg k_d/N$, the whole system can be considered well-mixed and has the critical value of α, $\alpha_c^{\text{system}} = 1$, from the well-mixed results (see Section 3.2). Note that α scales with the volume, and the volume of the whole system is two times the volume of each patch, *i.e.* $2V$. This indicates that in a single patch

$$\alpha_c \approx \frac{1}{2}, \quad \text{for } \delta \gg 0. \tag{4.16}$$

Now we can interpolate between these extreme limits, asymptotic to $1/2$ for large δ and to Eq. (4.15) for small δ:

$$\alpha_c = \frac{\delta + 2\delta^*}{2\delta + 2\delta^*}, \qquad \delta^* = \frac{k_d}{N}. \tag{4.17}$$

Figure (4.1) shows agreement between α_c measured from Gillespie simulations of the two-patch system, and the Eq. (4.17). At the parameter regime below the α_c curve in Fig. (4.1), individual patches are homochiral. Also, we find that the correlation between the homochiral states of the two patches increases with diffusion rate δ and become completely correlated when $\delta \sim k_d/N$ or more. In this regime the system reaches global homochirality.

4.4 One-Dimensional Model of Homochirality and the Correlation Function

In Section 4.3 we saw that chiral molecules produced through autocatalytic processes in a spatial model stay at least locally homochiral even in the presence of diffusion, when autocatalysis the dominant production mechanism. In other words, the noise-induced mechanism for homochirality is robust with respect to diffusion. But does the system stay globally homochiral? To answer this question, let us examine the continuous limit of Eq. (4.2). In the continuum limit, the noise term ξ_i (a side effect of diffusion on a discrete lattice) can be neglected. What is left of Eq. (4.2) in the continuous form can be written as

$$\frac{\partial \omega}{\partial t} = -\frac{2k_n\, k_d}{n\, k_a}\omega(t,\vec{x}) + \mathcal{D}\,\nabla^2\omega + \sqrt{\frac{2k_d}{n}(1-\omega^2)}\,\eta(t,\vec{x}), \tag{4.18}$$

where the Gaussian noise $\eta(t,\vec{x})$ is defined by its moments

$$\langle \eta(t,\vec{x})\eta(t',\vec{x}')\rangle = \delta(t-t')\,\delta(\vec{x}-\vec{x}'), \quad \text{and} \quad \langle \eta(t,\vec{x})\rangle = 0. \tag{4.19}$$

After a change of variable (not shown here) Eq. (4.18) can be converted to a special case of what Korolev et al. [72] call "*stochastic Fisher-Kolmogorov-Petrovsky-Piscounov equation* [73, 74] *with additional terms describing mutation.*" We follow Ref. [72] to derive an equation for the time evolution of the two-point correlation function defined as

$$\phi(t,\vec{x}_1,\vec{x}_2) = \langle \omega(t,\vec{x}_1)\omega(t,\vec{x}_2)\rangle\,. \tag{4.20}$$

The correlation function $\phi(t,\vec{x}_1,\vec{x}_2)$ is a function of two stochastic variables $\omega(t,\vec{x}_1)$ and $\omega(t,\vec{x}_2)$, and its time derivative can be calculated using Itō's lemma (see Appendix A.3) from Eq. (4.18). The result has a beautiful closure property, where the right hand side can

be written in terms of ϕ:

$$\frac{\partial}{\partial t}\phi(t,\vec{x}_1,\vec{x}_2) = -\frac{4k_nk_d}{nk_a}\phi(t,\vec{x}_1,\vec{x}_2) + \frac{2k_d}{n}(1-\phi(t,\vec{x}_1,\vec{x}_1))\delta(\vec{x}_1-\vec{x}_2) + \mathcal{D}\left(\nabla^2_{\vec{x}_1}+\nabla^2_{\vec{x}_2}\right)\phi(t,\vec{x}_1,\vec{x}_2). \tag{4.21}$$

The two point correlation function, $\phi(t,\vec{x}_1,\vec{x}_2)$, in Eq. (4.21) only depends on t and $\vec{x} = \vec{x}_1 - \vec{x}_2$ for spatially homogeneous initial conditions. With this simplification we have

$$\frac{\partial}{\partial t}\phi(t,\vec{x}) = 2\mathcal{D}\nabla^2\phi(t,\vec{x}) - \frac{2k_d}{n}\left(\phi(t,\vec{x})-1\right)\delta(\vec{x}) - \frac{4k_nk_d}{nk_a}\phi(t,\vec{x}) \tag{4.22}$$

In one dimension, the steady state solution of Eq. (4.22) can be obtained by setting the right hand side equal to zero, and for $\phi(x) = \phi(\infty, x)$, we have

$$2\mathcal{D}\frac{\partial^2}{\partial x^2}\phi(x) - \frac{2k_d}{n}\left(\phi(x)-1\right)\delta(x) - \frac{4k_nk_d}{nk_a}\phi(x) = 0. \tag{4.23}$$

Let us solve this differential equation: for $x > 0$, $\delta(x) = 0$ and we can solve for $\phi(x)$

$$\frac{\partial^2}{\partial x^2}\phi(x) - \frac{2k_nk_d}{n\mathcal{D}k_a}\phi(x) = 0 \implies \phi(x) = C_1 e^{-\sqrt{\frac{2k_nk_d}{n\mathcal{D}k_a}}x} + C_2 e^{\sqrt{\frac{2k_nk_d}{n\mathcal{D}k_a}}x} \tag{4.24}$$

The limit of $x \to \infty$ of $\phi(x)$ should be finite therefore $C_2 = 0$, and

$$\phi(x) = C_1 e^{-\sqrt{\frac{2k_nk_d}{n\mathcal{D}k_a}}x}, \quad \text{for } x > 0. \tag{4.25}$$

Similarly, for $x < 0$:

$$\phi(x) = C_1 e^{\sqrt{\frac{2k_nk_d}{n\mathcal{D}k_a}}x}, \quad \text{for } x < 0. \tag{4.26}$$

At $x = 0$, the second derivative of ϕ is proportional to a δ-function, and therefore, its derivative is discontinuous, but the function itself is continuous, and we have

$$\lim_{x\to 0^-}\phi(x) = \lim_{x\to 0^+}\phi(x) \implies C_1 = C_2. \tag{4.27}$$

To find the discontinuity in the derivative at $x = 0$, we need to integrate the second derivative given by

$$\frac{\partial^2}{\partial x^2}\phi(x) = \frac{k_d}{\mathcal{D}n}\left(\phi(x) - 1\right)\delta(x) - \frac{2k_n k_d}{n\mathcal{D}k_a}\phi(x), \tag{4.28}$$

on the interval $(-\epsilon, \epsilon)$ and take the limit of $\epsilon \to 0$:

$$\lim_{\epsilon\to 0}\int_{-\epsilon}^{\epsilon}\frac{\partial^2}{\partial x^2}\phi(x)dx = \lim_{\epsilon\to 0}\int_{-\epsilon}^{\epsilon}\frac{k_d}{\mathcal{D}n}\left(\phi(x) - 1\right)\delta(x) - \frac{2k_n k_d}{n\mathcal{D}k_a}\phi(x)dx. \tag{4.29}$$

The left hand side becomes the difference between the right and left derivative of ϕ, while only the term involving the δ-function survives under the limit on the right hand side:

$$\lim_{\epsilon\to 0^+}\left.\frac{\partial\phi}{\partial x}\right|_{\epsilon} - \lim_{\epsilon\to 0^-}\left.\frac{\partial\phi}{\partial x}\right|_{\epsilon} = \frac{k_d}{\mathcal{D}n}\left(\phi(0) - 1\right). \tag{4.30}$$

substituting ϕ from Eqs. (4.25) and (4.26), we have

$$-2\sqrt{\frac{2k_n k_d}{n\mathcal{D}k_a}}C_1 = \frac{k_d}{n\mathcal{D}}(C_1 - 1) \implies C_1 = \frac{1}{1 + \sqrt{\frac{8n\mathcal{D}k_n}{k_a k_d}}}, \tag{4.31}$$

which gives the steady state solution to the two-point correlation function

$$\phi(x) = \frac{e^{-\sqrt{\frac{2k_n k_d}{n\mathcal{D}k_a}}|x|}}{1 + \sqrt{\frac{8n\mathcal{D}k_n}{k_a k_d}}}. \tag{4.32}$$

The expected value of ω^2 is given by $\phi(0)$, and $\phi(x)$ exponentially decays from this value with the length scale

$$\zeta = \sqrt{\frac{n\mathcal{D}k_a}{2k_n k_d}}. \tag{4.33}$$

Therefore this length scale ζ defines a correlation length. This correlation length diverges as k_n approaches zero, indicating that in the pure autocatalytic limit of this model, at steady state, the entire space synchronizes its choice of homochirality to the same uniformly homochiral state. Figure (4.2) shows the result of simulation of reactions (4.1) in one dimension with $M = 100$ patches at the limit $k_n \to 0$. The simulation is initialized with a uniformly

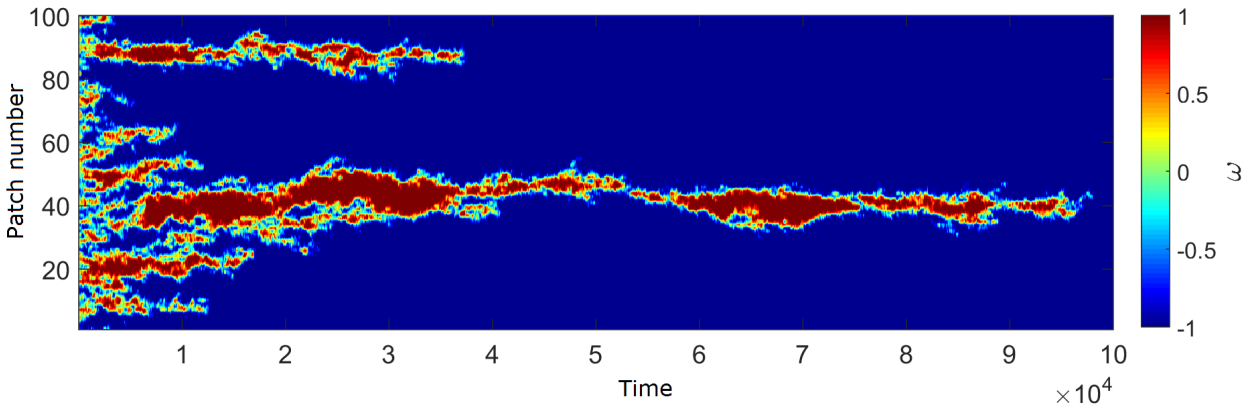

Figure 4.2: Gillespie simulation of scheme reaction (4.1) for a one-dimensional system of $M = 100$ patches, starting from racemic state and ending with all the patches in the same homochiral state $\omega = -1$. Simulation parameters: $N = 1000$, $k_a = k_d = 1$, $\delta = 10^{-3}$, and $k_n = 0$.

racemic state. The homochiral islands of D and L form very quickly at the beginning of the simulation and compete until the entire space becomes uniformly homochiral.

Here is a cute fact about this spatial extension: Let us define the correlation volume $\mathcal{V} = (2\zeta)^D$ (this is the volume of the correlated cube from $-\zeta$ to ζ on each dimension), where the dimension $D = 1$ in this case. In term of the correlation length and the correlation volume, the two-point correlation function is given by

$$\phi(x) = \frac{e^{-\left|\frac{x}{\zeta}\right|}}{1 + 2\frac{k_n \mathcal{V}}{k_a}} = \frac{e^{-\left|\frac{x}{\zeta}\right|}}{1 + 2\bar{\alpha}}. \tag{4.34}$$

The new $\bar{\alpha} = k_n \mathcal{V}/k_a$ is the α from the well-mixed case defined in Eq. (3.20) with the volume substituted by the correlation volume, $V = \mathcal{V}$. The expected value of ω^2 at each point is given by $\phi(0) = 1/(1 + 2\bar{\alpha})$ which is exactly the same if calculated from Eq. (3.20):

$$\left\langle \omega^2 \right\rangle = \int_{-1}^{1} \omega^2 P(\omega) d\omega = \frac{\Gamma\left(\alpha + \frac{1}{2}\right)}{\sqrt{\pi}\Gamma(\alpha)} \int_{-1}^{1} \omega^2 \left(1 - \omega^2\right)^{\alpha - 1} d\omega = \frac{1}{1 + 2\alpha}. \tag{4.35}$$

This shows that there is a correlation volume around every point in space in which the system behaves as though it is a well-mixed system with that volume.

4.5 Conclusion

In conclusion, a racemic population of self-replicating chiral molecules far from equilibrium, even in the absence of other nonlinearities that have previously been invoked, such as chiral inhibition, transitions to complete homochirality when the efficiency of self-replication exceeds a certain threshold. This transition occurs due to the drift of the chiral order parameter under the influence of the intrinsic stochasticity of the autocatalytic reactions. The functional form of the multiplicative intrinsic noise from autocatalysis directs this drift toward one of the homochiral states. Unlike some other mechanisms in the literature, this process does not require an initial enantiomeric excess. In our model, the homochiral states are not deterministic dynamical fixed points, but are instead stabilized by intrinsic noise. Moreover, in the spatial extension of our model, we have shown that diffusively coupled autocatalytic systems synchronize their final homochiral states, allowing a system solely driven by autocatalysis to reach global homochirality. We conclude that autocatalysis alone is a viable mechanism for homochirality, without the necessity of imposing chiral inhibition or other nonlinearities.

Part II

Nonnormality of Stochastic Turing Patterns

Chapter 5

Nonnormality and Steady State Amplification in Stochastic Dynamics

It is widely assumed that deterministic dynamical systems close to their stable fixed points respond to small perturbations by damping those perturbations exponentially. However, this is not necessarily the case: in *nonnormal* systems (*i.e.* systems with non-orthogonal eigenvectors) the response may initially consist of amplifying perturbations, as shown in Fig. 5.1. Systems that exhibit these amplifications are called *reactive* [75]. This surprising feature, initially found in fluid dynamics [76, 77, 78], and later in ecology [75, 79], shows that a stable deterministic system can in theory produce a response that exceeds by several order of magnitude the amplitude of the perturbation the system is subject to — a feature not detectable by the analysis of the system's eigenvalues.

In deterministic systems, where this phenomenon is most widely studied, the effect of growth is transient, and at long time, the system damps the perturbations exponentially at the rate determined by the largest eigenvalue of the system. In this chapter, we will see that the effect of nonnormality on stochastic dynamical systems is permanent, where the system maintains an amplified mean distance from its steady state. First, I discuss some background work on deterministic nonnormal dynamical systems in Section 5.1. Linear stability analysis of a stochastic dynamical system near its equilibrium point is shown in Section 5.2. Equilibrium systems are time reversally symmetric and have hermitian linear stability operators. However, near a nonequilibrium steady state, the system is generally nonnormal. The linear stability analysis of a system near a nonnormal fixed point is given in Section 5.3, which is used in Section 5.4 to calculate the amplification of the steady state mean distance from the fixed point due to nonnormality. This amplification factor, as a new

measure of nonnormality, with its geometric interpretation is the main result of this chapter and is used in Chapter 6 and Chapter 7 to study the effect of nonnormality on stochastic Turing patterns.

5.1 Introduction to Nonnormality and Transient Growth in Deterministic Dynamics

Recent work in ecological dynamics has emphasized the importance of both transient and asymptotic behavior of an ecological systems near their equilibrium when subject to an initial perturbation [80, 81, 82, 75]. Near a stable fixed point, a nonlinear dynamical system can be linearized to the following system of ordinary differential equations

$$\frac{d\vec{y}}{dt} = \boldsymbol{A}\,\vec{y}, \tag{5.1}$$

where the so called *community matrix* $\boldsymbol{A}$ has eigenvalues with negative real parts. It is straightforward to show that asymptotically, $\vec{y}$ decays with the time scale set by the real part of the largest eigenvalue λ_1 of $\boldsymbol{A}$, since all of the other eigenmodes decay faster (see Appendix B.2). It can also be shown that if $\boldsymbol{A}$ has a complete set of orthogonal eigenvectors, the same time scale sets an upper bound for the exponential decay of $\vec{y}$ (see Appendix B.1). However, for a nonnormal matrix $\boldsymbol{A}$, in short time, not only the norm of $\vec{y}$ could decay slower than this time scale, it may transiently grow, despite the fact that all the component of $\vec{y}$ along the eigenvectors of $\boldsymbol{A}$ exponentially decay. This is possible because of the fact that the transformation that gives the component of vector $\vec{y}$ in the eigenbasis of $\vec{A}$ is not unitary if the eigenvectors of $\boldsymbol{A}$ are not orthogonal, and does not preserve the norm of $\vec{y}$. We will see an intuitive explanation of this phenomenon in Section 5.4.

The rate of change of norm of $\vec{y}$ (*i.e.* $\|\vec{y}\| = \sqrt{\vec{y}^{\mathsf{T}}\vec{y}}$) is bound by the largest eigenvalue of the hermitian part, $\boldsymbol{H}$, of the matrix $\boldsymbol{A}$ defined as $\boldsymbol{H} = 1/2(\boldsymbol{A} + \boldsymbol{A}^{\mathsf{T}})$. If this eigenvalue is positive, for some initial conditions, $\|\vec{y}\|$ transiently grows. In this case, the matrix $\boldsymbol{A}$ is

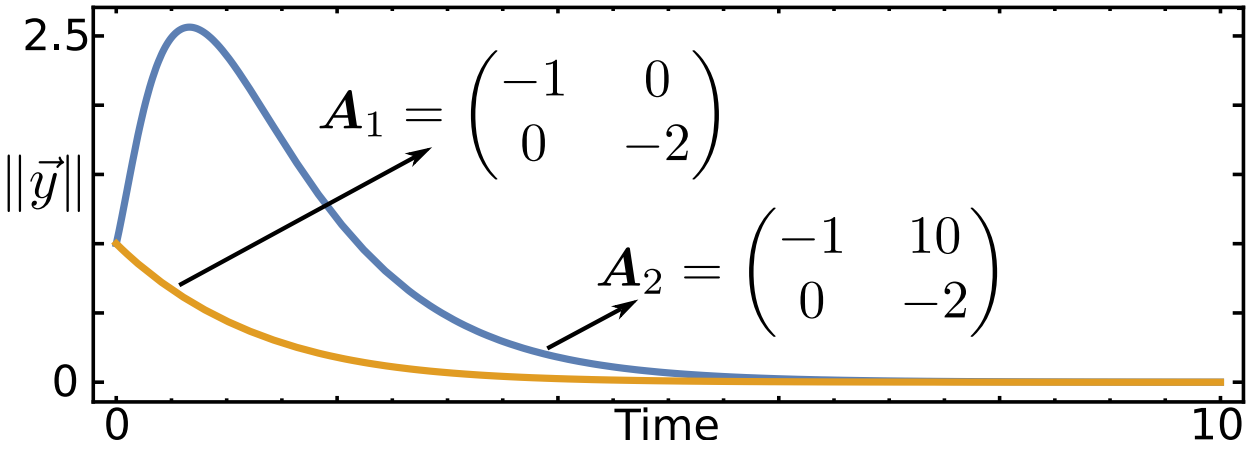

Figure 5.1: Stable linear systems can amplify perturbations. Dynamics of the Euclidean norm $\|\vec{y}\|$ obtained by solving $\dot{\vec{y}} = \boldsymbol{A}_i \vec{y}$. Reactive systems exhibit transient amplification before relaxing to fixed point (blue lines), in contrast with conventional response of stable systems (yellow lines). Matrices $\boldsymbol{A}_1$ and $\boldsymbol{A}_2$ have same eigenvalues [75].

called reactive, and the largest eigenvalue of $\boldsymbol{H}$ is called the *reactivity* of $\boldsymbol{A}$ [75]. The operator norm of the time evolution operator $\exp(\boldsymbol{A}t)$ is also used as upper bound for $\|\vec{y}(t)\| \,/\, \|\vec{y}(0)\|$ and is called the *amplification envelope*. The maximum of the amplification envelope and the time t_{max} at which it occurs are also used as alternative measures of reactivity [75] (see Appendix B.2 for more details).

5.2 Steady State Amplitude in Stochastic Dynamics Near Equilibrium

Consider the real-valued linear stochastic differential equation for an m-component state vector $\vec{y}$

$$\dot{\vec{y}} = \boldsymbol{A}\,\vec{y} + \sigma\,\vec{\eta}(t), \tag{5.2}$$

where η_i, $i = 1, \ldots, m$, the components of $\vec{\eta}$, are independent zero mean Gaussian white noises with unit variance, and the eigenvalues of the model-dependent matrix $\boldsymbol{A}$ have negative real parts. Therefore, the fixed point $\vec{y}_0 = 0$ is stable. The coefficient σ represents the strength of the fluctuations and scales with $\Omega^{-1/2}$ in the case of demographic noise. For sim-

plicity, the noise is chosen to be diagonal, however, partial results for non-diagonal noise are presented in Appendices A.5, A.6, and A.7. Equation (5.2) is the prototypical linearization of stochastic dynamics near a stable fixed point.

The condition of detailed balance corresponds to matrix $\boldsymbol{A}$ being symmetric (*i.e.* $\boldsymbol{A} = \boldsymbol{A}^{\mathsf{T}}$). When this condition is satisfied, $\vec{y}_0 = 0$ is an equilibrium point, and the driving force $\boldsymbol{A}\vec{y}$ can be written as the gradient of the potential $U = 1/2\,\vec{y}^{\,\mathsf{T}}\boldsymbol{A}\,\vec{y}$. The equilibrium probability density of $\vec{y}$ is given by the Boltzmann factor

$$P(\vec{y}) = \mathcal{Z}\exp\left(\frac{\vec{y}^{\,\mathsf{T}}\boldsymbol{A}\,\vec{y}}{\sigma^2}\right), \tag{5.3}$$

where the normalization constant $\mathcal{Z}$ is given by

$$\mathcal{Z} = \sqrt{\det\left(-\frac{\boldsymbol{A}}{\pi\sigma^2}\right)}. \tag{5.4}$$

Under the influence of the stochastic noise, the system maintains an average distant form the equilibrium point. The mean square value of this distant is given by

$$\left\langle \|\vec{y}\|^2 \right\rangle = \int P(\vec{y})\,\|\vec{y}\|^2\,d\vec{y} = -\frac{1}{2}\sigma^2\mathrm{Tr}\left(\boldsymbol{A}^{-1}\right) \leq \frac{m}{2}\sigma^2\tau, \tag{5.5}$$

where $\tau = -\lambda_1^{-1}$ is the time scale set by largest eigenvalue of $\boldsymbol{A}$. Alternatively, we could find this upper bound through the following heuristic argument: Since all the eigenvalues of $\boldsymbol{A}$ are negative, under the deterministic part of Eq. (5.2), all the components of $\vec{y}$ along the eigenvectors of $\boldsymbol{A}$ decay exponentially to zero with decay time scales $\tau_i = \lambda_i^{-1}$, where λ_i are the associated eigenvalues. An upper bound for the norm of $\vec{y}$ could be found by replacing all the eigenvalues by $\lambda = max\{\lambda_i\}$. Therefore, the norm of $\vec{y}_u$ obeying

$$\frac{d\vec{y}_u}{dt} = \lambda\,\vec{y}_u + \sigma\,\vec{\eta}(t), \tag{5.6}$$

should provide an upper bound for $\|\vec{y}\|$. The mean square norm of $\vec{y}_u$ for Eq. (5.6) is given

by

$$\left\langle \|\vec{y}_u\|^2 \right\rangle = \left\langle \left\| \int_0^{\tau/2} \vec{\eta}(t) dt \right\|^2 \right\rangle = \frac{m}{2} \tau \sigma^2. \tag{5.7}$$

Although, the exact amplitude calculated in Eq. (5.3) obviously depends on Eq. (5.2) having a potential solution and is only applicable to a symmetric $\boldsymbol{A}$, one could naively think that the heuristic argument above should hold for a nonsymmetric $\boldsymbol{A}$ as well. In this chapter, we show that this upper bound is only valid when the matrix $\boldsymbol{A}$ is normal, *i.e.* it has an orthogonal set of eigenvectors, since for a nonnormal $\boldsymbol{A}$ (when the fixed point $\vec{y}_0$ is a nonequilibrium steady state violating detailed balance), the argument that $\|\vec{y}\|$ decays at least as fast as the slowest eigenvalue does not hold. As a result, we can show that this transient effect in the deterministic part of Eq. (5.2) has a lasting effect on the steady state amplitude of the stochastic dynamics [78]. This can be demonstrated by solving the steady state probability density of $\vec{y}$ for Eq. (5.2).

5.3 Nonnormal Stochastic Dynamics Near a Nonequilibrium Steady State

If $\boldsymbol{A}$ is nonnormal, Eq. (5.2) does not satisfy detailed balance. This indicates that the fixed point $\vec{y}_0 = 0$ is a nonequilibrium steady state. In this case there does not exist a potential function whose gradient is given by driving force $\boldsymbol{A}\,\vec{y}$. Therefore, the steady state solution to the corresponding Fokker-Planck equation is not given by Boltzmann factor. The steady state solution to a more general form of Eq. (5.2) can be found in Appendix A.5. Here, I present the final results in terms of what I call the *hermitianizer* of $\boldsymbol{A}$: the unique matrix $\boldsymbol{G}$ such that its product with $\boldsymbol{A}$ is a hermitian matrix, and the hermitian part of its inverse is the identity,

$$\begin{aligned} &\frac{1}{2}\left(\boldsymbol{G}^{-1} + \left(\boldsymbol{G}^{-1}\right)^{\mathsf{T}}\right) = \mathbb{1} \\ &(\boldsymbol{G}\boldsymbol{A})^{\mathsf{T}} = \boldsymbol{G}\boldsymbol{A}. \end{aligned} \tag{5.8}$$

Note that $\boldsymbol{G}$ is the identity matrix if $\boldsymbol{A}$ is hermitian, and its deviation from identity measures how far $\boldsymbol{A}$ is from being hermitian. In terms of this matrix $\boldsymbol{G}$, the steady state probability density of $\vec{y}$ can be written as

$$P\left(\vec{y}\right) = \mathcal{N} \exp\left(\frac{\vec{y}^{\,\mathsf{T}} \boldsymbol{G} \boldsymbol{A} \vec{y}}{\sigma^2}\right), \tag{5.9}$$

where the normalization constant $\mathcal{N}$ is given by

$$\mathcal{N} = \sqrt{\det\left(-\frac{\boldsymbol{G}\boldsymbol{A}}{\pi\sigma^2}\right)} \tag{5.10}$$

Note that, even though it looks like that $1/2\,\vec{y}^{\,\mathsf{T}} \boldsymbol{G} \boldsymbol{A} \vec{y}$ is a potential function, the statistics of the approach to steady state is different in the system described by Eq. (5.2) compared to a system defined by the potential $1/2\,\vec{y}^{\,\mathsf{T}} \boldsymbol{G} \boldsymbol{A} \vec{y}$.

5.4 Steady State Amplification and New Measure of Nonnormality

Given the steady state probability density of $\vec{y}$ from Eq. (5.9), we can evaluate the mean square value of $\|\vec{y}\|$ (see Appendix A.6 for the derivations):

$$\left\langle \|\vec{y}\|^2 \right\rangle = -\frac{\sigma^2}{2} \mathrm{Tr}\left(\boldsymbol{G}^{-1} \boldsymbol{A}^{-1}\right). \tag{5.11}$$

For a hermitian matrix $\boldsymbol{A}$, $\boldsymbol{G}$ is the identity (recovering Eq. (5.3)), and the right hand side of Eq. (5.11) would depend only on the eigenvalues of $\boldsymbol{A}$ and the strength of the noise σ^2 (not the eigenvectors). Therefore, to measure the effect of nonnormality of the eigenvectors, we can divide Eq. (5.11) for a nonnormal matrix $\boldsymbol{A}$ by the same equation evaluated for a hermitian matrix whose eigenvalues have the same real parts. Thus, we define the nonnormality index $\mathcal{H}$ as

$$\mathcal{H}(\boldsymbol{A}) = \mathrm{Tr}\left(\boldsymbol{G}^{-1} \boldsymbol{A}^{-1}\right) / \mathrm{Tr}\left(\boldsymbol{A}^{-1}\right). \tag{5.12}$$

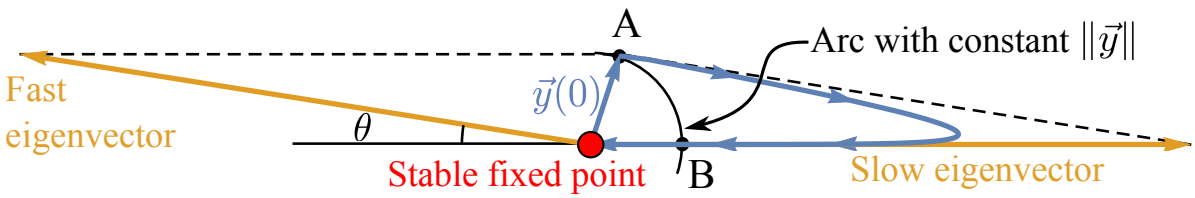

Figure 5.2: Reactivity is caused by nonorthogonal eigenvectors and a separation of timescales. The stable fixed point is subject to the perturbation $\vec{y}_0$. Because of the separation of timescales, the deterministic trajectory (blue arrowed line) is initially parallel to the fast eigenvector before relaxing to the slow manifold. From A to B, the trajectory has magnitude greater than $||\vec{y}_0||$, hence the system is reactive.

In terms of $\mathcal{H}$, Eq. (5.11) can be written as

$$\left\langle \|\vec{y}\|^2 \right\rangle = -\frac{\sigma^2}{2}\mathcal{H}(A)\,\mathrm{Tr}\left(\boldsymbol{A}^{-1}\right). \tag{5.13}$$

The nonnormality index $\mathcal{H}$ is always $\mathcal{H} \geq 1$, and the farther $\boldsymbol{A}$ is from normal, the larger is the index $\mathcal{H}$ (compare Eq. (5.13) with Eq. (5.5)). This becomes more clear in two dimensions where Eq. (5.11) simplifies to

$$\left\langle \|\vec{y}\|^2 \right\rangle = -\frac{\sigma^2}{2}\det\left(\boldsymbol{G}^{-1}\right)\mathrm{Tr}\left(\boldsymbol{A}^{-1}\right), \tag{5.14}$$

and therefore, the nonnormality index of $\boldsymbol{A}$ become the inverse determinant of the hermitianizer of $\boldsymbol{A}$. When the eigenvalues are real, we can solve directly for $\det(\boldsymbol{G})$ in term of the eigenvalues of $\boldsymbol{A}$ and the angle θ between its eigenvectors, resulting in the intuitive expression

$$\mathcal{H} = 1 + \cot^2(\theta)\left(\frac{\lambda_1 - \lambda_2}{\lambda_1 + \lambda_2}\right)^2, \tag{5.15}$$

relating the nonnormality index to the separation of time scales, and the non-orthogonality of the eigenvectors.

When the eigenvectors are not orthogonal, $\cot^2(\theta)$ will be greater than zero. In this case, for some initial conditions (*e.g.* the blue vector in Fig. (5.2)), the component along the eigenvectors can be larger than the vector itself. If one of the eigenvalues is much smaller than the other (separation of time scales), the component of $\vec{y}$ along the eigenvector associated with the smaller eigenvalue (the vector pointing to the left in Fig. (5.2)) decays quickly, and

as a result, the norm of $\vec{y}$ approaches the length of its other component, causing a transient growth of the vector $\vec{y}$, before decaying with rate associated with the larger eigenvector. It is clear from this simple geometric picture that the separation of time scales, and the non-orthogonality of the eigenvectors are requirements for the transient growth that leads to a steady state amplification of $\|\vec{y}\|$.

There are several other measures of nonnormality used in literature, such as the largest eigenvalue of the hermitian part of $\boldsymbol{A}$ and the operator norm of the time evolution operator $||\exp(\boldsymbol{A}t)||$ [75]. Although they all beautifully capture various aspects of the effect of nonnormality on the transient dynamics, in the context of stochastic dynamics, the non-normality index from Eq. (5.12) is the natural measure for this effect on steady state, as it directly measures the amplification of the steady state magnitude compared to a normal dynamical system with the same eigenvalues.

Chapter 6

Nonnormality and Spatial Patterns in Reaction Diffusion Equations

In the past decade, there has been an ever increasing attention to demographic fluctuations in gene expressions, populations biology, and ecology [83, 84]. While one of the most fundamental problems in ecology and developmental biology, *i.e.* the emergence of spatial and temporal patterns from homogeneity, has recently been linked to demographic fluctuations [85, 86], as it resolves the fine tunning problem [87, 88, 89] of Turing mechanism [90]. However, the amplitude of the fluctuation-induced patterns far from the fine tune parameter regime as estimated by current mathematical techniques [2] is expected to be small, casting a shadow on the prospect of ever observing spatially extended patterns due to demographic fluctuations. I show that the current mathematical analyses miss an important amplifying effect due to nonnormality that is a built-in feature of these pattern-forming systems. In this chapter, I will show that stochastic patterns are in fact observable and likely to be ubiquitous in systems characterized by demographic stochasticity.

Since the seminal paper of Turing [90], it has been thought that diffusion instabilities may underlie various cases of biological pattern formation [91]. The Turing mechanism, which I will describe in detail in Section 6.1, shows that diffusion, which is typically thought of as a process that stabilize the uniform solution, can indeed destabilize it in some reaction diffusion systems. These systems typically consist of activator-inhibitor reactions with diffusion constants of widely different magnitude [92]. This latter condition has not been found in experimental observations [93, 94], and has led to the conclusion that Turing-like patterns are not widespread [95].

Recently, it was noted that reaction diffusion systems subject to demographic noise can

also exhibit spatial patterns very similar to Turing patterns. They are known as stochastic Turing patterns and have constraints on the diffusions constant that are much weaker than the requirement for Turing patterns [85, 86, 96, 3, 97, 98]. I will review the mechanism underlaying these stochastic patterns in Section 6.2.

Stochastic Turing patterns can exist over a wide range of parameter values, even where the diffusion constants of activator and inhibitor are of similar magnitudes. Yet, unlike deterministic patterns, the amplitude of stochastic pattern scales as $\Omega^{-1/2}$ (where Ω is the correlated system size), meaning that in large populations, these patterns might be very small [85], and are expected to be smaller the farther the system from the parameter regime of deterministic Turing patterns. Therefore, it remains unclear whether stochastic patterns are a sound paradigm for biological and ecological pattern formation.

In Section 6.3, I show that all stochastic Turing patterns are far from normal, and therefore, their amplitudes are significantly larger than the upper bound expected from the eigenvalue analysis. The effect of this nonnormality is persistent at steady state due to the presence of noise, and the methods developed in Chapter 5 are applicable for the analysis of this amplification. I conclude that the mechanism underlying the observed pattern formation in many of biological systems is that of the reactive stochastic patterns, since they have large amplitudes and do not require an unphysically large separation of diffusion constants.

6.1 Deterministic Turing Patterns

The Turing mechanism in simplest form, consist of a system of two species, an activator and an inhibitor that react and diffuse with different diffusion constants. The *activator* is a species that catalyzes the production of itself and the other species, while the *inhibitor* inhibits the production of itself and the activator. In the context of predator-prey models in ecology, the activators are the prey that self-replicate and feed the predators, while predators that compete and prey on the prey are the inhibitors. In the absence of diffusion, such

systems typically reach a steady state solution with the coexistence of both activator and inhibitor species at certain densities.

My first intuition would say that in the spatially extended case with diffusion, the uniform solution with the well-mixed steady state densities should be a stable solution, since both the reaction kinetics and the diffusion process would suppress inhomogeneous deviations from the steady state value. However, Turing showed that if the inhibitor (the predator) diffuses much faster than the activator (the prey), a subtle interplay between the different rates of diffusion and the activation inhibition reactions can cause stable spatial inhomogeneities with well-define length scales.

The inhomogeneities in Turing patterns consist of localized areas with both densities of activator and inhibitor higher than the well-mixed steady state. Since the well-mixed steady state is stable, the high concentration of inhibitor should reduce the total density, but the inhibitor diffuses much faster and quickly leaves the high concentration area keeping the ratio of inhibitor to activator bellow the well-mixed steady state. This shortage of inhibitors is responsible for maintaining the high local density. But where would the inhibitors go? As inhibitors leave the high density area, they enter the low density area where the densities of both species are bellow their steady-state well-mixed values. Since the density of the activator is low in these regions, a significant portion of the local population would be migrants that are produced in high density areas. The inhibitors migrate faster, and therefore, the ratio of the inhibitor to activator in these regions is higher than the well-mixed. This excess density of inhibitor is what maintains the low density in these regions.

In summary, the high density spots are sources where most of both species are produced. The activators are slower and stay in the spots, while the inhibitors leave and keep the density of the surrounding area low. This mechanism highlights the out of equilibrium aspect of activator-inhibitor systems by separating the source and the sink locally in space. This nonequilibrium aspect, as mentioned in Chapter 5, hints at the possibility of nonnormal dynamics which we will see in Section 6.3. Before going there, we need to understand a more general form of the above dynamics in a quantitative sense and be able to predict the regime

of parameters of such spatial instabilities. Consider the reaction diffusion equation of the form

$$\frac{\partial \vec{q}}{\partial t} = \vec{f}(\vec{q}) + \boldsymbol{D}\nabla^2\vec{q} \tag{6.1}$$

where the vector field $\vec{q}$ is the state vector, with components q_i representing population densities of species i with diffusion constant D_i, and the diffusion matrix $\boldsymbol{D} = \boldsymbol{diag}(D_1, D_2, \dots)$. The function $\vec{f}(\vec{q})$ determines the interactions of the species. We assume that $\vec{f}(\vec{q})$ has a stable fixed point, *i.e.* there exist $\vec{q}^*$ such that $\vec{f}(\vec{q}^*) = 0$, and all of the eigenvalues of

$$\boldsymbol{J} = \nabla_{\vec{q}} f(\vec{q})|_{\vec{q}^*} \tag{6.2}$$

have negative real parts.

Our goal is to study the stability of the uniform solution $\vec{q}(\vec{x}) = \vec{q}^*$. Equation (6.1) can be linearized around its fixed point $\vec{q}^*$, by defining the deviation from the fixed point

$$\vec{p} = \vec{q} - \vec{q}^* \tag{6.3}$$

and linearizing around the fixed point.

$$\frac{\partial \vec{p}}{\partial t} = \boldsymbol{J}\vec{p} + \boldsymbol{D}\nabla^2\vec{p} \tag{6.4}$$

The Laplacian in Eq. (6.4) can be diagonalized by a Fourier transform, resulting in

$$\frac{d\vec{p}_{\vec{k}}}{dt} = \boldsymbol{K}\vec{p}_{\vec{k}}, \qquad \boldsymbol{K} = \boldsymbol{J} - k^2\boldsymbol{D} \tag{6.5}$$

If the diffusion constants D_i's are all the same, the matrix $\boldsymbol{D}$ becomes a multiple of the identity, and the eigenvalues of $\boldsymbol{K}$ will be the eigenvalues of $\boldsymbol{J}$ shifted by $-k^2D$ for each $\vec{k}$, resulting in a more stable operator, making the homogeneous solution a deterministically stable solution of Eq. (6.1). This is the natural case, when one would expect that the diffusion would favor the uniform solution. However, in the case that the diffusion rates are

sufficiently different, the largest eigenvalue of $\boldsymbol{K}$ can have a non-monotonic behavior as a function of $\vec{k}$, and in some cases have positive eigenvalues for a small range of $\vec{k}$ peaked around some value $\vec{k}_0$ (see Fig. (6.1a)). In this case, in a neighborhood of the homogeneous solution, all the Fourier modes exponentially decay to zero except the modes near $\vec{k}_0$ that can grow so large that the linear approximation is no longer valid. The growth in a localized region of $\vec{k}$-space leads to the formation of patterns known as deterministic Turing patterns [90]. The formation of these Turing patterns is dependent on a large separation of the diffusion constants [92, 93, 94].

6.2 Stochastic Turing Patterns

Turing instabilities rely on the inhibitors having a diffusion constant orders of magnitude larger than the activators, making the observation of Turing patterns in natural systems unlikely [92]. It has been shown, however, that the presence of noise can expand the range of parameters (in particular the ratio of diffusion constants) in which spatial pattens can be observed. Let us review the mechanism for these noise-induced spatial patterns. Consider the stochastic extension of Eq. (6.1)

$$\frac{\partial \vec{q}}{\partial t} = \vec{f}(\vec{q}) + \boldsymbol{D}\nabla^2\vec{q} + \sigma\vec{\xi}(\vec{x},t). \tag{6.6}$$

where ξ_i's, the components of $\vec{\xi}(\vec{x},t)$ are δ-correlated Gaussian white noises with unit variances and zero means. Again, we assume that $\vec{f}(\vec{q})$ has a stable fixed point, *i.e.* there exist $\vec{q}^*$ such that $\vec{f}(\vec{q}^*) = 0$, and all of the eigenvalues of $\boldsymbol{J} = \nabla_{\vec{q}} f(\vec{q})|_{\vec{q}^*}$ have negative real parts.

Our goal is to study the stability of the uniform solution $\vec{q}(\vec{x}) = \vec{q}^*$ in the present noise. Equation (6.6) can be linearized around its fixed point $\vec{q}^*$, by defining the deviation from the fixed point $\vec{p} = \vec{q} - \vec{q}^*$ and linearizing around the fixed point.

$$\frac{\partial \vec{p}}{\partial t} = \boldsymbol{J}\vec{p} + \boldsymbol{D}\nabla^2\vec{p} + \sigma\vec{\xi}(\vec{x},t). \tag{6.7}$$

The Laplacian in Eq. (6.7) can be diagonalized by a Fourier transform, resulting in

$$\frac{d\vec{p}_{\vec{k}}}{dt} = \boldsymbol{K}\vec{p}_{\vec{k}} + \sigma\vec{\xi}(\vec{k},t), \qquad \boldsymbol{K} = \boldsymbol{J} - k^2\boldsymbol{D} \tag{6.8}$$

Obtaining the stochastic extension of Eq. (6.5). In Section 6.1, we saw that for a large separation of diffusion constants, if the real part of the largest eigenvalue of $\boldsymbol{K}$ is positive in a neighborhood of its maximum at $\vec{k} = \vec{k}_0$, deterministic Turing patterns are formed. In contrast, consider an intermediate scenario with diffusion constants different enough so that they can cause a non-monotonic behavior for the largest eigenvalue of $\boldsymbol{K}$ as a function of $\vec{k}$ peaked around some value $\vec{k}_0$, but not enough for the largest eigenvalue to become positive at any $\vec{k}$. In the absence of the noise term, if the largest eigenvalue at $\vec{k}_0$ is close enough to zero, in a neighborhood of the homogeneous state, all the $\vec{k}$ modes decay quickly to zero, while the modes with $\vec{k} \sim \vec{k}_0$ persist longer in the system, causing a transient pattern. In the presence of the noise term $\vec{\xi}(\vec{k},t)$ in Eq. (6.8), while the modes with smaller eigenvalues decay quickly to zero, the slow modes drift away from the fixed points under the influence of the noise. The drift of the $\vec{k}$ modes near $\vec{k}_0$ produces persistent steady-state patterns with well-defined length-scales known as stochastic Turing patterns [85, 86]. See Fig. (6.1b) for an example of λ_1 of $\boldsymbol{K}$ as a function of $k = ||\vec{k}||$ that could lead to stochastic patterns.

Equation (6.8), is the complex variable version of Eq. (5.2), and its steady state amplitude can be calculated through methods similar to those in Chapter 5. The complex extensions of some of the analyses in Chapter 5 are shown in Appendix A.7. The amplitude of such fluctuation-induced pattern is proportional to the amplitude of the noise, σ, which is of the order of inverse square root of the system size, $\Omega^{-1/2}$, in the case of demographic noise. A naive eigenvalue analysis would set an upper bound on the mean amplitude square of the patterns proportional to $\sigma^2\tau$, where τ is the decay time scale associated with the largest eigenvalue of $\boldsymbol{K}$, $\tau = \Re(\lambda_1)^{-1}$. Therefore, for these patterns to be experimentally observed, either the noise has to be very large, or the real part of λ_1 be very close to zero. But, for $\Re(\lambda_1)$ to be very close to zero, the parameters of the problem (in particular the ratio of

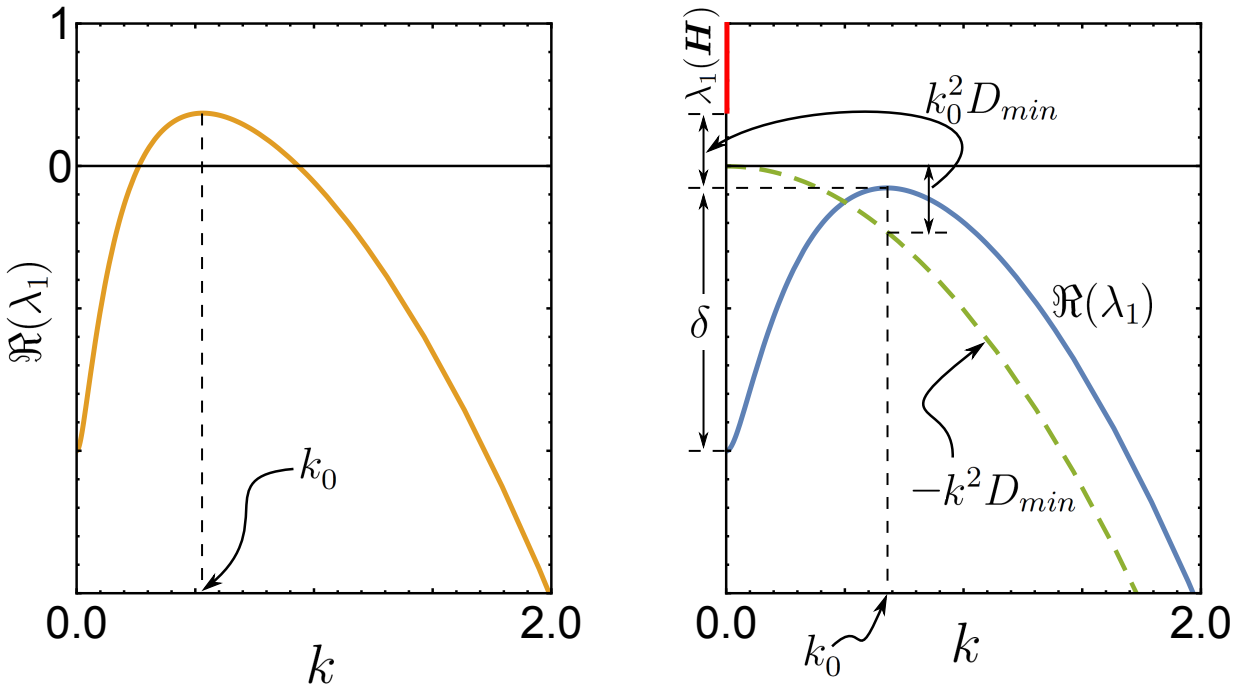

(a) Deterministic Pattern

(b) Stochastic Pattern

Figure 6.1: The real part of the largest eigenvalue, $\Re(\lambda_1)$, of $\boldsymbol{K}$, as a function of the length of the wave vector $k = \left\|\vec{k}\right\|$. (a) The real part of the largest eigenvalue of $\boldsymbol{K}$ is positive in a neighborhood of its peak at $k = k_0$ leading to spatial instabilities known as deterministic Turing patterns. (b) When $\Re(\lambda_1)$ at its peak at some $\vec{k}_0 \neq 0$ is close to zero, but still negative, the $\vec{k}$ modes in the neighborhood of k_0 maintain a larger steady state amplitude in the presence of noise compared to the other Fourier modes giving rise to spatial inhomogeneities known as stochastic Turing patterns

the diffusion constants) have to be very close to the parameter regime of the deterministic Turing patterns (see Fig. (6.1)).

This seems to suggest that we have not solved the problem of observability of Turing patterns, unless, we can show the system is far from normal. In which case, the amplitude of these patterns can be far larger than predicted from the eigenvalue analysis, as shown in Chapter 5. In the next section, I will show that all the pattern forming systems are far from normal. In particular, if a system can theoretically exhibit deterministic Turing patterns for some ratio of diffusion constants, that system is reactive, and can produce large amplitude stochastic Turing patterns at much smaller ratio of diffusion constants.

6.3 Nonnormality and Pattern Formation

In this section, I show that in order for a system described by Eq. (6.6) to produce stochastic patterns, it is necessary for the matrix $\boldsymbol{J}$ in Eq. (6.7) to be far from normal. I will show this by finding a lower bound on the difference between the largest eigenvalue of $\boldsymbol{H} = (\boldsymbol{J}+\boldsymbol{J}^T)/2$ and the real part of the largest eigenvalue of matrix $\boldsymbol{J}$.

The proof relies on the fact that for the system to exhibit stochastic patterns, the real part of the largest eigenvalue, λ_1, of $\boldsymbol{K}$ as a function of the wave vector $\vec{k}$ should have its maximum at some value $\vec{k}_0 \neq 0$ [2, 86], and therefore,

$$\delta = \Re(\lambda_1(\boldsymbol{K}_0)) - \Re(\lambda_1(\boldsymbol{J})) > 0, \tag{6.9}$$

for $\boldsymbol{K}_0 = \boldsymbol{K}(\vec{k}_0)$ (see Fig. (6.1b)). It is a well known fact that the real part of the largest eigenvalue of a matrix is less than or equal to that of its Hermitian part (see Appendix B.2 for a simple proof), therefore,

$$\Re(\lambda_1(\boldsymbol{K}_0)) \leq \lambda_1(\boldsymbol{H} - k_0^2\boldsymbol{D}). \tag{6.10}$$

Since both $\boldsymbol{H}$ and $-k_0^2\boldsymbol{D}$ are Hermitian, by Weyl inequality

$$\lambda_1(\boldsymbol{H} - k_0^2\boldsymbol{D}) \leq \lambda_1(\boldsymbol{H}) + \lambda_1(-k_0^2\boldsymbol{D}) = \lambda_1(\boldsymbol{H}) - k_0^2 D_{min}. \tag{6.11}$$

Adding $k_0^2\, D_{min} - \Re(\lambda_1(\boldsymbol{J}))$ to both sides of this inequality, we have

$$\lambda_1(\boldsymbol{H}) - \Re(\lambda_1(\boldsymbol{J})) \geq \delta + k_0^2 D_{min}. \tag{6.12}$$

Moreover, since the non-normality of $\boldsymbol{J}$ should be independent of the diffusion constants, this lower bound can be extended to the supremum of the right hand side of the inequality (6.12) over all the matrices $\boldsymbol{D}$ that produce spatial patterns and their corresponding $\vec{k}_0$. In particular, if a system is theoretically capable of producing deterministic Turing patterns

for some set of diffusion constants, *i.e.* $\Re(\lambda_1(\boldsymbol{K}_0)) > 0$, δ would be greater than $-\Re(\lambda_1(\boldsymbol{J}))$, and therefore $\boldsymbol{J}$ would be reactive (this special case was previously proven by Neubert et al. [99]). In this case, if experimentally measured values of diffusion constants do not fall within the Turing pattern regime, the system is still reactive and capable of exhibiting amplified stochastic patterns.

6.4 Conclusion

Deterministic Turing patterns suffer from their dependence on extremely large separation of the diffusion constant. Stochastic Turing patterns in nonreactive systems have amplitudes of order Eq. (5.7) and are unlikely to be experimentally observed. We argue that the observation of spatial order in reaction diffusion systems based on Turing mechanism is only possible in the case of stochastic Turing patterns with large reactivity. It is important to note that reactivity in a pattern forming system is not unexpected. We have shown that all stochastic pattern forming systems are far from normal. Neubert et al. have shown that reactivity is a necessary, but not sufficient condition for the formation of deterministic Turing patterns [99]. This implies that as we move in the parameter space of the problem out of the deterministic Turing pattern regime and enter the stochastic Turing pattern regime, the system is still reactive for all range of parameters in the stochastic regime. In other word, every system that is capable of producing deterministic patterns for some ratio of diffusion constants, will produce reactive stochastic Turing patterns for smaller ratios of diffusion constants.

In Chapter 7, we will study the patterns that emerge in the stochastic extension of a model whose deterministic behavior was previously examined by Ridolfi et al. [3], and show that the range of parameters in which the system exhibits steady state patterns is drastically expanded by the demographic noise, and the amplification of the stochastic patterns due to nonnormality makes it possible to observe these patterns far form the regime of deterministic pattern.

Chapter 7

Reactive Stochastic Patterns in an Activator-Inhibitor Model

In this chapter, we study the patterns that emerge in the stochastic extension of a model whose deterministic behavior was previously examined by Ridolfi et al. [3], and show that (1) the range of parameters in which the system exhibits steady state patterns is drastically expanded by the demographic noise, and (2) the nonnormality amplifies the amplitude of the stochastic patterns by orders of magnitudes.

7.1 Description of the Model

A special case of the deterministic part of Eq. (6.6) was studied by Ridolfi et al. with two species U and V with densities $\vec{q} = (u,\, v)$, and $\vec{f}(u, v)$ define as

$$\vec{f}(u,v) = \begin{pmatrix} u\,(a\,u\,v - e) \\ v\,(b - c\,u^2\,v) \end{pmatrix}, \tag{7.1}$$

where the the constants a, b, c and e are positive It was determined that the deterministic dynamics produces transient patterns [3]. Here, we use an individual level model whose deterministic dynamics is given by Ridolfi's model, and demonstrate that the resulting intrinsic noise induces steady state stochastic patterns that are highly amplified by the nonnormality of Jacobian of $\vec{f}$. This individual level model is defined by the following set of two-species

activator-inhibitor reactions on a discretized D-dimensional space with L^D lattice sites,

$$\begin{aligned} &2U_i + V_i \xrightarrow{a} 3U_i + V_i, \qquad V_i \xrightarrow{b} 2V_i, \\ &U_i \xrightarrow{e} \varnothing, \qquad 2V_i + 2U_i \xrightarrow{c} V_i + 2U_i, \\ &U_i \xrightarrow{\delta_u} U_j, \qquad V_i \xrightarrow{\delta_v} V_j, \qquad j \in \langle i \rangle \end{aligned} \tag{7.2}$$

where U_i and V_i are the species U and V on the site i for $i = 1 \dots L^D$ and $\langle i \rangle$ is the set of sites neighboring i. The state of the system is specified by the concentration vectors $\vec{q}_i \equiv (u_i, v_i) \equiv (U_i, V_i)/\Omega$, where Ω is the volume of each site. The diffusion rates δ_u and δ_v are related to the diffusion constants by $(\delta_u,\, \delta_v) = (D_U,\, D_V)/\Omega^{2/D}$.

For $b > e$, the deterministic dynamics of the well-mixed reactions has a stable fixed point. The stability of the homogeneous state associated with this fixed point in the spatial-extended system can be analyzed by the methods explained in the previous chapter. In the following sections, the discrete-space version of Eqs. (6.6) (6.7) (6.8) are derived by expanding the master equation for the time evolution of the probability of the system being at a density $\vec{q}$. Then, the stability of the homogeneous state is determined by analyzing the behavior of the eigenvalues of $\boldsymbol{K}$ as a function of $\vec{k}$. The audience not interested in the details of the analysis can skip to Section 7.6 were the main results are summarized.

7.2 Master Equation, Fokker-Planck Equation, and Langevin Equation

In this section we derive the stochastic extension of the model by Redolfi et al. [3] by expanding the master equation corresponding to the individual level model defined by reactions (7.2). Each reaction of reaction scheme (7.2) takes the system from a state $\{\vec{q}_i\}$ to $\{\vec{q}_i'\}$ with probability per unit time $T(\{\vec{q}_i'\}|\{\vec{q}_i\})$. These transition rates are given from the

law of mass action:

$$\begin{aligned} T\left(\vec{q}_i + \vec{s}_1 | \, \vec{q}_i\right) &= \Omega a u_i^2 v_i, \quad T\left(\vec{q}_i + \vec{s}_2 | \, \vec{q}_i\right) = \Omega b v_i, \\ T\left(\vec{q}_i - \vec{s}_1 | \, \vec{q}_i\right) &= \Omega e u_i, \quad T\left(\vec{q}_i - \vec{s}_2 | \, \vec{q}_i\right) = \Omega c u_i^2 v_i^2, \end{aligned} \tag{7.3}$$

and for every $j \in \langle i \rangle$

$$\begin{aligned} T\left(\vec{q}_i - \vec{s}_1, \vec{q}_j + \vec{s}_1 | \, \vec{q}_i, \vec{q}_j\right) &= \Omega \delta_u u_i, \\ T\left(\vec{q}_i - \vec{s}_2, \vec{q}_j + \vec{s}_2 | \, \vec{q}_i, \vec{q}_j\right) &= \Omega \delta_v v_i, \end{aligned} \tag{7.4}$$

where

$$\vec{s}_1 = \Omega^{-1} \begin{pmatrix} 1 \\ 0 \end{pmatrix}, \qquad \vec{s}_2 = \Omega^{-1} \begin{pmatrix} 0 \\ 1 \end{pmatrix}. \tag{7.5}$$

The master equation for the time evolution of the probability of finding the system at a state $\{\vec{q}_i\}$, $P(\{\vec{q}_i\}, t)$ can be written as

$$\frac{dP(\{\vec{q}_i\}, t)}{dt} = \sum_{\{\vec{q}_i'\}} \left(T(\{\vec{q}_i\} | \{\vec{q}_i'\}) - T(\{\vec{q}_i'\} | \{\vec{q}_i\}) \right) \tag{7.6}$$

Following [2], we can expand the right hand side of Eq. (7.6) to second order in Ω^{-1} obtaining a Fokker-Planck equation corresponding the following set of stochastic differential equations

$$\begin{aligned} \frac{du_i}{dt} &= u_i(a u_i v_i - e) + \delta_u \sum_{j \in \langle i \rangle} (u_j - u_i) + \xi_i(t), \\ \frac{dv_i}{dt} &= v_i(b - c u_i^2 v_i) + \delta_v \sum_{j \in \langle i \rangle} (v_j - v_i) + \eta_i(t), \end{aligned} \tag{7.7}$$

where ξ_i's and η_i's are zero mean Gaussian noise with correlations

$$\begin{aligned} \langle \xi_i(t) \xi_j(t') \rangle &= \frac{\delta(t - t')}{\Omega} \left(\left(u_i(a u_i v_i + e) + \delta_u \sum_{k \in \langle i \rangle} (u_i + u_k) \right) \delta_{i,j} - \delta_u (u_i + u_j) \chi_{\langle i \rangle}(j) \right) \\ \langle \eta_i(t) \eta_j(t') \rangle &= \frac{\delta(t - t')}{\Omega} \left(\left(v_i(b + c u_i^2 v_i) + \delta_v \sum_{k \in \langle i \rangle} (v_i + v_k) \right) \delta_{i,j} - \delta_v (v_i + v_j) \chi_{\langle i \rangle}(j) \right) \end{aligned} \tag{7.8}$$

and the characteristic function, $\chi_{\langle i \rangle}$, of $\langle i \rangle$ is defined as

$$\chi_{\langle i \rangle}(j) = \begin{cases} 1 & j \in \langle i \rangle \\ 0 & j \notin \langle i \rangle \end{cases}. \tag{7.9}$$

By defining $\vec{f}(\vec{q}) \equiv (f,\ g) \equiv (u(auv - e),\ v(b - cu^2 v))$, $\vec{\xi}_i \equiv (\xi_i,\ \eta_i)$, $\boldsymbol{\delta} \equiv \boldsymbol{diag}(\delta_u,\ \delta_v)$, and $(\Delta\vec{q})_i \equiv \sum_{j \in \langle i \rangle}(\vec{q}_j - \vec{q}_i)$, Eq. (7.7) can be written in the simple form

$$\frac{d\vec{q}_i}{dt} = \vec{f}(\vec{q}_i) + \boldsymbol{\delta}\,(\Delta\vec{q})_i + \vec{\xi}_i(t). \tag{7.10}$$

Equation (7.10) is the discrete space version of Eq. (6.6). Continuous limit can be taken at any point in the following analysis to recover the continuous space stochastic partial differential equations of type analyzed in Chapter 6. We continue with the discrete version where the analytic results can be more readily compared to the simulation.

The deterministic part of our model has a fixed point $\vec{q}^{\,*} \equiv (u^*,\ v^*) = (ba/ce,\ e^2c/a^2b)$, obtained by setting $\vec{f}(\vec{q})$ equal to zero. We can linearize Eq. (7.10) around the fixed point $\vec{q}^{\,*}$, by defining $\vec{p}_i \equiv \big((u_i - u^*)/\sqrt{2u^*e},\ (v_i - v^*)/\sqrt{2v^*b}\big)$ which are the rescaled deviations of $\vec{q}_i$ from $\vec{q}^{\,*}$,

$$\frac{d\vec{p}_i}{dt} = \boldsymbol{J}\vec{p}_i + \boldsymbol{\delta}(\Delta\vec{p})_i + \vec{\xi}_i(t), \tag{7.11}$$

where the linear stability operator $\boldsymbol{J}$ is defined as the Jacobian of the transformed function f at the fixed point $\vec{p} = 0$ is given by

$$\boldsymbol{J} = \begin{pmatrix} e & \frac{b^{\frac{3}{2}}a^{\frac{3}{2}}}{ce} \\ -\frac{2e^2c}{a^{\frac{3}{2}}b^{\frac{1}{2}}} & -b \end{pmatrix} \tag{7.12}$$

Evaluating Eq. (7.8) at $\vec{q}^{\,*}$

$$\begin{aligned} \langle \xi_i(t)\xi_j(t') \rangle &= \frac{\delta(t-t')}{\Omega}\Big(\big(1 + \delta_u n/e\big)\delta_{i,j} - \delta_u \chi_{\langle i \rangle}(j)\Big), \\ \langle \eta_i(t)\eta_j(t') \rangle &= \frac{\delta(t-t')}{\Omega}\Big(\big(1 + \delta_v n/b\big)\delta_{i,j} - \delta_v \chi_{\langle i \rangle}(j)\Big), \end{aligned} \tag{7.13}$$

where $n \equiv |\langle i \rangle|$ is the number of neighbors of each site. Note that for $b > e$, both of the eigenvalues of $\boldsymbol{J}$ have negative real parts, making $\vec{q}^*$ an attractor of the dynamics in the absence of the diffusion.

7.3 Pattern Formation and Stability of the Uniform State

To examine the spatial stability of the uniform solution $\vec{q}_i = \vec{q}^*$ of Eq. (7.10), we need to diagonalize the discrete Laplacian operator Δ in Eq. (7.11) to obtain a discrete-$\vec{k}$ version of Eq. (6.8) whose pattern forming behavior was analyzed in Section 6.2. The discrete Laplacian operators is diagonalized by discrete Fourier transform: we define the discrete Fourier transform for a sequence $\{s_{\vec{n}}\}$ as

$$\tilde{s}_{\vec{k}} \equiv (\mathcal{F}[\{s_{\vec{n}}\}])_{\vec{k}} \equiv \frac{1}{\sqrt{N^D}} \sum_{\vec{n}} \epsilon^{-2\pi \vec{k}.\vec{n}/N} s_{\vec{n}}. \tag{7.14}$$

We drop the tildes on the Fourier variable with the convention that the variables with index k are Fourier variables. Equation (7.11) under this transformation becomes

$$\frac{d\vec{p}_{\vec{k}}}{dt} = \boldsymbol{K}\vec{p}_{\vec{k}} + \vec{\xi}_{\vec{k}}(t), \qquad \boldsymbol{K} = \boldsymbol{J} + \Delta(\vec{k})\boldsymbol{\delta}, \tag{7.15}$$

where $\Delta(\vec{k})$ is the discrete Fourier transform of the discrete Laplacian operator given by

$$\Delta(\vec{k}) \equiv -2 \sum_{l=1}^{D} \big(1 - \cos(2\pi k_l/N)\big) \tag{7.16}$$

and

$$\begin{aligned} \langle \xi_{\vec{k}}(t) \xi^*_{\vec{k}'}(t') \rangle &= \Omega^{-1} \left(1 - e^{-1}\delta_u \Delta(\vec{k})\right) \delta_{\vec{k},\vec{k}'} \delta(t - t'), \\ \langle \eta_{\vec{k}}(t) \eta^*_{\vec{k}'}(t') \rangle &= \Omega^{-1} \left(1 - b^{-1}\delta_v \Delta(\vec{k})\right) \delta_{\vec{k},\vec{k}'} \delta(t - t'). \end{aligned} \tag{7.17}$$

For the regime that we observe stochastic patterns, the contribution of the diffusion

process in the amplitude of the noise in Eq. (7.17) is very small and will be neglected for simplicity. This approximation is not necessary, since there is always a change of variables that simplifies the correlation matrix to a multiple of the identity matrix (this is the reason for the rescaling in the definition of $\vec{p}$). With this approximation

$$\left\langle \vec{\xi}_{\vec{k}}(t)\vec{\xi}^{\dagger}_{\vec{k}'}(t')\right\rangle = \Omega^{-1}\delta_{\vec{k},\vec{k}'}\delta(t-t')\,\mathbb{1} \tag{7.18}$$

where $\vec{\xi}^{\dagger}_{\vec{k}'}$ is the conjugate transpose of $\vec{\xi}_{\vec{k}'}$, and $\mathbb{1}$ is the 2×2 identity matrix. Equation (7.15) is of the form Eq. (7.11) and its pattern forming behavior is determined by the eigenvalues of $\boldsymbol{K}$ as explained in Chapter 6.

7.4 Phase Diagram

The pattern forming behavior of the model defined by reactions (7.2) can be understood by analyzing the eigenvalues of $\boldsymbol{K}$ as a function of $\vec{k}$. Matrix $\boldsymbol{K}$ can be written in elements from Eq. (7.15) and Eq. (7.12):

$$\boldsymbol{K} = \begin{pmatrix} e+\Delta(\vec{k})\delta_u & \frac{b^{\frac{3}{2}}a^{\frac{3}{2}}}{ce} \\ -\frac{2e^2c}{a^{\frac{3}{2}}b^{\frac{1}{2}}} & -b+\Delta(\vec{k})\delta_v \end{pmatrix} \tag{7.19}$$

As it will become clear, most of the properties of the system depend on the following three parameters

$$\rho = \frac{b}{e}, \qquad \nu = \frac{e\,c}{a^{\frac{3}{2}}b^{\frac{1}{2}}}, \qquad r = \frac{\delta_v}{\delta_u} = \frac{D_V}{D_U}. \tag{7.20}$$

In the following analysis, I rewrite various expression in terms of these parameters, wherever possible. We start with $\boldsymbol{K}$

$$\boldsymbol{K} = \begin{pmatrix} e+\Delta(\vec{k})\delta_u & b/\nu \\ -2e\,\nu & -b+\Delta(\vec{k})\delta_v \end{pmatrix} \tag{7.21}$$

The largest eigenvalue of $\boldsymbol{K}$ is given by

$$\lambda(\vec{k}) = \frac{1}{2}\left(\sqrt{b^2 - 2b\Delta(\vec{k})(\delta_v - \delta_u) - 6be + \left(e - \Delta(\vec{k})(\delta_v - \delta_u)\right)^2} - b + \Delta(\vec{k})(\delta_v + \delta_u) - e\right). \tag{7.22}$$

Notice that the eigenvalues of $\boldsymbol{K}$ are independent of ν. For small $\vec{k}$, $\Delta(\vec{k})$ is a monotonically decreasing function of $\vec{k}$ (proportional to $-k^2$). We define $y = -\Delta(\vec{k})$. To determine if λ monotonically decays or if it has a maximum at some $\vec{k}_0 \neq 0$, we can differentiate λ with respect to y and see if it has a positive root. The largest root of $\frac{d\lambda}{dy}$ is given by

$$y_0 = -\Delta(\vec{k}_0) = \frac{(r+1)\sqrt{2\,b\,e\,r} - b\,r - e\,r}{\delta_u\,(r-1)\,r}. \tag{7.23}$$

For y_0 to be greater than zero we need

$$\rho < \frac{\left(1 + r + r^2 + (r+1)\sqrt{r^2+1}\right)}{r}. \tag{7.24}$$

We can find the condition on the ratio of the diffusion constants by inverting this inequality:

$$r > \frac{1 - 2\,\rho + \rho^2 + (1+\rho)\sqrt{1 + \rho\,(\rho - 6)}}{4\,\rho} = f_1(\rho). \tag{7.25}$$

The condition for formation of stochastic pattern is $\lambda(\vec{k}_0) > \Re(\lambda(0))$. We can find $\lambda(\vec{k}_0)$ and $\lambda(0)$ by substituting $y_0 = y(\vec{k}_0)$ from Eq. (7.23) and $y(0) = 0$ in Eq. (7.22):

$$\lambda(\vec{k}_0) = \frac{b + e\,r - \sqrt{8\,b\,e\,r}}{r-1}, \qquad \lambda(0) = \frac{1}{2}\left(\sqrt{b^2 - 6\,b\,e + e^2} - b + e\right). \tag{7.26}$$

Then, $\lambda(\vec{k}_0) > \Re(\lambda(0))$ simplifies to

$$r > \frac{-1 + 14\,\rho - \rho^2 + 4\sqrt{-2\,\rho\,(1 + \rho\,(\rho - 6))}}{(1+\rho)^2} = f_2(\rho). \tag{7.27}$$

The condition for a deterministic Turing pattern is a lot simpler; we just need $\lambda(\vec{k}_0) > 0$

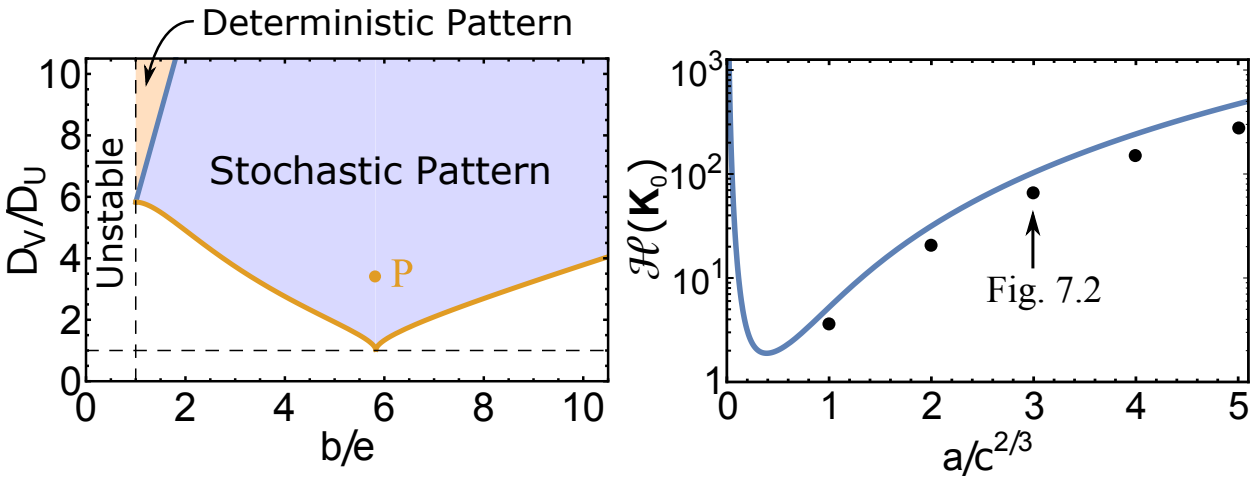

Figure 7.1: **Stochasticity expands the parameter regime of pattern formation**. (left) Phase diagram of model defined by reactions (7.2) showing that the pattern forming behavior of this model depends only on the ratios b/a and D_V/D_U. (right) Semi-log plot of nonnormality index for the point P as a function of $a/c^{2/3}$. Black markers are amplifications measured in simulation.

which simplifies to

$$r > \left(3 + 2\sqrt{2}\right)\rho = f_3(\rho). \tag{7.28}$$

When r is greater than $f_1(\rho)$ and $f_2(\rho)$ but less than $f_3(\rho)$, the system exhibits stochastic patterns (blue region in Fig. (7.1)-left), while we observe the deterministic patterns when r is greater than f_3 (orange region of Fig. (7.1)-left).

7.5 Nonnormality

The amplification of our stochastic patterns depend on the nonnormality index of $\boldsymbol{K}_0 = \boldsymbol{K}(\vec{k}_0)$ given by

$$\boldsymbol{K}_0 = \begin{pmatrix} e - y_0\,\delta_u & b/\nu \\ -2\,e\,\nu & -b - y_0\,\delta_v \end{pmatrix}, \tag{7.29}$$

where $y_0 = -\Delta(\vec{k}_0)$. The nonnormality index of 2×2 matrices is calculated explicitly in Appendix B.3. We use Eq. (B.14) to calculate the nonnormality index of $\boldsymbol{K}_0$:

$$\mathcal{H}(\boldsymbol{K}_0) = 1 + \left(\frac{b + 2e\nu^2}{\nu(b - e + y_0\,(\delta_u + \delta_v))}\right)^2. \tag{7.30}$$

We substitute y_0 from Eq. (7.23) and rewrite the resulting expression in terms of ρ, r, and ν:

$$\mathcal{H}(\boldsymbol{K}_0) = 1 + \left(\frac{2\nu^2 + \rho}{\nu \left(\rho - 1 + \frac{(r+1)\left(-\rho r + (r+1)\sqrt{2\rho r} - r\right)}{(r-1)r} \right)} \right)^2 \tag{7.31}$$

Since the eigenvalues of $\boldsymbol{K}$ do not depend on ν, one can change $\mathcal{H}(\boldsymbol{K}_0)$ by changing ν without moving the system in its phase diagram (see Fig. (7.1)-right). This can be done by changing the ratio of $a/c^{2/3}$ without affecting ρ.

7.6 Summary

The pattern forming behavior of the model described by reaction (7.2) only depends on the ratio of the diffusion constants D_V/D_U and the ratio of the reaction rates of the two linear reactions b/e. Figure (7.1)-left shows the regime of parameters in which the system exhibits either stochastic or deterministic Turing patterns. As expected, deterministic patterns emerge only when the ratio D_V/D_U of diffusion constants is very large (above the blue line in Fig. (7.1) which steeply grows outside of the figure), while the requirement on this ratio for the stochastic patterns is drastically reduced (see the Section 7.4 for analytic expressions for the boundaries). In the absence of the nonnormality effect, one would expect that only stochastic patterns with the parameters very close to the deterministic regime would be observed, since far from this regime, the amplitude of the patterns would be too small to detect.

However, since for all $b/e > 1$, there is a D_V/D_U above which the system exhibits deterministic Turing patterns, $\boldsymbol{J}$ is reactive for all $b/e > 1$. Therefore, even when the system is far from the parameter regime of deterministic patterns, the amplitude of the resulting stochastic pattern is far larger than what one would expect from the analysis of the eigenvalues from Eq. (5.7). We can see this by analyzing the amplitude of the patterns at the point P in Fig. (7.1). This point has the ratios $b/e = 5.8$ and $D_V/D_U = 3.4$ and is chosen to

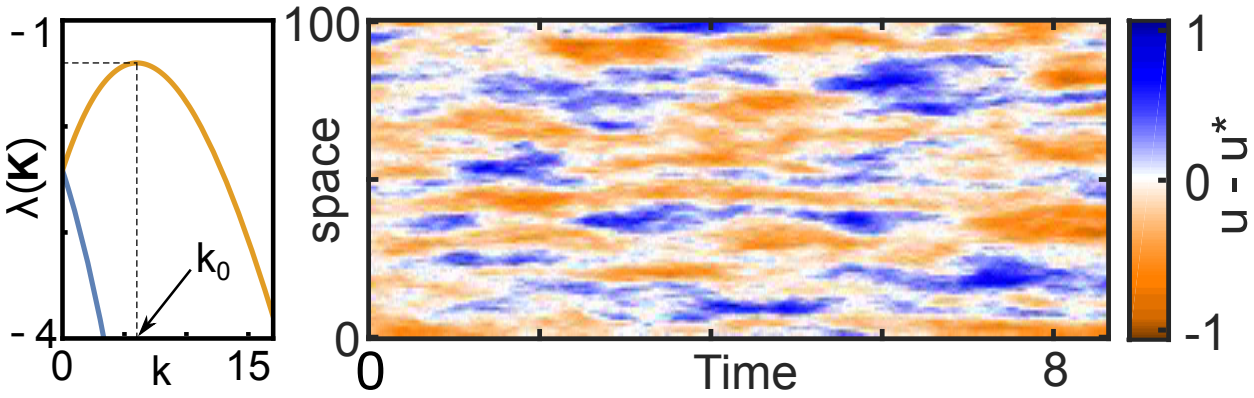

Figure 7.2: **Reactivity amplifies the amplitude of stochastic patterns**. (right) An example of stochastic patterns obtained by Gillespie simulations [60] of the model defined by reactions (7.2) at the point P of Fig. (7.1) showing two orders of magnitude amplification. (left) Eigenvalues of $\boldsymbol{K}$ as a function of k; the largest eigenvalue peaks at $k_0 = 6$. Simulation parameters: $a = 3$, $b = 5.8$, $c = e = 1$, $\delta_u = 3.9$, $\delta_v = 3.4\,\delta_u$, and $\Omega = 10^4$.

be very far from the deterministic Turing pattern regime. At this b/e ratio, the ratio of the diffusion constants has to be at least ten time larger than the chosen value for the system to exhibit deterministic Turing patterns. The amplitude of the patterns as determined by Eq. (5.13) is dependent on the eigenvalues of $\boldsymbol{K}$ (fixed by the choice of the point P) and the nonnormality index $\mathcal{H}(\boldsymbol{K})$ which can be tuned by changing the ratio $a/c^{2/3}$ without changing the point P (see Section 7.5 for the analytic expression). Figure (7.1)-right shows that the amplification of stochastic patterns for the point P varies over orders of magnitude for a small range of $a/c^{2/3}$.

Figure (7.2)-right shows the time series of the amplified stochastic Turing patterns in the concentration of the species U, in a simulation of our model in one dimension. The mean square amplitude of these spatial patterns is about 0.21, while the upper bound for the amplitude of the pattern in the absence of reactivity from Eq. (5.7) is 2.5×10^{-3}. The nonnormality index $\mathcal{H}$ of the slowest Fourier mode $k_0 = 6$ is about 103 justifying the two order of magnitude amplification in the amplitude of the stochastic patterns (see Fig. (7.1)-right).

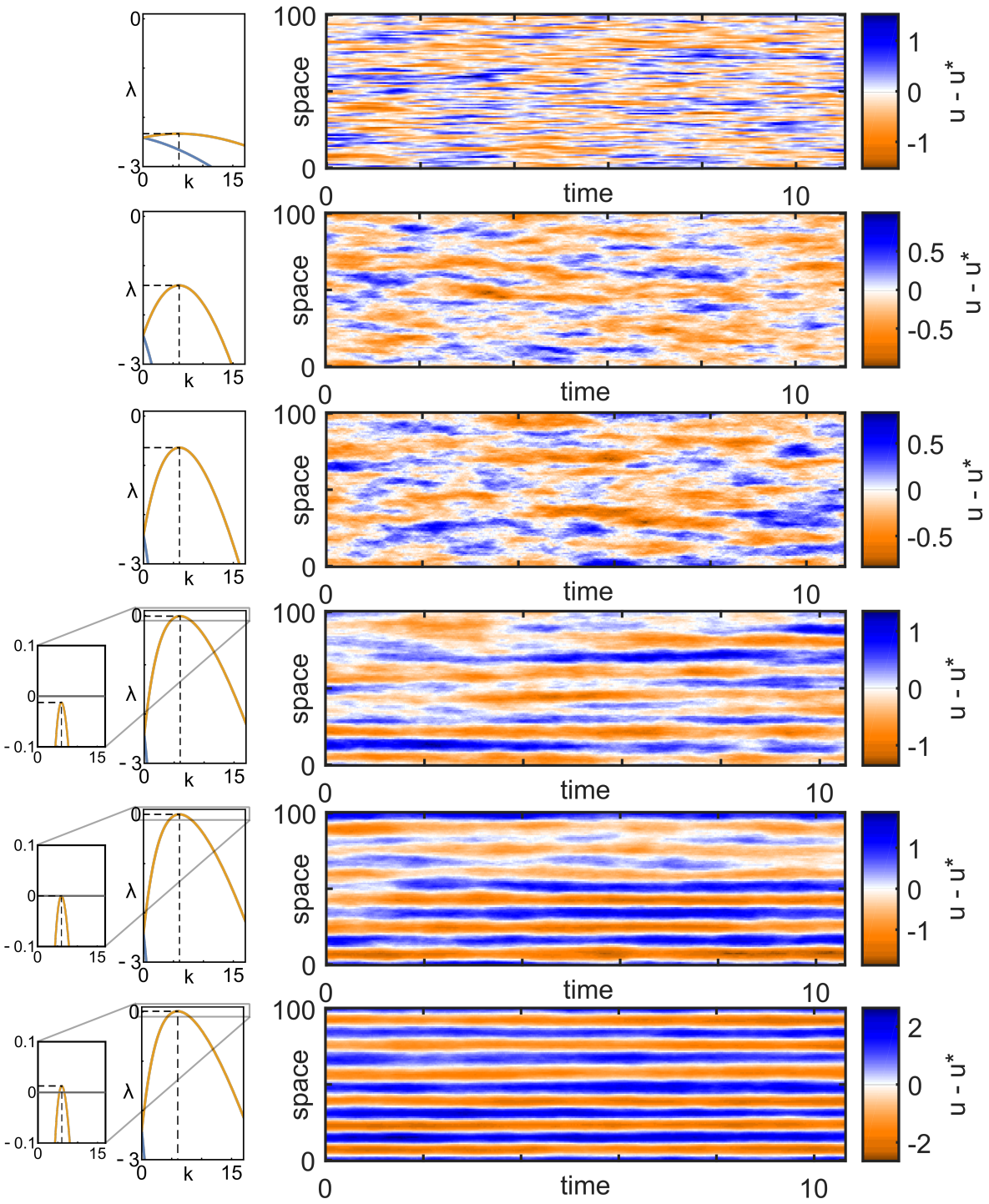

Figure 7.3: The effect of the ratio r of the diffusion constants $r = D_V/D_U$ on the pattern formation of the model defined by reactions (7.2). The Gillespie simulations are run for r values 1.1, 3.4, 10, 33, 34, and 35 (top to bottom). For $r > 34$, the system is in the regime of deterministic Turing patterns, while the values of $1 < r < 34$ are stochastic patterns. Unlike what is expected from the eigenvalue analysis, the amplitude of the patterns is not strongly dependent on how far the system is form the deterministic Turing pattern regime, but the regularity of the patterns is affected by moving away from this regime. Simulation parameters: $a = 3$, $b = 5.8$, $c = e = 1$, and $\Omega = 10^4$.

Part III

Plasticity and Dyson model of 2D Electron Gas

Chapter 8

Velocity Statistics of Edge Dislocations in Plastic Flow

8.1 Introduction

At mesoscopic scales, crystalline materials under stress exhibit intermittent behavior through plastic slip avalanches that follow the power-law statistics predicted by the mean field theory of interface depinning transition [4, 5, 6, 7, 8, 9, 10, 11, 12, 13]. The origin of intermittency in plastic strain rate fluctuations is attributed to the collective dynamics of dissipative structures, such as dislocations, where shear deformation is localized. In addition to the heterogeneous strain response, the long range elastic interactions between dislocations lead to complex spatial-temporal patterning and correlations [100]. Plastic slip avalanches mediated by dislocations have been studied numerically using discrete dislocation dynamics models [5, 101, 102] and phase field crystal models [13].

A point edge dislocation generates in two-dimensions a shear stress that decays as $1/|\vec{r}|$ with a quadrupole anisotropy of the form

$$\tau\left(\vec{r}\right) = b\mu \frac{x\left(x^2 - y^2\right)}{2\pi(1-\nu)(x^2+y^2)^2}, \tag{8.1}$$

where $\vec{r} = (x,\ y)$ is a position vector with respect to the dislocation origin, b is the length of the Burgers vector parallel to the x-direction ($\vec{b} = b\hat{x}$), μ is the shear modulus, and ν is the Poisson ratio [103]. The discrete dislocation dynamics (DDD) model describes a collection of N edge dislocations with pairwise interactions mediated by the internal shear stress τ from Eq. (8.1). Each dislocation performs overdamped motion along the x-direction described

by [104, 5, 101]

$$\frac{\eta}{b}\frac{dx_i}{dt} = b\sum_{j\neq i}\tau(\vec{r}_i - \vec{r}_j), \qquad \forall i = 1, \cdots, N \tag{8.2}$$

where η/b is an effective friction coefficient per unit dislocation length [105]. Most of the DDD simulations are done at zero temperature and focus on the collective effects of dislocations in the presence of an external, uniform stress. Starting from a random configuration, the system relaxes according to Eq. (8.3) towards a frozen metastable configuration. At a non-vanishing external stress below a critical threshold, the relaxation dynamics follows a power-law scaling in time with exponents depending on the physical setup [106, 105]. Above a critical threshold and after a transient power-law relaxation, the system approaches a stress-dependent plateau corresponding to steady-state plastic flow.

Since the velocity of each dislocation is proportional to the stress at the position of the dislocation, in a translationally invariant system, where the probability density of position of dislocations is uniform, the distribution of velocity v of dislocations has the same functional form as the distribution of internal stress. Although the velocity distribution of individual dislocations (or, equivalently, the distribution of internal stress) has not been directly measured, from a theoretical point of view, it is a better defined quantity compared to the distribution of acoustic energy of plastic slip avalanches, as one does not need to deal with the arbitrarily defined thresholds and coarse-graining time scales that show up in the definition of slip events in avalanches. Also, in a discrete dislocation dynamics simulation, as a measure of the statistical properties of the system, the stress distribution can be numerically calculated and analysed more effectively than the pair correlation function [107].

While the local stress fluctuations are known to be power-law distributed, different exponents have been found in the literature depending on the details of the models and methods used in the particular studies. The probability distribution of stress is analytically studied in Ref. [108] for a two-dimensional statistical model, and a power-law scaling τ^{-3} is found for the high stress tail of the stress distribution in equilibrium configurations. A similar power-law, found in the high velocity tail of the velocity distribution in both two and three

dimensions in discrete dislocation dynamics simulation in Ref. [16], is attributed to the avalanche dynamics, and has been shown to be independent of the value of the external stress. However, at intermediate stresses, when a pair of oppositely-oriented dislocations can be approximated by ideal dipoles, the stress distribution has been shown to have the exponent -2 [107]. Reference [5] shows that the $E^{-3/2}$ distribution of the acoustic energy, E, of avalanches that is measured experimentally is associated with the power-law distribution of velocity of dislocations with an exponent -2.5 that is again independent of the value of the external stress. In this study, the presence of avalanches and intermittency of the system was attributed to dislocation pair-creation through Frank-Read sources.

In Refs. [15, 16, 8, 5] discussed above, the robust power-law distributions for the different avalanche variables of the collective dislocation dynamics are attributed to self-organized criticality, while other studies [17, 13, 11, 18] show that in fact the avalanche statistics is a signature of a fine-tuned critical behavior predicted by the mean field depinning transition. Reference [17] derives the density dependence of the critical stress below which the system of dislocations are jammed, and proposes a phase diagram by analogy with the jamming transition in granular materials [109] in which stress and temperature play symmetric roles.

Although the DDD method has been extensively used to investigate plastic flow problems, most studies are based on a deterministic, athermal approach. Hence, the classical DDD model is not suitable for simulating thermally-activated processes, such as dislocation-obstacle interactions. In athermal DDD simulations, the system gets trapped into a metastable configuration, causing unphysical freezing of dislocation motion. Hence, it is challenging to study equilibrium properties of dislocation ensembles in athermal configurations. Instead, we consider a stochastic approach by including in the dislocation motion, given by Eq. (8.3), random stress pulses that mimic, to a first approximation, thermal agitations. Another source of stochasticity in dislocation dynamics is the fluctuating local strain field arising from random dislocation arrangements. This approach has been applied to study the distribution of stress fluctuations [108] and fractal dislocation patterning during plastic deformations [110, 111].

The purpose of this project is to investigate the statistical properties of equilibrium dislo-

cation configurations in the presence of thermal fluctuations. Thermal agitations arise from random collisions of dislocations with surrounding particles, such as phonons, and result in random forces acting on dislocations. The stochastic version of Eq. (8.2) that we consider is given by

$$\frac{\eta}{b}\frac{dx_i}{dt} = b\sum_{j\neq i}\tau(\vec{r}_i - \vec{r}_j) + \xi_i(t), \tag{8.3}$$

where the fluctuations are Gaussian distributed with zero mean and variance

$$\langle \xi_i(t)\xi_j(t')\rangle = \frac{2k_BT\eta}{b^2}\delta_{i,j}\delta(t -' t), \tag{8.4}$$

that depends on the effective temperature k_BT and a damping coefficient consistent with the fluctuation-dissipation theorem. In particular, we study the distribution of velocities of dislocations in a relaxed configuration and show that the corresponding power-law probability distribution function $P(v)$ is not necessarily a collective effect arising from avalanches dynamics, non-equilibrium critical points, or self-organized criticality; rather, it is a consequence of the functional form of the stress in Eq. (8.1) and, in some cases, can be determined only by considering the nearest-neighbor interaction. In other cases, where the collective dynamics of dislocations has a significant effect on $P(v)$, this collective effect can be quantified by considering the deviation of the exponent of the power-law distribution of velocity from the one predicted using only the nearest-neighbor interaction. In section II, we show that Eq. (8.3) in one dimension is the same as the equation of motion for a two-dimensional (2D) Coulomb gas confined in one dimension (1D). This system is sometimes known as Dyson's model, and was first introduced to investigate the statistical properties of energy levels of heavy nuclei [1]. We find the probability distribution of velocity in Dyson's model and show that it follows a temperature dependent power-law distribution which can be predicted simply by considering the nearest-neighbor interaction, and thus is a consequence of the logarithmic interaction energy.

The nearest-neighbor analysis in 2D is performed in section III, where we find a power-law distribution of velocities with an exponent -2 independent of the effective temperature.

We show the presence of a phase transition analogous to the pairing transition in a 1D plasma with logarithmic interaction [112] at a temperature where the effective thermal energy becomes equal to the mutual interaction energy scale $\frac{\mu b^3}{2\pi(1-\nu)}$. Above this temperature, the dislocations are no longer bound to their nearest neighbor in the long time limit. At temperatures well below the transition temperature, we show that the nearest-neighbor approximation is valid, and the probability distribution of velocities of dislocations follows a power-law with the exponent -2, while at temperatures comparable with the transition temperature or above, the exponent of the power-law distribution of velocity deviates from -2, and is thus a presumptive indication of the collective dynamics of dislocations.

8.2 Velocity distribution in Dyson's model

In 1D, Eq. (8.1) for the internal stress simplifies to a $1/r$- force, such that Eq. (8.3) reduces to the stochastic equation of motion for a 2D Coulomb gas confined in 1D, which was first studied by Dyson [1] to investigate the statistics of the energy levels of heavy nuclei. Dyson's model has also been used to model a wide variety of phenomena in nuclear physics and other fields, including random matrix theory [113, 114], the theory of orthogonal polynomials [115, 116], and quantum transport theory [113, 117]. Since a system of Coulomb particles with the same charge (in our case, dislocations with the same Burgers vector) does not have a stable equilibrium, a uniform background of opposite charge is added to the model through a parabolic potential term, keeping the particles from flying off to infinity.

Here we work with a dimensionless spatial variable $\hat{x}$ by rescaling the length in units of the Burgers vector, $x = b\hat{x}$ and define a dimensionless time variable $\hat{t}$ through $t \equiv \hat{t}t_0$ with $t_0 = 2\pi(1-\nu)\eta/(b\mu)$. In these units and dropping the hat symbol over the dimensionless variables, Eq. (8.3) with an additional term $-\kappa x_i$, added to ensure the charge neutrality condition, can be written as:

$$\frac{dx_i}{dt} = \sum_{j \neq i} \frac{1}{x_i - x_j} - \kappa x_i + \xi_i(t), \tag{8.5}$$

which is the same as the equation of motion in Dyson's model [1]. The value of the dimensionless parameter κ is an indication of the strength of the parabolic potential originating from the uniform opposite charge background, and it introduces a new length scale in the problem. We will show that the addition of the parabolic potential does not influence the power-law distribution of the velocity of dislocations, and its only function is to keep the system bounded. The variance of the dimensionless fluctuations is then given by

$$\langle \xi_i(t)\xi_j(t') \rangle = 2\sigma\delta_{ij}\delta(t-t'), \tag{8.6}$$

where $\sigma = 2\pi(1-\nu)k_BT/(\mu b^3)$ which is the ratio between the effective thermal energy and the elastic interaction energy. From Eq. (8.5), the Fokker-Plank equation for the joint probability distribution of the positions of dislocations $\rho(x_1, \cdots, x_N, t)$ follows as

$$\frac{\partial \rho}{\partial t} = \sigma \sum_i \frac{\partial^2 \rho}{\partial x_i^2} - \sum_i \frac{\partial}{\partial x_i}\left[\rho\left(\sum_{j\neq i} \frac{1}{x_i - x_j} - kx_i\right)\right] \tag{8.7}$$

The equilibrium configurational probability distribution is determined from Eq. (8.7) and is given by [1]:

$$\rho(x_1, ..., x_N) \propto \left(\prod_{i<j} |x_i - x_j|^{1/\sigma}\right) \exp\left(-\frac{\kappa}{2\sigma}\sum_i x_i^2\right). \tag{8.8}$$

However, the exact probability distribution of particle velocities in this system is very difficult to determine, due to the nonlinear relationship between the x_i's and the v_i's in Eq. (8.5). Nonetheless, we show that the velocity distribution can be computed analytically in the limit where only the nearest-neighbor interactions are dominant. This is done by solving the system of two particles and comparing with the numerical result for a simulated system of $N = 100$ particles. The strength of the parabolic potential for the two-body system is tuned to give the same average separation between the particles as the one in the simulation.

Let the vector $\vec{x} \equiv (x_1,\ x_2)$ be the position vector of two particles and $\vec{v} \equiv (v_1,\ v_2)$ be the deterministic part of the velocity vector:

$$\vec{v}(\vec{x}) = \left(\frac{1}{x_1 - x_2} - \kappa x_1, \frac{1}{x_2 - x_1} - \kappa x_2\right). \tag{8.9}$$

The joint probability distribution of velocities can be found by the change of variables $\vec{x} \to \vec{v}$ in the probability distribution of positions

$$P(\vec{v}) = \sum_{\vec{x}(\vec{v})} \rho(\vec{x}(\vec{v})) \begin{vmatrix} \frac{\partial x_1}{\partial v_1} & \frac{\partial x_1}{\partial v_2} \\ \frac{\partial x_2}{\partial v_1} & \frac{\partial x_2}{\partial v_2} \end{vmatrix}, \tag{8.10}$$

where the summation is performed over all the positions $\vec{x}$ associated with the same velocity

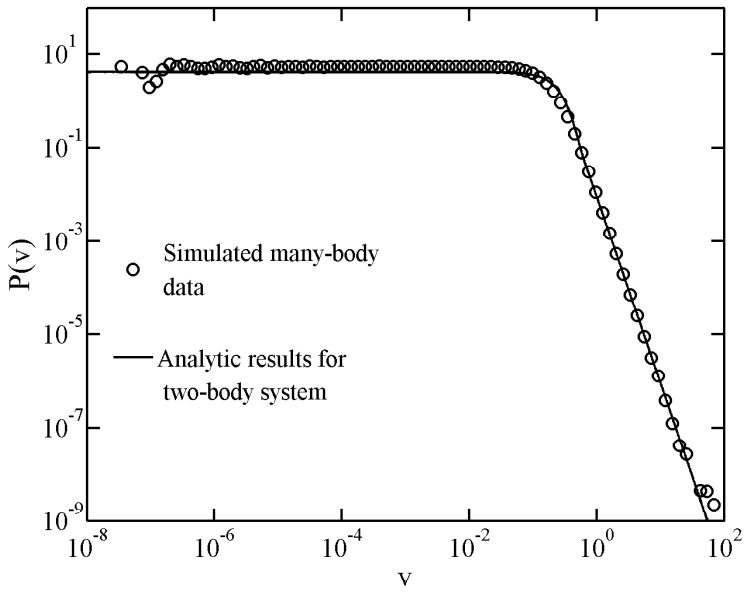

Figure 8.1: Probability distribution of velocity of particles at $\sigma = 1/2$. The solid line is the result of numerical integration of Eq. (8.11) with $\kappa = 0.05$. The circles are the data from the simulation of a system of $N = 100$ particles with $\kappa = 10^{-3}$.

$\vec{v}$ in Eq. (8.9). By inverting Eq. (8.9) and substituting in Eq. (8.8), the joint probability distribution of velocities $P(\vec{v})$ can be written as:

$$P(\vec{v}) = C \exp\left(\frac{w^2}{\kappa\sigma}\right) \sum_{+,-} \frac{1}{\sqrt{u^2+8\kappa}} \left(\mp u + \sqrt{u^2+8\kappa}\right)^{1+\frac{1}{\sigma}} \exp\left(-\frac{u^2 \mp u\sqrt{u^2+8\kappa}}{8\kappa\sigma}\right) \quad (8.11)$$

where $u = v_1 - v_2$ and $w = \frac{1}{2}(v_1+v_2)$ are the relative and center of mass velocities respectively, and C is a normalization constant. Eq. (8.11) can be numerically integrated over either v_1 or v_2 to obtain the probability distribution of velocity. In Fig. (8.1), we compare the result of numerical integration of Eq. (8.11) with the simulation of a system of $N = 100$ particles at $\sigma = \frac{1}{2}$. In order to obtain the same transition velocity (the velocity at which $P(v)$ becomes a power-law), κ was scaled up by a factor of 50 to keep κN constant.

In the high velocity limit (either $v_1 \to \infty$ or $v_2 \to \infty$), Eq. (8.11) scales as:

$$P(\vec{v}) \sim |u|^{-2-1/\sigma} \quad (8.12)$$

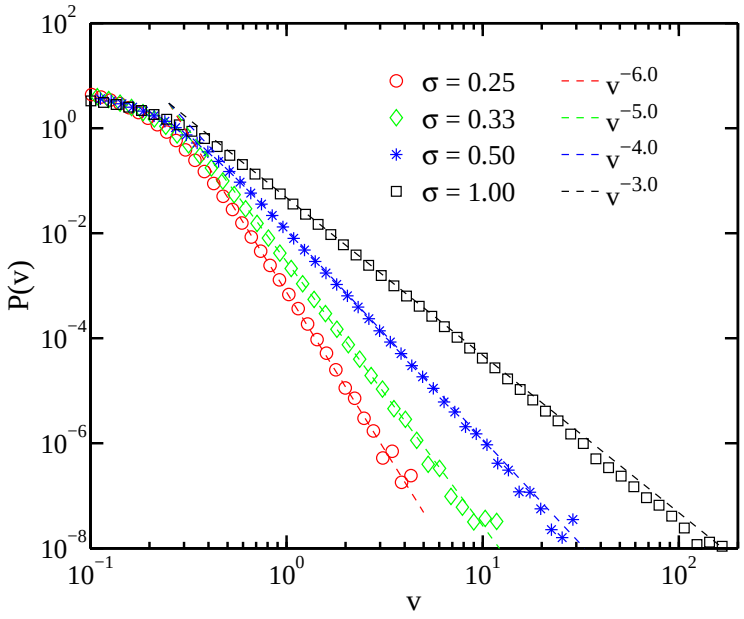

Figure 8.2: (Color online) High velocity tail of probability distribution of velocities for $\sigma \in \{\frac{1}{4}, \frac{1}{3}, \frac{1}{2}, 1\}$ for $N = 100$ particles with $\kappa = 10^{-3}$. The exponent of the power-law distribution agrees with predicted values from Eq. (8.13).

We claim that almost all of the high velocity events result from the pair interaction of two particles that are very close to each other. Therefore, in this limit, v_1 and v_2 would be correlated ($v_1 \sim -v_2$), implying that $P(v)$ also scales as

$$P(v) \sim |v|^{-2-1/\sigma}, \tag{8.13}$$

where $v = |v_1| = |v_2|$. Figure (8.2) shows how the tail of the probability distribution of velocities scales for different values of σ. The exponent $\beta = -2 - 1/\sigma$ is independent of κ as expected. In fact, the same result can be obtained without the parabolic potential, by calculating the probability distribution for the velocity of a moveable particle trapped in between two fixed particles. In this case, to get the correct transition velocity, the separation of two fixed particles should be set to twice the most likely next-neighbor separation of particles obtained from a many-body simulation. This is a clear indication that the only effect of the background parabolic potential is to keep the system bounded, and that it does not affect the scaling of the velocity distribution.

Given the functional form of the pair interaction ($1/r$ force) and the claim that high velocity events are consequences of very close neighbor interactions, we can understand the power-law tail of the velocity distribution through the following scaling argument: Since $r \to 0$ is a singular limit, for two very close particles, both the external force (the force from the parabolic potential in this case) and the superposition of all forces from other distant particles can be neglected compared to the force of the closest particle. Therefore, $v(r)$ scales as $v \sim 1/r$. Also, from Eq. (8.8), $\rho(r)$ scales as $\rho(r) \sim r^{1/\sigma}$. Using

$$\rho(r)dr = P(v)dv, \tag{8.14}$$

we have

$$P(v) \sim \rho\left(r(v)\right)\left|\frac{dr}{dv}\right| \sim v^{-2-1/\sigma}. \tag{8.15}$$

It is important to confirm that $\rho(r) \sim r^{1/\sigma}$, that is, we can neglect the contribution of the interactions with other particles in the scaling of the probability distribution separation of a pair of particles with very small distance. Equivalently, we need to confirm that the distribution of nearest-neighbor separation is the same as the two-particle distribution in the limit of small distance. Figure (8.3) compares the probability distribution $P_{nn}(d)$ of the nearest-neighbor separation, d, with the distribution of relative distance in a two-body system. Although the distribution at large separations behaves differently in the many-body system from the two-body system, the small separation limits of both systems are essentially identical.

From the simple argument above, it is clear that the temperature-dependent power-law distribution of velocities in one dimension is not a collective effect, and it is only a consequence of the logarithmic interaction potential. The distribution of velocities and the short distant limit of the distribution of nearest-neighbor separations can be very well approximated with those of the two-body system. The long distance limit of the distribution of the nearest-neighbor separations is the only quantity that can not be predicted from the two-body analysis (see Fig. (8.3)).

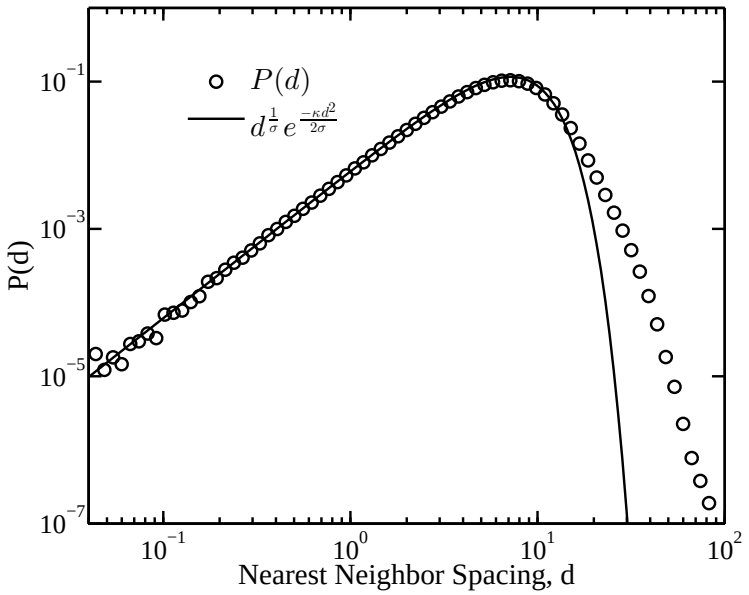

Figure 8.3: Probability distribution P_{nn} of the nearest-neighbor separation, d, for a system of $N = 100$ particles compared with the distribution of relative distance in a two-body system.

8.3 Two-dimensional model and pairing transition

A neutral system of dislocations with opposite charges in 1D is difficult to study without introducing ad-hoc rules of pair creation and annihilation. Forrester has studied a 2D generalization of Eq. (8.5) for a system with two opposite charges and isotropic logarithmic interaction potential [118]. For nanocrystals with strong crystal anisotropy, the assumption of straight edge dislocations with parallel Burgers vectors is a good approximation, and, in this case, the motion is confined to discrete, parallel glide lines. However, the dislocation interaction is not a simple isotropic logarithmic potential, but it obeys Eq. (8.1). We can generalize Dyson's model with an anisotropic interaction as following.

Consider a system of $2N$ particles (N of each charge) with position vectors $\vec{r}_i^{\pm} = (x_i^{\pm},\ y_i^{\pm})$ $(1 \leq i \leq N)$, where $y_i^{\pm}$'s are a set of $2N$ uniformly distributed random variables between 0 and L, and $x_i^{\pm}$'s satisfy the following equations of motion:

$$\frac{dx_i^{\pm}}{dt} = \sum_{j \neq i} \tau(\vec{r}_i^{\pm} - \vec{r}_j^{\pm}) - \sum_{j} \tau(\vec{r}_i^{\pm} - \vec{r}_j^{\mp}) + \sqrt{2\sigma}\xi_i^{\pm}(t). \tag{8.16}$$

Here

$$\tau(\vec{r}) = \frac{x\left(x^2 - y^2\right)}{\left(x^2 + y^2\right)^2}, \tag{8.17}$$

and $\langle \xi_i^{\pm}(t)\xi_j^{\pm}(t')\rangle = \delta_{ij}\delta(t - t')$.

Since the system is charge-neutral, the term from the parabolic potential is no longer necessary. We notice that Eq. (8.17) can be derived from a potential of the form

$$V(\vec{r}) = -\frac{y^2}{|\vec{r}|^2} - \log\left(|\vec{r}|\right). \tag{8.18}$$

The equilibrium joint probability distribution for the positions of these particles is given by the generalization of Eq. (8.8) to a neutral system of particles and has the following

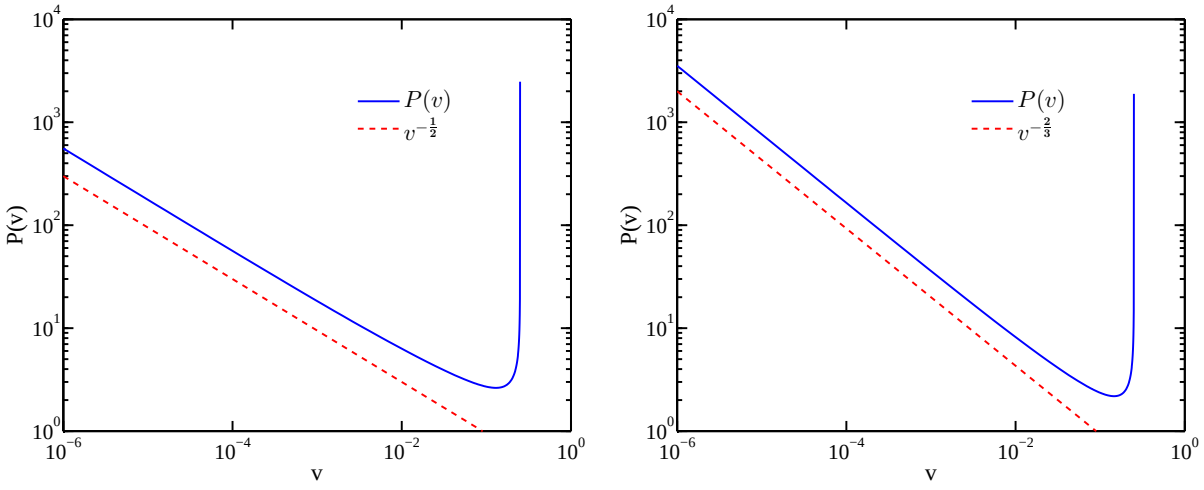

(a) $\sigma = \frac{2}{3}$ (b) $\sigma = \frac{3}{4}$

Figure 8.4: (Color online) Relative velocity distribution calculated from Eq. (8.25) for temperatures $\sigma \in \{\frac{2}{3},\ \frac{3}{4}\}$ compared with the predicted power-law in Eq. (8.26)

expression

$$\rho(\vec{r}_1^{+}, \ldots,\ \vec{r}_N^{+},\ \vec{r}_1^{-}, \ldots,\ \vec{r}_N^{-}) = \frac{1}{\mathcal{Z}} \frac{\prod_{i<j} \left|\vec{r}_i^{+} - \vec{r}_j^{+}\right|^{\frac{1}{\sigma}} \exp\left(\frac{\left(y_i^{+}-y_j^{+}\right)^2}{\sigma\left|\vec{r}_i^{+}-\vec{r}_j^{+}\right|^2}\right) \prod_{n<m} \left|\vec{r}_n^{-} - \vec{r}_m^{-}\right|^{\frac{1}{\sigma}} \exp\left(\frac{\left(y_n^{-}-y_m^{-}\right)^2}{\sigma\left|\vec{r}_n^{-}-\vec{r}_m^{-}\right|^2}\right)}{\prod_{i,j} \left|\vec{r}_i^{+} - \vec{r}_j^{-}\right|^{\frac{1}{\sigma}} \exp\left(\frac{\left(y_i^{+}-y_j^{-}\right)^2}{\sigma\left|\vec{r}_i^{+}-\vec{r}_j^{-}\right|^2}\right)}, \tag{8.19}$$

where the partition function is expressed as

$$\mathcal{Z} = L^{2N} \int d^{2N}r \frac{\prod_{i<j} \left|\vec{r}_i^{+} - \vec{r}_j^{+}\right|^{\frac{1}{\sigma}} \exp\left(\frac{\left(y_i^{+}-y_j^{+}\right)^2}{\sigma\left|\vec{r}_i^{+}-\vec{r}_j^{+}\right|^2}\right) \prod_{n<m} \left|\vec{r}_n^{-} - \vec{r}_m^{-}\right|^{\frac{1}{\sigma}} \exp\left(\frac{\left(y_n^{-}-y_m^{-}\right)^2}{\sigma\left|\vec{r}_n^{-}-\vec{r}_m^{-}\right|^2}\right)}{\prod_{i,j} \left|\vec{r}_i^{+} - \vec{r}_j^{-}\right|^{\frac{1}{\sigma}} \exp\left(\frac{\left(y_i^{+}-y_j^{-}\right)^2}{\sigma\left|\vec{r}_i^{+}-\vec{r}_j^{-}\right|^2}\right)}. \tag{8.20}$$

We show that the logarithmic term in Eq. (8.18) results in a power-law velocity distribution for a system of two particles. If the power-law distribution of velocities is a consequence of the nearest-neighbor pair interaction, as was the case in a 1D system with one charge, we should be able to predict the exponent of the velocity distribution in a many-body system by studying a system of two particles. However, if the high velocity events are dominated by collective effects such as avalanches, we should see different exponents in the many-body

simulation compared to the analysis of the two-body system. We will show that, in fact, the latter is true, and at a non-zero temperature, the high velocity events are dominated by collective interactions.

In contrast to the case of same-charge particles in 1D, the opposite charges have attractive forces, and therefore, the nearest neighbor of each particle is expected to have opposite charge for the majority of the time when the system is at equilibrium. Consider a system of two opposite charges moving on two parallel lines with separation $y = y^+ - y^-$, and relative longitudinal displacement $x = x^+ - x^-$ obeying the equation of motion

$$\frac{dx}{dt} = -2\frac{x(x^2 - y^2)}{(x^2 + y^2)^2} + \sqrt{4\sigma}\xi(t). \tag{8.21}$$

This equation imposes a limit of $v_{max} = \frac{1}{4y}$ on the absolute value of the velocity of these particles. The absolute value of velocity attains its maxima at $x = \pm(1 \pm \sqrt{2})y$.

Equation (8.21) is simplified through rescaling x by y. This corresponds to the changes of variables $\frac{x}{y} \to x$, $\frac{t}{y^2} \to t$, and $y\xi \to \xi$. Under these changes of variables, Eq. (8.21) becomes

$$\frac{dx}{dt} = -2\frac{x(x^2 - 1)}{(x^2 + 1)^2} + \sqrt{4\sigma}\xi(t), \tag{8.22}$$

which is the same equation obtained by setting $y = 1$. From Eq. (8.19) and Eq. (8.20), we have

$$\rho(x) = \frac{1}{\mathcal{Z}}\left(x^2 + 1\right)^{-\frac{1}{2\sigma}} \exp\left(-\frac{1}{\sigma\left(x^2 + 1\right)}\right) \tag{8.23}$$

and

$$\mathcal{Z} = \int_{-\infty}^{+\infty} \left(x^2 + 1\right)^{-\frac{1}{2\sigma}} \exp\left(-\frac{1}{\sigma\left(x^2 + 1\right)}\right) dx. \tag{8.24}$$

The integral above, converges only for $\sigma < 1$, meaning that for $\sigma \geq 1$, at equilibrium, the probability of finding the particles at any finite separation is zero. At low temperatures, the particles remain in a bound state at equilibrium. Above the critical temperature $\sigma_c = 1$, the particles are no longer bound and fly off to infinity in the long-time limit. This is the

analogue of the pairing transition in a 1D plasma with logarithmic interaction with a short distance cut-off [112].

The probability distribution for the relative velocity of these particles can be found using the change of variable

$$P(v) = \sum_{x(v)} \rho\left(x(v)\right) \left|\frac{dx}{dv}\right|. \tag{8.25}$$

Fig. (8.4) shows the resulting velocity distribution calculated from Eq. (8.25) for temperatures $\sigma = \frac{2}{3}$ and $\frac{3}{4}$. The divergence of $P(v)$ at v_{max} is due to the singular change of variable Jacobian $\left|\frac{dx}{dv}\right|$. For $\sigma > \frac{1}{2}$, away from the maximum velocity, corresponding to $|x| \gg 1$, $P(v)$ decays as

$$P(v) \sim v^{-2+1/\sigma}. \tag{8.26}$$

In this region, the system can be approximated by the 1D system, and an argument similar to the one in the previous section can be used to explain the scaling behavior of $P(v)$. For $\sigma \leq 1/2$, however, the $x \gg 1$ region has a finite contribution in the low velocity limit ($\lim_{v\to 0} P(v)$ is finite for $\sigma \leq 1/2$ in Eq. (8.26)), and therefore, the contributions of other zeros of velocity near $x = 0$ become important. In this region, the low velocity scaling of $P(v)$ can be determined by considering the contributions of all the competing terms from zeros of velocity including both the ones near zero and the one at infinity in the scaling argument.

$P(v)$ calculated above is, in fact, the conditional probability distribution for the velocity given the separation $y = 1$ or $P(v|y = 1)$. The relation

$$P(v|y) = yF(yv) \tag{8.27}$$

can be obtained by a reverse change of variable to the original x, y, and v, where $F(v) = P(v|y = 1)$ is the distribution calculated above. In order to calculate the probability distri-

bution for the velocity, independent of y,

$$P(v) = \int_0^\infty P(v|y) f(y) dy, \tag{8.28}$$

the distribution of y, $f(y)$, is needed. In the original many-body problem, y_i's were chosen to be uniformly distributed. However, the two-body problem that approximates the many-body problem is constructed to represent a pair of nearest neighbors in the many-body problem. Thus, $f_N(y)$ should be defined to be the probability distribution of the distance from the nearest neighbor in an ensemble of N uniformly distributed y_i's, $0 \leq y_i \leq L = Nd$, for some average separation d. In other words, $f_N(y)$ is the probability of finding y_i at any point $0 \leq s \leq L = dN$ finding another y_j at the distance y from y_i, and finding all the other y_k's outside of the interval $(s-y,\ s+y)$, given that the probability density of finding each y_i at each point in $(0,\ L)$ is $L^{-1} = (Nd)^{-1}$:

$$\begin{aligned} f_N(y) &= \int_0^{Nd} P(y_i = s) \sum_{j \neq i} \left(P\left(y_j = s \pm y\right) \prod_{k \neq i,j} \left(1 - \int_{max\{s-y,0\}}^{min\{s+y,Nd\}} P(y_k = x) dx \right) \right) ds \\ &\approx Nd \left(\frac{1}{Nd}\right) (N-1) \left(\frac{2}{Nd} \left(1 - \frac{2y}{Nd}\right)^{N-2} \right) = \frac{2(N-1)}{Nd} \left(1 - \frac{2y}{Nd}\right)^{N-2} \end{aligned} \tag{8.29}$$

Now, $f(y)$ can be defined as

$$f(y) = \lim_{N \to \infty} f_N(y) = \lambda e^{-\lambda y}, \tag{8.30}$$

where $\lambda = \frac{2}{d}$. The limit of $N \to \infty$ is taken by keeping $d = \frac{L}{N}$ constant. In order to perform the integral in Eq. (8.28), $F(v)$ was analytically calculated and numerically evaluated over its range of definition and stored in an array. 10^8 random numbers from an exponential distribution were generated as y values, and at each v, $P(v|y)$ was calculated using Eq. (8.27) for all y's, and it was summed over all y's. The resulting function $P(v)$ then was normalized. Fig. (8.5) shows $P(v)$ calculated for different values of σ. The low velocity tail follows the scaling law for the low velocity tail of $F(v)$ discussed above, while the high velocity tail is

independent of σ and has the exponent $\beta = -2$.

Although the behavior of the low velocity tail can be understood by the same scaling argument used in 1D system, since the low velocity tail is heavily influenced by the long distance behavior, the nearest-neighbor approximation does not hold for this region. The high velocity tail of a the two-body system, however, can be used as the nearest-neighbor approximation for the many-body system. The -2 exponent of the high velocity tail can be understood through a similar argument, but this time, by expanding $v(x)$ near its maxima. v can be written near each of its maxima as

$$v \approx v_{max} + k_i(x - x_i)^2, \tag{8.31}$$

where $k_i = \frac{1}{2}\frac{\partial^2 v}{\partial x^2}\big|_{x_i}$ and $|v(x_i)| = v_{max}$. Thus, using Eq. (8.25), near v_{max}, $F(v)$ can be approximated as

$$F(v) \approx \left(\sum_i \frac{\rho(x_i)}{k_i}\right)(v_{max} - v)^{-\frac{1}{2}}. \tag{8.32}$$

In other words, $F(v)$ diverges as $(v_{max}-v)^{-\frac{1}{2}}$ in the limit that v approaches v_{max}. It is important to note that the exponent does not depend on the functional form of the interaction, and this scaling holds as long as the interaction stress has a non-singular maximum at which its second derivative does not vanish. Using Eq. (8.28), it is straightforward to see that the -2 exponent of the high velocity tail can be obtained only by considering the near maximum functional form $F(v)$,

$$P(v) \sim \int_0^{\frac{v_{max}}{v}} y(v_{max} - yv)^{-\frac{1}{2}} e^{-\lambda y} dy \sim v^{-2} \tag{8.33}$$

Figure (8.6) shows the probability distribution for the velocity in a simulation with 200 particles ($N = 100$). The weakly temperature-dependent exponent β has the value -2 as

predicted from the nearest-neighbor analysis for $\sigma \ll \sigma_c = 1$, while it has a smaller value for σ close to or larger than σ_c. This deviation from the predicted exponent in the nearest-neighbor approximation is an indication that the dislocation motion is dominated by more than just the nearest-neighbor interactions. The numerical exponent has the value $\beta = -2.4$ at the critical temperature $\sigma_c = 1$ which is consistent with the exponent found in externally driven systems at zero temperature [5].

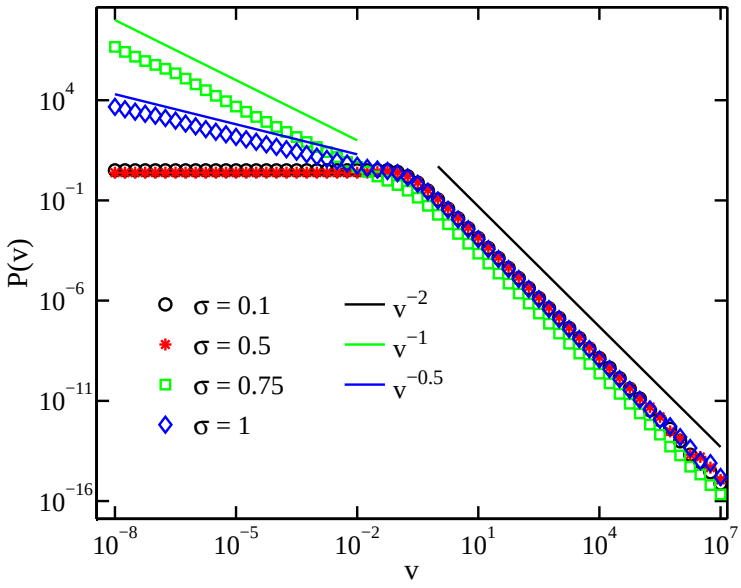

Figure 8.5: (Color online) Probability distribution of velocities in ensembles of system of two particles confined in parallel lines with exponentially distributed separations, y, for $\sigma \in \{0.1,\ 0.5,\ 1.0,\ 1.5\}$.

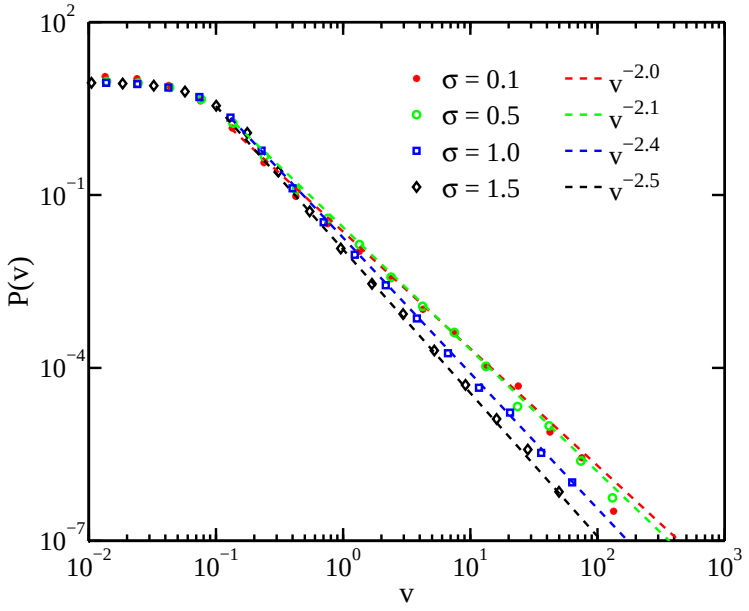

Figure 8.6: (Color online) Probability distribution of velocities in a system of 200 particles ($N = 100$) for $\sigma \in \{0.1,\ 0.5,\ 1.0,\ 1.5\}$.

8.4 Conclusions

In this project, we have studied the statistics of velocity fluctuations in a simplified system of dislocations with parallel Burgers vectors in one and two dimensions.

In one dimension, the probability density function for the velocities of the dislocations at high velocities scales as $v^{-2-1/\sigma}$ with a power law exponent that quantifies the strength of background noise fluctuations relative to the pairwise interaction energy. We have shown that this power-law distribution can be derived by considering only the nearest-neighbor interactions of dislocations, and therefore, is not a consequence of collective interactions.

In two dimensions, at an effective temperature where the noise energy k_BT becomes equal to the pairwise interaction energy $\frac{\mu b^3}{2\pi(1-\nu)}$, we have found that there is a transition between a state at which the nearest neighbors are bound to each other and a state where they can escape from each other's attractive force. For temperatures significantly smaller than this transition temperature, the velocity probability density function for dislocations agrees with the scaling v^{-2} found from the nearest-neighbor analysis, while for temperatures close to or larger than this transition temperature, the probability density function follows a power-law with an exponent steeper than -2 suggesting that the high velocity events are dominated by collective effects due to the interaction of more than two dislocations. This exponent is very weakly temperature dependent and has the value -2.4 at the transition temperature.

It remains to be further investigated how our results relate to the velocity statistics in more complicated three-dimensional models with features such as junctions of dislocations and line tension effects.

Appendix A

Useful Results from Stochastic Dynamics

A.1 Stochastic Differential Equations

A stochastic differential equation in Itō sense is the continuous-time limit of a Markov process defined by

$$X_{t+\delta t} = X_t + \delta t \left(f(X_t) + \sqrt{g(X_t)}\xi(t) \right), \tag{A.1}$$

where X_t is a random variable describing the state of a system, f and g are continuously differentiable functions, and $\xi(t)$ at each time t, is an independent Gaussian distributed random number with zero mean and variance $1/\delta t$.

In contrast, a stochastic differential equation in the Stratonovich sense is defined as the continuous-time limit of the Markov process

$$X_{t+\delta t} = X_t + \delta t \left(f'\left(\frac{X_t + X_{t+\delta t}}{2} \right) + \sqrt{g'\left(\frac{X_t + X_{t+\delta t}}{2} \right)}\xi(t) \right), \tag{A.2}$$

where the functions f' and g' depend on the average of the variable X in the interval $[X_t, X_{t+\delta t}]$. In ordinary calculus, evaluating the functions at different points in the interval $[X_t, X_{t+\delta t}]$ does not make a difference, and by continuity, the $\delta t \to 0$ limit of both processes would converge to the same value. However, in stochastic calculus, since the function $\xi(t)$ is a discontinuous function of time, it matters at which point the function g' is evaluated. Of course, there are infinitely many types of processes where g' is evaluated at different points in the interval.

At $\delta t \to 0$ limit, Eq. (A.1) and Eq. (A.2) converge to the same continuous process only if

$$g'(x) = g(x), \quad \text{and} \quad f'(x) = f(x) - \frac{1}{4}\frac{dg}{dx}. \tag{A.3}$$

This can be shown by finding an equation of motion for the corresponding probability density $P(X_t)$ for Eq. (A.1) and Eq. (A.2), and showing that in the $\delta t \to 0$ limit, both equations converge to the same equation.

The conditions of Eq. (A.3) can be understood from the fact that zero mean random fluctuation of a variable X that depend on the initial value of X in the time interval (as is the case in Eq. (A.1)) induce a probability current down the gradient of g. I would like to clarify this by a simple example: suppose you invest your money in a volatile stock, and on average, the value of the stock changes 10% a day. The strength of the fluctuations is dependent on the initial value of the stock everyday, and it increases as the stock value increases (it is a fixed fraction of the stock value[1]). According to the claim I made earlier, there should be a probability current down the gradient of the function describing the dependence of fluctuations on the stock value, and therefore, you should be more likely to lose money. Of course, since the fluctuations have zero mean (the stock is equally likely to go up and down with the same amount every day), the expected value of your final amount of money stays the same, but still you are more likely to lose money. Here is why: the most likely scenario is that over a long time you gain and lose money about the same number of times, let's say n gains and n losses. Each time you lose money, the value of your stock is multiplied by 0.9, while each time you gain, it is multiplied by 1.1. The final value of the stock is its initial value multiplied by $(1.1 \times 0.9)^n$, which is less than one. This probability flux down the gradient of g persists in the continuous limit of Eq. (A.1).

In contrast, if the value of your stock fluctuates in a way that its fluctuation is proportional to the average value of stock over the day[2], one can show that on average, you are equally likely to lose or gain over time. This is why a term proportional to the gradient of g is subtracted in f' in Eq. (A.2) to make up for the probability flux down the gradient of g in

[1] The continuous version of this process with Gaussian noise is known as geometric random walk.

[2] Of course, this requires that either the system have some knowledge of future events before making a change, or the fluctuations to be a result of some underlying coarse-grained behavior over the whole day.

Eq. (A.1) that results from evaluating the fluctuations at the beginning of the interval.

Most of the processes described in this thesis are neither one of Eq. (A.1) nor Eq. (A.2). They are Markov processes defined by an equation of the form

$$X_{t+\delta t} = X_t + \sum_{t' \in [t,\, t+\delta t]} \zeta(X_{t'}), \tag{A.4}$$

where $\zeta(X_{t'})$ are independent (usually Poisson distributed) random variables with finite X-dependent variance, added at some time $t' \in [t,\, t+\delta t]$. In the limit of the model where many such stochastic events are happening per unit time, the Central Limit Theorem implies that, for a mesoscopic δt, the sum

$$\mu(X,t) = \sum_{t' \in [t, t+\delta t]} \zeta(X_{t'}), \tag{A.5}$$

is a Gaussian distributed random variable with an X-dependent variance proportional to δt. We can define the mean and the X-dependent part of the variance of $\mu(X,t)$ by

$$f''(X) = \langle \mu(X,t) \rangle \tag{A.6}$$

$$g''(X) = \frac{1}{\delta t} \left\langle (\mu(X,t) - f''(X))^2 \right\rangle . \tag{A.7}$$

Then the zero mean Gaussian random variable

$$\xi(t) = \frac{1}{\delta t \sqrt{g(X)}} (\mu(X,t) - f''(X)) \tag{A.8}$$

is independent of X. In terms of these new functions, Eq. (A.5) can be written as

$$X_{t+\delta t} = X_t + \delta t \left(f''(X) + \sqrt{g''(X)}\, \xi(t) \right) . \tag{A.9}$$

Due to the coarse-graining process through which the noise function $\xi(t)$ is defined, it is ambiguous to know at which point in the time interval $[t,\, t+\delta t]$, X in $g''(X)$ should be evaluated. As we saw earlier, the continuous limit of this process converges to different

limits depending on this choice of evaluation. To avoid this ambiguity, in this thesis, I never derive a stochastic differential equation by taking the continuous limit of an equation of the type Eq. (A.5). Instead, I write a master equation for the time evolution of the probability of X. The probability function is continuous and differentiable, and the Gaussian noise approximation and the continuous limit are unambiguous and can be evaluated using the Kramers-Moyal expansion, as explained in Section 3.2. The resulting partial differential equation for the time evolution of the probability density of X, which is known as the Fokker-Planck equation, describes the time evolution of two related processes: one is the probability density of a stochastic differential equation in the Itō sense and the other is a somewhat different stochastic differential equation in the Stratonovich sense. The two equations are related by the conditions of Eq. (A.3).

In this thesis, I use stochastic differential equations in the Itō sense and not that of Stratonovich. There are two good reasons to do so:

1. The Gaussian noise produced at each time step in Itō does not require knowledge of the future state of the system. This makes the computer simulation of such processes more readily accessible.

2. The noise term $\xi(t)$ in Itō is independent of the variable X in $g(X)$, while that is not the case in Stratonovich differential equations. For example, in Itō, we know that the expected value of the fluctuation term is zero,

$$\langle g(X)\xi(t)\rangle = \langle g(X)\rangle \langle \xi(t)\rangle = 0, \tag{A.10}$$

   due to the independence of $g(X)$ and $\xi(t)$.

However, it is important to keep in mind that the choice of Itō over Stratonovich means that we have to deal with the counter intuitive effect of the probability current down the gradient of g (also known as noise-induced drift) that is produced by zero mean random fluctuations. This drift plays a crucial role in Section 3.3.

In this thesis, I write the Itō stochastic differential equation describing the continuous

limit ($\delta t \to 0$) of Eq. (A.1) as

$$\frac{dX}{dt} = f(X) + \sqrt{g(X)}\xi(t), \tag{A.11}$$

A.2 Decoupling Gaussian Noise

Consider a set of coupled stochastic differential equations

$$\frac{d\vec{x}}{dt} = \vec{H}(\vec{x}) + \vec{\xi}(t), \tag{A.12}$$

where ξ_i's ($i \in \{1, \ldots, n\}$), the components of $\vec{\xi}(t)$, are zero mean Gaussian noise functions with correlation

$$\langle \xi_i(t)\xi_j(t') \rangle = B_{i,j}\delta(t - t'). \tag{A.13}$$

We would like to rewrite Eq. (A.12) in terms of some set of independent Gaussian white noise functions $\eta_i(t)$'s ($i \in \{1, \ldots, m\}$ for some m) with the correlation

$$\langle \eta_i(t)\eta_j(t') \rangle = \delta_{i,j}\delta(t - t'). \tag{A.14}$$

If we can find an $n \times m$ matrix $\boldsymbol{G}$ such that $\boldsymbol{B} = \boldsymbol{G}\boldsymbol{G}^{\mathsf{T}}$, then it is straightforward to show that $\vec{\xi}(t) = \boldsymbol{G}\vec{\eta}(t)$:

$$\begin{aligned}
\langle \xi_i(t)\xi_j(t') \rangle &= \left\langle \sum_k G_{i,k}\eta_k(t) \sum_l G_{j,l}\eta_l(t') \right\rangle \\
&= \sum_{k,l} G_{i,k}G_{j,l} \langle \eta_k(t)\eta_l(t') \rangle \\
&= \sum_{k,l} G_{i,k}G_{j,l}\delta_{k,l}\delta(t - t') \\
&= \sum_k G_{i,k}G^{\mathsf{T}}_{k,j}\delta(t - t') = B_{i,j}\delta(t - t').
\end{aligned} \tag{A.15}$$

Now Eq. (A.12) in terms of $\vec{\eta}(t)$ is given by

$$\frac{d\vec{x}}{dt} = \vec{H}(\vec{x}) + \boldsymbol{G}\vec{\eta}(t). \tag{A.16}$$

This decomposition is not unique and multiple choices for $\boldsymbol{G}$ exist [61]. Perhaps the simplest choice is given by the $n \times n$ matrix $\boldsymbol{G} = \boldsymbol{B}^{1/2}$. Note that matrix $\boldsymbol{B}$ is symmetric positive

definite, and therefore, is diagonalizable and has well-defined real symmetric square root. Hence $\boldsymbol{G}\boldsymbol{G}^{\mathsf{T}} = \boldsymbol{G}\boldsymbol{G} = \boldsymbol{G}^2 = \boldsymbol{B}$.

Many of the Fokker-Planck Equations in this thesis are derived from a set of reactions or species interactions, and therefore have a $\boldsymbol{B}$ matrix with the particular structure (see *e.g.* Section 3.2)

$$\boldsymbol{B} = \sum_{i=1}^{m} T_i \, \vec{s}_i \otimes \vec{s}_i, \tag{A.17}$$

where $\vec{s}_i$ is the i'th row of an $m \times n$ stoichiometry matrix $\boldsymbol{S}$. For such $\boldsymbol{B}$, there is a particular choice of matrix $\boldsymbol{G}$ whose matrix elements have simpler analytic expressions compared to the square root choice:

$$G_{i,j} = \sqrt{T_j} \, S_{j.i} \tag{A.18}$$

It is easy to show that $\boldsymbol{G}\boldsymbol{G}^{\mathsf{T}} = \boldsymbol{B}$:

$$\left(\boldsymbol{G}\boldsymbol{G}^{\mathsf{T}}\right)_{i,j} = \sum_k G_{i,k} \, G_{j,k} = \sum_k \sqrt{T_k} S_{k.i} \sqrt{T_k} S_{k,j} = \left(\sum_k T_k \, \vec{s}_k \otimes \vec{s}_k \right)_{i,j} = B_{i,j}. \tag{A.19}$$

The number of columns, m, of matrix $\boldsymbol{G}$ from this method is the same as the number of reactions from which the Fokker-Planck Equation is derived. In the special case, where the stoichiometry matrix $\boldsymbol{S}$ has rows that are multiples of each other, there are simpler choices of $\boldsymbol{G}$ obtained by reducing the rows of $\boldsymbol{S}$ before calculating $\boldsymbol{G}$ through the following procedure: Suppose, for example $\vec{s}_j = a \, \vec{s}_i$. Then, we simply remove the row j of $\boldsymbol{S}$ (and the corresponding T_j) and replace T_i by $T_i + a^2 \, T_j$. The reason that this row reduction works is that the reduced matrix $\boldsymbol{S}$ and corresponding T's define the same matrix $\boldsymbol{B}$ as before:

$$\begin{aligned} \boldsymbol{B} = \sum_{k=1}^{m} T_k \, \vec{s}_k \otimes \vec{s}_k &= \cdots + T_i \, \vec{s}_i \otimes \vec{s}_i + \cdots + T_j \, \vec{s}_j \otimes \vec{s}_j + \ldots \\ &= \cdots + T_i \, \vec{s}_i \otimes \vec{s}_i + \cdots + a^2 \, T_j \, \vec{s}_i \otimes \vec{s}_i + \ldots \\ &= \sum_{k \neq i,j} T_k \, \vec{s}_k \otimes \vec{s}_k + (T_i + a^2 \, T_j) \vec{s}_i \otimes \vec{s}_i. \end{aligned} \tag{A.20}$$

A.3 Itō's lemma

Consider a set of coupled stochastic differential equations

$$\frac{d\vec{x}}{dt} = \vec{H}(\vec{x}) + \boldsymbol{G}(\vec{x})\vec{\eta}(t). \tag{A.21}$$

where η_i's ($i \in \{1, \ldots, n\}$), the components of $\vec{\eta}(t)$, are zero mean Gaussian noise functions with correlation

$$\langle \eta_i(t)\eta_j(t')\rangle = \delta_{i,j}\delta(t-t'). \tag{A.22}$$

Itō's lemma is used to find the time evolution of an arbitrary function f of $\vec{x}$. The normal chain rule does not apply to a function $f(\vec{x})$ since the variable $\vec{x}$ is a stochastic variable in Itō's sense [54]. The rate of change of f is given by

$$\frac{df}{dt} = \sum_i H_i \frac{\partial f}{\partial x_i} + \frac{1}{2}\sum_{i,j} B_{i,j}\frac{\partial^2 f}{\partial x_i \partial x_j} + \sum_{i,j} G_{i,j}\frac{\partial f}{\partial x_i}\eta_j(t), \tag{A.23}$$

where $\boldsymbol{B} = \boldsymbol{G}\boldsymbol{G}^{\mathsf{T}}$.

In particular, one can use Itō's lemma to change of variables from $\vec{x}$ to some $\vec{y} = \vec{f}(\vec{x})$. We obtain the time evolution in the new variables $\vec{y}$,

$$\frac{d\vec{y}}{dt} = \vec{H}'(\vec{y}) + \boldsymbol{G}'(\vec{y})\vec{\eta}(t), \tag{A.24}$$

where $\vec{H}'$ and $\boldsymbol{G}'$ are given by:

$$\vec{H}' = \sum_i H_i \frac{\partial \vec{f}}{\partial x_i} + \frac{1}{2}\sum_{i,j} B_{i,j}\frac{\partial^2 \vec{f}}{\partial x_i \partial x_j}, \qquad {G'}_{i,j} = \sum_k \frac{\partial f_i}{\partial x_k} G_{k,j}. \tag{A.25}$$

A.4 Steady-State Solution of One-Dimensional Fokker-Planck Equation

Consider a one-dimensional stochastic differential equations

$$\frac{dx}{dt} = h(x) + g(x)\eta(t). \tag{A.26}$$

where $\eta(t)$ is zero mean Gaussian noise with correlation $\langle \eta(t)\eta(t') \rangle = \delta(t-t')$. The probability density function, $P(x,t)$, of x obeys the Fokker-Planck Equation

$$\frac{\partial}{\partial t}P(x,t) = -\frac{\partial}{\partial x}(h(x)P(x,t)) + \frac{1}{2}\frac{\partial^2}{\partial x^2}(b(x)P(x,t)), \tag{A.27}$$

where $b(x) = (g(x))^2$. Equation (A.27) can be written as a continuity equation for probability density

$$\frac{\partial P(x,t)}{\partial t} = -\frac{\partial J}{\partial x} \tag{A.28}$$

where the probability current J is given by

$$J = h(x)P(x,t) - \frac{1}{2}\frac{\partial}{\partial x}\left(b(x)P(x,t)\right), \tag{A.29}$$

with $J = 0$ at the boundaries. Equation (A.28) implies that at steady state the probability current J is constant, and since it is zero at the boundaries, it has to be zero everywhere. Therefore, the steady state solution for $P_s(x) = \lim_{t\to\infty} P(x,t)$ is obtained by setting J from Eq. (A.29) to zero:

$$\begin{aligned} h(x)P_s(x) = \frac{1}{2}\frac{d}{dx}\left(b(x)P_s(x)\right) &= \frac{1}{2}\left(\frac{db}{dx}P_s(x) + b(x)\frac{dP_s}{dx}\right) \\ \implies \int \frac{dP_s}{P_s} &= \int 2\left(b(x)\right)^{-1}\left(h(x) - \frac{1}{2}\frac{db}{dx}\right)dx \\ \implies P_s(x) &= \mathcal{N}\frac{1}{b(x)}\exp\left(-2\int_0^x \frac{h(y)}{b(y)}dy\right), \end{aligned} \tag{A.30}$$

where the normalization constant $\mathcal{N}$ is given by

$$\mathcal{N} = \left(\int \frac{1}{b(x)} \exp\left(-2 \int_0^x \frac{h(y)}{b(y)} dy \right) dx \right)^{-1}. \tag{A.31}$$

A.5 Steady State Solution of Multivariate Linear Fokker-Planck Equation

Consider the linear stochastic differential equation of the form

$$\frac{d\vec{y}}{dt} = \boldsymbol{A}\vec{y} + \vec{\eta}(t), \tag{A.32}$$

where $\boldsymbol{A}$ is independent of $\vec{y}$ and $\vec{\eta}$ are Gaussian white noises with zero mean and correlator

$$\langle \vec{\eta}(t)\, \vec{\eta}^{\mathsf{T}}(t') \rangle = \boldsymbol{B}\delta(t - t'). \tag{A.33}$$

The noise matrix $\boldsymbol{B}$ is symmetric (*i.e.* $\boldsymbol{B}^{\mathsf{T}} = \boldsymbol{B}$) and independent of $\vec{y}$. Equation (A.32) is tantamount to the Fokker-Planck equation for the probability density $P(\vec{y}, t)$:

$$\frac{\partial P(\vec{y}, t)}{\partial t} = -\sum_{i,j} A_{ij} \frac{\partial}{\partial y_i}(y_j P) + \frac{1}{2}\sum_{i,j} \frac{\partial^2}{\partial y_i \partial y_j}(B_{ij} P). \tag{A.34}$$

As shown in *e.g.* [59], the stationary distribution is Gaussian and takes the form

$$P_s(\vec{y}) = \frac{1}{\sqrt{\det(2\pi\boldsymbol{\Xi})}} \exp\left(-\frac{1}{2}\vec{y}^{\mathsf{T}}\, \boldsymbol{\Xi}^{-1}\, \vec{y}\right), \tag{A.35}$$

where the symmetric covariance matrix $\boldsymbol{\Xi}$ satisfies the Sylvester's equation,

$$\boldsymbol{A}\boldsymbol{\Xi} + \boldsymbol{\Xi}\boldsymbol{A}^{\mathsf{T}} + \boldsymbol{B} = 0. \tag{A.36}$$

In two dimensions, this equation can be solved [54] leading to an explicit formula for $\boldsymbol{\Xi}$:

$$\boldsymbol{\Xi} = \frac{(\boldsymbol{A} - \mathbb{1}_2 \operatorname{tr}\boldsymbol{A})\, \boldsymbol{B}\, (\mathbb{1}_2 \operatorname{tr}\boldsymbol{A} - \boldsymbol{A})^{\mathsf{T}} - \boldsymbol{B} \det \boldsymbol{A}}{2 \operatorname{tr}\boldsymbol{A} \det\boldsymbol{A}}. \tag{A.37}$$

In the following, I assume for convenience that the noise matrix $\boldsymbol{B}$ is a multiple of the identity matrix $\mathbb{1}$ ($\boldsymbol{B} = \sigma^2\mathbb{1}$), a choice that can be made without losing in generality. In fact, since $\boldsymbol{B}$ is symmetric, it is diagonalized by an orthogonal matrix which one can use

to transform the noises; the resulting diagonal matrix can then be mapped to the identity matrix simply by rescaling the variables $\vec{y}$. Now, I will write the matrix $\boldsymbol{\Xi}$ in terms of $\boldsymbol{A}$ and what I call the hermitianizer of $\boldsymbol{A}$, defined as

$$\boldsymbol{G} = -\frac{1}{2}\,\sigma^2\,\boldsymbol{\Xi}^{-1}\boldsymbol{A}^{-1}, \tag{A.38}$$

which yields a symmetrization of matrix $\boldsymbol{A}$: even though $\boldsymbol{A}$ is not generally symmetric, $\boldsymbol{A} \neq \boldsymbol{A}^{\mathsf{T}}$, the product $\boldsymbol{G}\boldsymbol{A} = -2^{-1}\sigma^2\boldsymbol{\Xi}^{-1}$ is a symmetric matrix. Sylvester equation (A.36) written in terms of $\boldsymbol{G}$ simplifies to

$$\frac{1}{2}(\boldsymbol{G}^{-1} + (\boldsymbol{G}^{-1})^{\mathsf{T}}) = \mathbb{1}, \tag{A.39}$$

indicating that the hermitian part of $\boldsymbol{G}^{-1}$ is the identity. Alternatively, the hermitianizer of $\boldsymbol{A}$ can be defined as the unique matrix satisfying Eq. (A.39) whose product with $\boldsymbol{A}$ is hermitian. In terms of $\boldsymbol{G}$, Eq. (A.35) can be written as

$$P_s(\vec{y}) = \sqrt{\det\left(-\frac{\boldsymbol{G}\boldsymbol{A}}{\pi\sigma^2}\right)}\,\exp\left(\frac{\vec{y}^{\,\mathsf{T}}\boldsymbol{G}\boldsymbol{A}\,\vec{y}}{\sigma^2}\right). \tag{A.40}$$

If $\boldsymbol{A}$ is hermitian, $\boldsymbol{G}$ is the identity matrix, and the Boltzmann distribution is recovered.

A.6 Steady State Mean Square Norm in Linear Fokker-Planck Equation

We now wish to find an expression for the mean amplification factor, $\langle \|\vec{y}\|^2 \rangle$, used in the main text to quantify the linear response of a stochastic reactive system. The norm of $\vec{y}$ is the Euclidean norm $\|\vec{y}\| = \sqrt{\sum_i |y_i^2|}$. Specifically, we want to compute the integral:

$$\langle \|\vec{y}\|^2 \rangle = \int_{\mathbb{R}^D} d\vec{y}\, P_s(\vec{y})\, \|\vec{y}\|^2 \,, \tag{A.41}$$

where the distribution $P_s(\vec{y})$ is given by Eq. (A.35). Therefore,

$$\left\langle \|\vec{y}\|^2 \right\rangle = \frac{1}{\sqrt{\det(2\pi \boldsymbol{\Xi})}} \int d\vec{y} \exp\left(-\frac{1}{2} \vec{y}^{\mathsf{T}}\, \boldsymbol{\Xi}^{-1}\, \vec{y} \right) \|\vec{y}\|^2 \,. \tag{A.42}$$

To evaluate this integral, we use the identity

$$\int \|\vec{p}\|^2\, e^{-\vec{p}^T \boldsymbol{M} \vec{p}} d\vec{p} = \frac{1}{2} \mathrm{Tr}\left(\boldsymbol{M}^{-1}\right) \int e^{-\vec{p}^T \boldsymbol{M} \vec{p}} d\vec{p}, \tag{A.43}$$

with $\boldsymbol{M} = 1/2\, \boldsymbol{\Xi}^{-1}$, which yields the compact expression:

$$\langle \|\vec{y}\|^2 \rangle = \mathrm{Tr}(\boldsymbol{\Xi}) \tag{A.44}$$

Now we can rewrite Eq. (A.44) in terms of $\boldsymbol{A}$ and $\boldsymbol{G}$ by substituting Eq. (A.38) in Eq. (A.44):

$$\langle \|\vec{y}\|^2 \rangle = -\frac{1}{2} \sigma^2\, \mathrm{Tr}\left(\boldsymbol{A}^{-1} \boldsymbol{G}^{-1}\right) \tag{A.45}$$

When $\boldsymbol{A}$ is a 2×2 matrix, the trace of the inverse can be written as trace over determinant:

$$\langle \|\vec{y}\|^2 \rangle = -\frac{1}{2} \sigma^2\, \frac{\mathrm{Tr}\left(\boldsymbol{G}\boldsymbol{A}\right)}{\det(\boldsymbol{G})\det(\boldsymbol{A})} \tag{A.46}$$

$\mathrm{Tr}(\boldsymbol{GA})$ can be simplified by taking the trace of Eq. (A.38)

$$\mathrm{Tr}(\boldsymbol{GA}) = -\frac{1}{2}\,\sigma^2\,\mathrm{Tr}(\boldsymbol{\Xi}^{-1}). \tag{A.47}$$

Also, by multiplying the right-hand side of the Sylvester equation Eq. (A.36) by $\boldsymbol{\Xi}^{-1}$:

$$\boldsymbol{A} + \boldsymbol{\Xi}\boldsymbol{A}^{\mathsf{T}}\boldsymbol{\Xi}^{-1} = -\sigma^2\,\boldsymbol{\Xi}^{-1}. \tag{A.48}$$

and taking the trace we have (recalling that $\mathrm{Tr}(\boldsymbol{\Xi}\boldsymbol{A}^{\mathsf{T}}\boldsymbol{\Xi}^{-1}) = \mathrm{Tr}(\boldsymbol{A}^{\mathsf{T}}) = \mathrm{Tr}(\boldsymbol{A})$):

$$\sigma^2\,\mathrm{Tr}(\boldsymbol{\Xi}^{-1}) = -2\,\mathrm{Tr}(\boldsymbol{A}) \tag{A.49}$$

From Eq. (A.49) and Eq. (A.47) it follows that $\mathrm{Tr}(\boldsymbol{GA}) = \mathrm{Tr}(\boldsymbol{A})$, which we can use to simply Eq. (A.45):

$$\langle \|\vec{y}\|^2 \rangle = -\frac{\sigma^2}{2\,\det \boldsymbol{G}}\frac{\mathrm{Tr}\,\boldsymbol{A}}{\det \boldsymbol{A}} = -\frac{1}{2}\,\sigma^2\,\det\left(\boldsymbol{G}^{-1}\right)\mathrm{Tr}\left(\boldsymbol{A}^{-1}\right). \tag{A.50}$$

A.7 Multivariate Linear Fokker-Planck Equation with Complex Variables

Consider a linear stochastic differential equation of the the form

$$\frac{d\vec{y}}{dt} = \boldsymbol{A}\vec{y} + \vec{\eta}(t), \tag{A.51}$$

where $\vec{y}$ and $\vec{\eta}$ are vectors with complex-valued, and $\vec{\eta}$ is a Gaussian white noise with zero mean and correlation

$$\begin{aligned} \langle \vec{\eta}(t)\, \vec{\eta}^{\,\dagger}(t') \rangle &= \boldsymbol{B}\delta(t-t'), \\ \langle \vec{\eta}(t)\, \vec{\eta}^{\,\mathsf{T}}(t') \rangle &= 0. \end{aligned} \tag{A.52}$$

where the † symbol represents the transpose conjugate. These equations can show up, for example as the Fourier transform of a similar real valued equation, as it was the case in chapters (6) and (7). The analysis in the Appendices (A.5) and (A.6) can be generalized by evaluating the expected value of $\vec{y}(t)\vec{y}^{\,\dagger}(\tau)$ and $\vec{y}(t)\vec{y}^{\,\mathsf{T}}(\tau)$ at steady state for $t = \tau$ to obtain the following relationships for the covariance and relation matrices

$$\begin{aligned} \boldsymbol{A} \left\langle \vec{y}\vec{y}^{\,\dagger} \right\rangle + \left\langle \vec{y}\vec{y}^{\,\dagger} \right\rangle \boldsymbol{A}^{\dagger} + \boldsymbol{B} &= 0, \\ \boldsymbol{A} \left\langle \vec{y}\vec{y}^{\,\mathsf{T}} \right\rangle + \left\langle \vec{y}\vec{y}^{\,\mathsf{T}} \right\rangle \boldsymbol{A}^{\mathsf{T}} &= 0. \end{aligned} \tag{A.53}$$

The first equation is the analogue of equation of Sylvester Eq. (A.36) for the hermitian *covariance matrix* $\boldsymbol{\Xi} = \left\langle \vec{y}\vec{y}^{\,\dagger} \right\rangle$, while the second equation implies that the symmetric *relation matrix* $\boldsymbol{C} = \left\langle \vec{y}\vec{y}^{\,\mathsf{T}} \right\rangle$ is equal to zero. Therefore, at steady state, $\vec{y}$ obeys a circularly symmetric complex Gaussian distribution of the form

$$P_s(\vec{y}) = \frac{1}{\det(2\pi\boldsymbol{\Xi})} \exp\left(-\frac{1}{2} \vec{y}^{\,\dagger}\, \boldsymbol{\Xi}^{-1}\, \vec{y} \right). \tag{A.54}$$

Notice the different normalization factor compared to Eq. (A.35), as it is normalized over $\mathbb{C}^D$ instead of $\mathbb{R}^D$.

To compute the mean square value of the norm of $\vec{y}$, we can follow similar analysis to that of Appendix A.6. Here, we highlight the differences. The mean square norm is define as

$$\langle \|\vec{y}\|^2 \rangle = \int_{\mathbb{C}^D} d\vec{y}\, P_s(\vec{y})\, \|\vec{y}\|^2 \,, \tag{A.55}$$

with the norm $\|\vec{y}\| = \sqrt{\vec{y}^{\,\dagger}\vec{y}}$. The complex version of Eq. (A.43) can be evaluated by diagonalizing the matrix $\boldsymbol{M}$ and rewrite the integral on a 2-dimensional real space. The result is given by

$$\int_{\mathbb{C}^D} \|\vec{p}\|^2\, e^{-\vec{p}^{\,\dagger}\boldsymbol{M}\vec{p}} d\vec{p} = \mathrm{Tr}\left(\boldsymbol{M}^{-1}\right) \int_{\mathbb{C}^D} e^{-\vec{p}^{\,\dagger}\boldsymbol{M}\vec{p}} d\vec{p}, \tag{A.56}$$

where the factor $1/2$ is canceled due to the fact that each eigenvalue of $\boldsymbol{M}^{-1}$ should be counted twice in the 2-dimensional space, once for the real part and once for the imaginary part. As a result, there will be an extra factor 2 in Eq. (A.44), Eq. (A.45), and Eq. (A.50). In particular ,

$$\langle \|\vec{y}\|^2 \rangle = -\sigma^2\, \mathrm{Tr}\left(\boldsymbol{A}^{-1}\boldsymbol{G}^{-1}\right) \tag{A.57}$$

Appendix B

Nonnormality

B.1 Exponential Decay Under Normal Stable Operator

Consider the set of linear ordinary differential equations

$$\frac{d\vec{y}}{dt} = \boldsymbol{A}\vec{y}. \tag{B.1}$$

where $\boldsymbol{A}$ is an $n \times n$ matrix with eigenvalues $\lambda_1, \ldots, \lambda_n$, and $0 > \Re(\lambda_1) \geq \cdots \geq \Re(\lambda_n)$. Suppose $\boldsymbol{A}$ has a complete set of orthogonal eigenvectors; *i.e.* there exist a unitary matrix $\boldsymbol{U}$ and a diagonal matrix $\boldsymbol{\Lambda} = \boldsymbol{diag}(\lambda_1, \ldots, \lambda_n)$ such that $\boldsymbol{A} = \boldsymbol{U}\boldsymbol{\Lambda}\boldsymbol{U}^\dagger$. Then the rate of change $\|\vec{y}\|$ is given by

$$\begin{aligned}\frac{d\|\vec{y}\|}{dt} &= \frac{d\sqrt{\vec{y}^\dagger\vec{y}}}{dt} = \frac{1}{2\|\vec{y}\|}\left(\vec{y}^\dagger\boldsymbol{A}^\dagger\vec{y} + \vec{y}^\dagger\boldsymbol{A}\vec{y}\right) = \frac{1}{2\|\vec{y}\|}\left(\vec{y}^\dagger\boldsymbol{U}\boldsymbol{\Lambda}^*\boldsymbol{U}^\dagger\vec{y} + \vec{y}^\dagger\boldsymbol{U}\boldsymbol{\Lambda}\boldsymbol{U}^\dagger\vec{y}\right) \\ &= \frac{1}{2\|\vec{y}\|}\vec{y}^\dagger\boldsymbol{U}\left(\boldsymbol{\Lambda}^* + \boldsymbol{\Lambda}\right)\boldsymbol{U}^\dagger\vec{y} = \frac{1}{\|\vec{y}\|}\vec{y}^\dagger\boldsymbol{U}\Re(\boldsymbol{\Lambda})\boldsymbol{U}^\dagger\vec{y} \leq \frac{1}{\|\vec{y}\|}\vec{y}^\dagger\boldsymbol{U}\Re(\lambda_1)\mathbb{1}\boldsymbol{U}^\dagger\vec{y} = \Re(\lambda_1)\|\vec{y}\|\end{aligned} \tag{B.2}$$

Therefore, norm of $\vec{y}$ decays exponentially with a time scales $\tau = 1/\Re(\lambda_1)$,

$$\|\vec{y}(t)\| \leq \|\vec{y}(0)\| \exp\left(\Re(\lambda_1)t\right). \tag{B.3}$$

B.2 Transient Growth Under Nonnormal Stable Operator

Consider the set of linear ordinary differential equations

$$\frac{d\vec{y}}{dt} = \boldsymbol{A}\vec{y}. \tag{B.4}$$

where $\boldsymbol{A}$ is an $n \times n$ matrix with eigenvalues $\lambda_1, \ldots, \lambda_n$, and $0 > \Re(\lambda_1) \geq \cdots \geq \Re(\lambda_n)$.

Claim 1: The upper bound for the growth/decay rate of the $\|\vec{y}\|$ is set by the largest eigenvalue, ν_1, of the hermitian part, $\boldsymbol{H}$, of $\boldsymbol{A}$. Note that since $\boldsymbol{H}$ is hermitian, there exist a unitary matrix $\boldsymbol{V}$ and a real diagonal matrix $\boldsymbol{N} = \boldsymbol{diag}(\nu_1, \ldots, \nu_n)$ such that $\boldsymbol{H} = \boldsymbol{V}\boldsymbol{N}\boldsymbol{V}^\dagger$. Let b_i be the component of $\vec{y}$ along the i'th eigenvector, $\vec{v}_i$, of $\boldsymbol{H}$. Then rate of change of norm of $\vec{y}$ is given by

$$\begin{aligned}
\frac{d\|\vec{y}\|}{dt} &= \frac{d\sqrt{\vec{y}^\dagger\vec{y}}}{dt} = \frac{1}{2\|\vec{y}\|}\left(\vec{y}^\dagger\boldsymbol{A}^\dagger\vec{y} + \vec{y}^\dagger\boldsymbol{A}\vec{y}\right) = \frac{1}{\|\vec{y}\|}\vec{y}^\dagger\left(\frac{\boldsymbol{A}^\dagger + \boldsymbol{A}}{2}\right)\vec{y} \\
&= \frac{1}{\|\vec{y}\|}\vec{y}^\dagger\boldsymbol{H}\vec{y} = \frac{1}{\|\vec{y}\|}\vec{y}^\dagger\boldsymbol{V}\boldsymbol{N}\boldsymbol{V}^\dagger\vec{y} = \frac{1}{\|\vec{y}\|}\sum \nu_i |b_i|^2 \\
&\leq \frac{1}{\|\vec{y}\|}\sum \nu_1 |b_i|^2 = \frac{1}{\|\vec{y}\|}\vec{y}^\dagger\boldsymbol{V}\nu_1\mathbb{1}\boldsymbol{V}^\dagger\vec{y} = \nu_1\|\vec{y}\|
\end{aligned} \tag{B.5}$$

Therefore, the upper bound for the growth/decay rate of norm of $\vec{y}$ is give by the largest eigenvalue of the hermitian part of $\boldsymbol{A}$, ν_1. If $\nu_1 > 0$, there exist an initial condition (namely $\vec{y}(0) = \vec{v}_1$, where $\vec{v}_1$ is the eigenvector of $\boldsymbol{H}$ corresponding to the eigenvalue ν_1) such that $\|\vec{y}\|$ growth at the rate ν_1 at time $t = 0$. In this case, matrix $\boldsymbol{A}$ is called reactive.

Claim 2: The largest eigenvalue of $\boldsymbol{H}$ is greater than or equal to the real part of the largest eigenvalue of $\boldsymbol{A}$ [119], *i.e.* $\nu_1 \geq \Re(\lambda_1)$. Let $\vec{u}_1$ be the normalized eigenvector of $\boldsymbol{A}$ corresponding to the eigenvalue λ_1, then

$$\begin{aligned}
\nu_1 &= \sup_{\|\vec{x}\|=1} \vec{x}^\dagger\boldsymbol{H}\vec{x} = \sup_{\|\vec{x}\|=1} \vec{x}^\dagger\left(\frac{\boldsymbol{A}^\dagger + \boldsymbol{A}}{2}\right)\vec{x} = \sup_{\|\vec{x}\|=1}\left(\frac{\vec{x}^\dagger\boldsymbol{A}^\dagger\vec{x} + \vec{x}^\dagger\boldsymbol{A}\vec{x}}{2}\right) \\
&= \sup_{\|\vec{x}\|=1}\left(\frac{(\vec{x}^\dagger\boldsymbol{A}\vec{x})^\dagger + \vec{x}^\dagger\boldsymbol{A}\vec{x}}{2}\right) = \sup_{\|\vec{x}\|=1} \Re\left(\vec{x}^\dagger\boldsymbol{A}\vec{x}\right) \geq \Re\left(\vec{u}_1^\dagger\boldsymbol{A}\vec{u}_1\right) = \Re(\lambda_1)
\end{aligned} \tag{B.6}$$

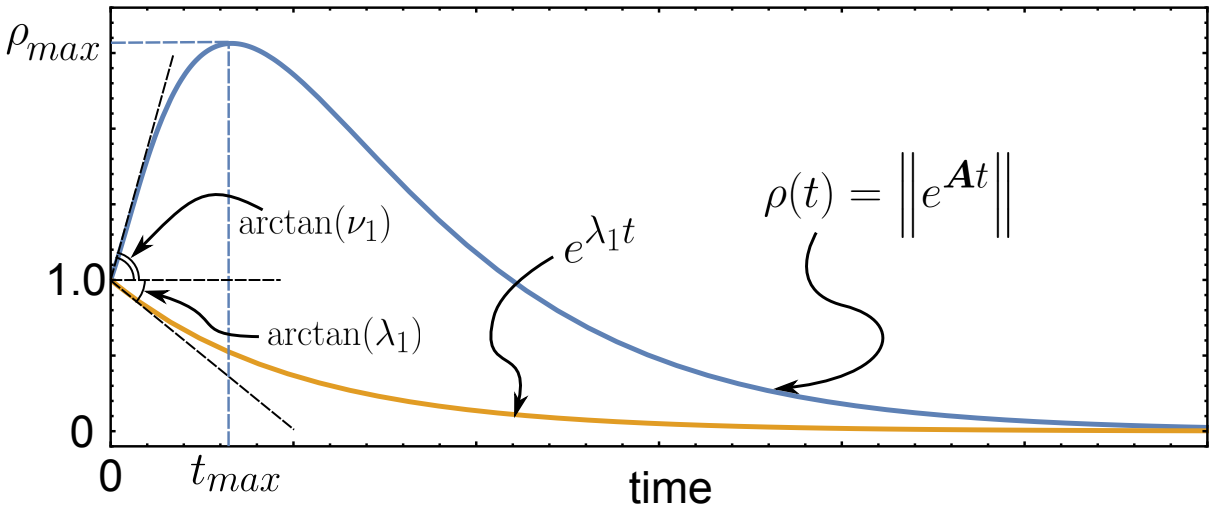

Figure B.1: Maximum value of $\|\vec{y}(t)\|$ over all normalized initial conditions, given by the amplitude envelope, $\rho(t)$, for a reactive matrix $\boldsymbol{A}$ (blue curve). The amplitude envelope for a hermitian matrix with the same eigenvalues is given by $\exp(\lambda_1 t)$ (orange curve). The initial slope of the amplitude envelope (*i.e.* maximum initial growth rate) is set by the largest eigenvalue, ν_1, of the hermitian part of $\boldsymbol{A}$.

Claim 3: At long time, $\|\vec{y}\|$ decays at the rate set by λ_1, *i.e.*

$$\lim_{t\to\infty} \frac{\|\vec{y}(t)\|}{\exp(\lambda_1 t)} = \mathcal{O}(1). \tag{B.7}$$

I prove this result for the case that the eigenvalue of $\boldsymbol{A}$ are distinct. Let $\vec{u}_1, \ldots, \vec{u}_n$ be the eigenvectors of $\boldsymbol{A}$. Then $\vec{y}(t)$ can be written as a linear combination of $\vec{u}_i$'s, *i.e.* $\vec{y}(t) = \sum a_i(t)\vec{u}_i$. By diagonalizing Eq. (B.4), we have

$$\frac{da_i}{dt} = \lambda_i a_i \implies a_i(t) = a_i(0)\exp(\lambda_i t) \tag{B.8}$$

Therefore

$$\begin{aligned}\lim_{t\to\infty} \frac{\|\vec{y}(t)\|}{\exp(\lambda_1 t)} &= \lim_{t\to\infty} \left\| \frac{\vec{y}(t)}{\exp(\lambda_1 t)} \right\| = \lim_{t\to\infty} \left\| \frac{\sum a_i(t)\vec{u}_i}{\exp(\lambda_1 t)} \right\| = \lim_{t\to\infty} \left\| \frac{\sum a_i(0)\exp(\lambda_i t)\vec{u}_i}{\exp(\lambda_1 t)} \right\| \\ &= \lim_{t\to\infty} \left\| \sum a_i(0)\exp((\lambda_i - \lambda_1)t)\vec{u}_i \right\| = a_i(0)\,\|\vec{u}_i\|\end{aligned} \tag{B.9}$$

For an operator $\boldsymbol{O}$, the operator norm with respect to some norm $\|\cdot\|$ on the vector space

is define as

$$\|\boldsymbol{O}\| = \sup_{\|\vec{x}\|=1} \|\boldsymbol{O}\vec{x}\| \,. \tag{B.10}$$

The amplitude envelope of $\boldsymbol{A}$ is defined as $\rho(t) = \|\exp(\boldsymbol{A}t)\|$. With this definition

$$\|\vec{y}(t)\| \leq \rho(t)\, \|\vec{y}(0)\| \,. \tag{B.11}$$

The maximum possible amplitude of $\|\vec{y}\|$, given $\|\vec{y}(0)\| = 1$, is $\rho_{max} = \max_t \rho(t)$, and the time at which this maximum is achieved is called t_{max}. At $t = 0$ the slope of $\rho(t)$ is given by ν_1, and when $\boldsymbol{A}$ is hermitian, $\rho(t) = \exp(\lambda_1 t)$ with slope λ_1 at $t = 0$ (see Fig. (B.1)).

B.3 Nonnormality Index of 2×2 Matrices

Consider a general 2×2 matrix $\boldsymbol{A}$ given by its elements

$$\boldsymbol{A} = \begin{pmatrix} a_{11} & a_{12} \\ a_{21} & a_{22} \end{pmatrix}. \tag{B.12}$$

To find an expression for $\mathcal{H}(\boldsymbol{A})$, the nonnormality index of $\boldsymbol{A}$, we start by solving for $\boldsymbol{\Xi}$ from Eq. (A.37) and substituting in Eq. (A.38) to find the matrix $\boldsymbol{G}$ in terms of matrix elements of $\boldsymbol{A}$:

$$\boldsymbol{G} = \begin{pmatrix} \frac{(a_{11}+a_{22})^2}{(a_{12}-a_{21})^2+(a_{11}+a_{22})^2} & -\frac{(a_{12}-a_{21})(a_{11}+a_{22})}{(a_{12}-a_{21})^2+(a_{11}+a_{22})^2} \\ \frac{(a_{12}-a_{21})(a_{11}+a_{22})}{(a_{12}-a_{21})^2+(a_{11}+a_{22})^2} & \frac{(a_{11}+a_{22})^2}{(a_{12}-a_{21})^2+(a_{11}+a_{22})^2} \end{pmatrix}. \tag{B.13}$$

The nonnormality index $\mathcal{H}$ is given by the inverse of the determinant of $\boldsymbol{G}$:

$$\mathcal{H}(\boldsymbol{A}) = \det\left(\boldsymbol{G}^{-1}\right) = 1 + \frac{(a_{12}-a_{21})^2}{(a_{11}+a_{22})^2}. \tag{B.14}$$

If the eigenvalues of $\boldsymbol{A}$ are real, we can rewrite this expression in terms of the eigenvalues and the angle between the eigenvectors of $\boldsymbol{A}$. Let $\Delta > 0$ be the discriminant of the characteristic polynomial of $\boldsymbol{A}$:

$$\Delta = (a_{11}-a_{22})^2 + 4\,a_{12}\,a_{21}. \tag{B.15}$$

If λ_1 and λ_2 are the two eigenvalues of $\boldsymbol{A}$, and $\vec{v}_1$ and $\vec{v}_2$ are the two eigenvectors, we have

$$\begin{aligned} &(\lambda_1+\lambda_2)^2 = (a_{11}+a_{22})^2, \qquad (\lambda_1-\lambda_2)^2 = \Delta, \\ &\cos^2(\theta) = \left(\frac{\vec{v}_1\cdot\vec{v}_2}{\|\vec{v}_1\|\,\|\vec{v}_2\|}\right)^2, \qquad \cot^2(\theta) = \frac{\cos^2(\theta)}{1-\cos^2(\theta)} = \frac{(a_{11}-a_{22})^2}{\Delta}. \end{aligned} \tag{B.16}$$

Now it is clear that

$$\mathcal{H}(\boldsymbol{A}) = 1 + \cot^2(\theta)\left(\frac{\lambda_1-\lambda_2}{\lambda_1+\lambda_2}\right)^2. \tag{B.17}$$

References

[1] F.J. Dyson. A brownian-motion model for the eigenvalues of a random matrix. *J. Math. Phys.*, 3(6):1191–1198, 1962.

[2] Alan J. McKane, Tommaso Biancalani, and Tim Rogers. Stochastic pattern formation and spontaneous polarisation: The linear noise approximation and beyond. *Bull. Math. Biol.*, 76:895–921, 2014.

[3] Luca Ridolfi, C Camporeale, P D'Odorico, and Francesco Laio. Transient growth induces unexpected deterministic spatial patterns in the turing process. *Eur. Phys. Lett.*, 95(1):18003, 2011.

[4] J. Weiss and J.R. Grasso. Acoustic emission in single crystals of ice. *J. Phys. Chem. B*, 101(32):6113–6117, 1997.

[5] M.C. Miguel, A. Vespignani, S. Zapperi, J. Weiss, and J.R. Grasso. Intermittent dislocation flow in viscoplastic deformation. *Nature*, 410(6829):667–671, 2001.

[6] M.D. Uchic, D.M. Dimiduk, J.N. Florando, and W.D. Nix. Sample dimensions influence strength and crystal plasticity. *Science*, 305(5686):986–989, 2004.

[7] C. Fressengeas, AJ Beaudoin, D. Entemeyer, T. Lebedkina, M. Lebyodkin, and V. Taupin. Dislocation transport and intermittency in the plasticity of crystalline solids. *Phys. Rev. B*, 79(1):014108, 2009.

[8] D.M. Dimiduk, C. Woodward, R. LeSar, and M.D. Uchic. Scale-free intermittent flow in crystal plasticity. *Science*, 312(5777):1188–1190, 2006.

[9] J. Weiss, T. Richeton, F. Louchet, F. Chmelik, P. Dobron, D. Entemeyer, M. Lebyodkin, T. Lebedkina, C. Fressengeas, and R.J. McDonald. Evidence for universal intermittent crystal plasticity from acoustic emission and high-resolution extensometry experiments. *Phys. Rev. B*, 76(22):224110, 2007.

[10] Michael Zaiser, Brett Marmo, and Paolo Moretti. The yielding transitionin crystal plasticity-discrete dislocations and continuum models. In *Proceedings of the International Conference on Statistical Mechanics of Plasticity and Related Instabilities*, 2005.

[11] Michael Zaiser. Scale invariance in plastic flow of crystalline solids. *Adv. Phys.*, 55(1-2):185–245, 2006.

[12] M. Koslowski, R. LeSar, and R. Thomson. Avalanches and scaling in plastic deformation. *Phys. Rev. Lett.*, 93(12):125502, 2004.

[13] Pak Yuen Chan, Georgios Tsekenis, Jonathan Dantzig, Karin A Dahmen, and Nigel Goldenfeld. Plasticity and dislocation dynamics in a phase field crystal model. *Phys. Rev. Lett.*, 105(1):15502, 2010.

[14] Farshid Jafarpour, Luiza Angheluta, and Nigel Goldenfeld. Velocity statistics for interacting edge dislocations in one dimension from dyson's coulomb gas model. *Physical Review E*, 88(4):042123, 2013.

[15] T. Richeton, P. Dobron, F. Chmelik, J. Weiss, and F. Louchet. On the critical character of plasticity in metallic single crystals. *Mat. Sci. Eng. A*, 424(1):190–195, 2006.

[16] P.D. Ispánovity, I. Groma, G. Györgyi, F.F. Csikor, and D. Weygand. Submicron plasticity: yield stress, dislocation avalanches, and velocity distribution. *Phys. Rev. Lett.*, 105(8):85503, 2010.

[17] Georgios Tsekenis, Nigel Goldenfeld, and Karin A Dahmen. Dislocations jam at any density. *Phys. Rev. Lett.*, 106(10):105501, 2011.

[18] Nir Friedman, Andrew T Jennings, Georgios Tsekenis, Ju-Young Kim, Molei Tao, Jonathan T Uhl, Julia R Greer, and Karin A Dahmen. Statistics of dislocation slip avalanches in nanosized single crystals show tuned critical behavior predicted by a simple mean field model. *Physical Review Letters*, 109(9):095507, 2012.

[19] Farshid Jafarpour, Tommaso Biancalani, and Nigel Goldenfeld. Noise-induced mechanism for biological homochirality of early life self-replicators. *Physical review letters*, 115(15):158101, 2015.

[20] J Podlech. Origin of organic molecules and biomolecular homochirality. *Cellular and Molecular Life Sciences CMLS*, 58(1):44–60, 2001.

[21] Marcelo Gleiser and Sara Imari Walker. Life's chirality from prebiotic environments. *Int. J. Astrobiol.*, 11(04):287–296, 2012.

[22] Yukio Saito and Hiroyuki Hyuga. Colloquium: Homochirality: Symmetry breaking in systems driven far from equilibrium. *Rev. Mod. Phys.*, 85(2):603, 2013.

[23] F. C. Frank. On spontaneous asymmetric synthesis. *Biochimica et Biophysica Acta*, 11:459–463, 1953.

[24] Louis Pasteur. *Recherches sur les relations qui peuvent exister entre la forme cristalline, la composition chimique et les sens de la polarisation rotatoire.* Impr. Bachelier, 1848.

[25] Jacobus Henricus vant Hoff. A suggestion looking to the extension into space of the structural formulas at present used in chemistry, and a note upon the relation between the optical activity and the chemical constitution of organic compounds. *Archives Néerlandaises des Sciences exactes et naturelles*, 9:445–454, 1874.

[26] Joseph Achille Le Bel. Sur les relations qui existent entre les formules atomiques des corps organiques et le pouvoir rotatoire de leurs dissolutions. *Bull. soc. chim. France*, 22:337–347, 1874.

[27] GP Moss. Basic terminology of stereochemistry (iupac recommendations 1996). *Pure and applied chemistry*, 68(12):2193–2222, 1996.

[28] Paul M Kim, Xin Duan, Alex S Huang, Cindy Y Liu, Guo-li Ming, Hongjun Song, and Solomon H Snyder. Aspartate racemase, generating neuronal d-aspartate, regulates adult neurogenesis. *Proceedings of the National Academy of Sciences*, 107(7):3175–3179, 2010.

[29] Horst Kleinkauf and Hans von Döhren. Review nonribosomal biosynthesis of peptide antibiotics. In *EJB Reviews 1990*, pages 151–165. Springer, 1990.

[30] Felipe Cava, Hubert Lam, Miguel A de Pedro, and Matthew K Waldor. Emerging knowledge of regulatory roles of d-amino acids in bacteria. *Cellular and Molecular Life Sciences*, 68(5):817–831, 2011.

[31] Jeremy Bailey. Astronomical sources of circularly polarized light and the origin of homochirality. *Origins of Life and Evolution of the Biosphere*, 31(1-2):167–183, 2001.

[32] S Pizzarello and JR Cronin. Alanine enantiomers in the murchison meteorite. *Nature*, 394(6690):236–236, 1998.

[33] Michael H Engel and SA Macko. Isotopic evidence for extraterrestrial non-racemic amino acids in the murchison meteorite. *Nature*, 389(6648):265–268, 1997.

[34] John R Cronin and Sandra Pizzarello. Enantiomeric excesses in meteoritic amino acids. *Science*, 275(5302):951–955, 1997.

[35] Tsung-Dao Lee and Chen-Ning Yang. Question of parity conservation in weak interactions. *Physical Review*, 104(1):254, 1956.

[36] Yukio Yamagata. A hypothesis for the asymmetric appearance of biomolecules on earth. *Journal of Theoretical Biology*, 11(3):495–498, 1966.

[37] William A Bonner. Parity violation and the evolution of biomolecular homochirality. *Chirality*, 12(3):114–126, 2000.

[38] James D Watson and Francis HC Crick. The structure of dna. In *Cold Spring Harbor Symposia on Quantitative Biology*, volume 18, pages 123–131. Cold Spring Harbor Laboratory Press, 1953.

[39] Stanley L Miller et al. A production of amino acids under possible primitive earth conditions. *Science*, 117(3046):528–529, 1953.

[40] Kenso Soai, Takanori Shibata, Hiroshi Morioka, and Kaori Choji. Asymmetric autocatalysis and amplification of enantiomeric excess of a chiral molecule. *Nature*, 378:767–768, 1995.

[41] GF Joyce, GM Visser, CAA Van Boeckel, JH Van Boom, LE Orgel, and J Van Westrenen. Chiral selection in poly (c)-directed synthesis of oligo (g). *Nature*, 310:602–604, 1984.

[42] PGH Sandars. A toy model for the generation of homochirality during polymerization. *Orig. Life Evol. Biosph.*, 33(6):575–587, 2003.

[43] Marcelo Gleiser and Sara Imari Walker. An extended model for the evolution of prebiotic homochirality: A bottom-up approach to the origin of life. *Orig. Life Evol. Biosph.*, 38(4):293–315, 2008.

[44] Marcelo Gleiser, Bradley J Nelson, and Sara Imari Walker. Chiral polymerization in open systems from chiral-selective reaction rates. *Orig. Life Evol. Biosph.*, 42(4):333–346, 2012.

[45] Raphaël Plasson, Hugues Bersini, and Auguste Commeyras. Recycling frank: spontaneous emergence of homochirality in noncatalytic systems. *Proc. Natl. Acad. Sci. USA*, 101(48):16733–16738, 2004.

[46] Axel Brandenburg, Harry J Lehto, and Kirsi M Lehto. Homochirality in an early peptide world. *Astrobiology*, 7(5):725–732, 2007.

[47] Jonathan T Sczepanski and Gerald F Joyce. A cross-chiral rna polymerase ribozyme. *Nature*, 515(7527):440–442, 2014.

[48] Gábor Lente. The role of stochastic models in interpreting the origins of biological chirality. *Symmetry*, 2(2):767–798, 2010.

[49] Ryo Shibata, Yukio Saito, and Hiroyuki Hyuga. Diffusion accelerates and enhances chirality selection. *Phys. Rev. E*, 74(2):026117, 2006.

[50] Raphaël Plasson, Dilip K Kondepudi, and Kouichi Asakura. Three-dimensional description of the spontaneous onset of homochirality on the surface of a conglomerate crystal phase. *J. Phys. Chem. B*, 110(16):8481–8487, 2006.

[51] David Hochberg and María-Paz Zorzano. Reaction-noise induced homochirality. *Chem. Phys. Lett.*, 431(1):185–189, 2006.

[52] David Hochberg and María Paz Zorzano. Mirror symmetry breaking as a problem in dynamic critical phenomena. *Phys. Rev. E*, 76(2):021109, 2007.

[53] Gábor Lente. Homogeneous chiral autocatalysis: a simple, purely stochastic kinetic model. *J. Phys. Chem. A*, 108(44):9475–9478, 2004.

[54] C W Gardiner. *Handbook of Stochastic Methods for Physics, Chemistry and the Natural Sciences*. Springer, New York, fourth edition, 2009.

[55] Yuichi Togashi and Kunihiko Kaneko. Transitions induced by the discreteness of molecules in a small autocatalytic system. *Phys. Rev. Lett.*, 86(11):2459, 2001.

[56] Maxim N Artyomov, Jayajit Das, Mehran Kardar, and Arup K Chakraborty. Purely stochastic binary decisions in cell signaling models without underlying deterministic bistabilities. *Proc. Natl. Acad. Sci. USA*, 104(48):18958–18963, 2007.

[57] DI Russell and RA Blythe. Noise-induced dynamical transition in systems with symmetric absorbing states. *Phys. Rev. Lett.*, 106(16):165702, 2011.

[58] Tommaso Biancalani, Louise Dyson, and Alan J McKane. Noise-induced bistable states and their mean switching time in foraging colonies. *Phys. Rev. Lett.*, 112(3):038101, 2014.

[59] N G van Kampen. *Stochastic Processes in Physics and Chemistry*. Elsevier Science, Amsterdam, third edition, 2007.

[60] Daniel T Gillespie. Exact stochastic simulation of coupled chemical reactions. *J. Phys. Chem.*, 81(25):2340–2361, 1977.

[61] Alan J. McKane, Tommaso Biancalani, and Tim Rogers. Stochastic pattern formation and spontaneous polarisation: The linear noise approximation and beyond. *Bull. Math. Biol.*, 76:895–921, 2014.

[62] Tommaso Biancalani, Louise Dyson, and Alan J McKane. The statistics of fixation times for systems with recruitment. *J. Stat. Mech.*, 2015(1):P01013, 2015.

[63] Donna G Blackmond. if pigs could fly chemistry: a tutorial on the principle of microscopic reversibility. *Angewandte Chemie International Edition*, 48(15):2648–2654, 2009.

[64] Rud Wegscheider. Über simultane gleichgewichte und die beziehungen zwischen thermodynamik und reactionskinetik homogener systeme. *Monatshefte für Chemie/Chemical Monthly*, 32(8):849–906, 1911.

[65] Jeremy R Knowles. Enzyme-catalyzed phosphoryl transfer reactions. *Annual review of biochemistry*, 49(1):877–919, 1980.

[66] Raphal Plasson. Comment on re-examination of reversibility in reaction models for the spontaneous emergence of homochirality. *The Journal of Physical Chemistry B*, 112(31):9550–9552, 2008. PMID: 18630862.

[67] Jeffrey L Bada. Kinetics of racemization of amino acids as a function of ph. *Journal of the American Chemical Society*, 94(4):1371–1373, 1972.

[68] Jeffrey L Bada, Xueyun S Wang, Hendrik N Poinar, Svante Pääbo, and George O Poinar. Amino acid racemization in amber-entombed insects: implications for dna preservation. *Geochimica et cosmochimica acta*, 58(14):3131–3135, 1994.

[69] Jeffrey L Bada. Origins of homochirality. *Nature*, 374(6523):594–595, 1995.

[70] William Martin, John Baross, Deborah Kelley, and Michael J Russell. Hydrothermal vents and the origin of life. *Nature Reviews Microbiology*, 6(11):805–814, 2008.

[71] A. J. McKane and T. J. Newman. Stochastic models in population biology and their deterministic analogs. *Phys. Rev. E*, 70:041902, 2004.

[72] Kirill S Korolev, Mikkel Avlund, Oskar Hallatschek, and David R Nelson. Genetic demixing and evolution in linear stepping stone models. *Reviews of modern physics*, 82(2):1691, 2010.

[73] Ronald Aylmer Fisher. The wave of advance of advantageous genes. *Annals of eugenics*, 7(4):355–369, 1937.

[74] Andrei N Kolmogorov, IG Petrovsky, and NS Piskunov. Etude de léquation de la diffusion avec croissance de la quantité de matiere et son applicationa un probleme biologique. *Moscow Univ. Math. Bull*, 1:1–25, 1937.

[75] Michael G Neubert and Hal Caswell. Alternatives to resilience for measuring the responses of ecological systems to perturbations. *Ecology*, 78(3):653–665, 1997.

[76] Lloyd N Trefethen, Annee Trefethen, Satishc Reddy, Tobina Driscoll, et al. Hydrodynamic stability without eigenvalues. *Science*, 261(5121):578–584, 1993.

[77] Lloyd Nicholas Trefethen and Mark Embree. *Spectra and pseudospectra: the behavior of nonnormal matrices and operators*. Princeton University Press, 2005.

[78] Brian F Farrell and Petros J Ioannou. Variance maintained by stochastic forcing of non-normal dynamical systems associated with linearly stable shear flows. *Physical review letters*, 72(8):1188, 1994.

[79] Si Tang and Stefano Allesina. Reactivity and stability of large ecosystems. *Population Dynamics*, 2:21, 2014.

[80] Evelyn Buckwar and Cónall Kelly. Asymptotic and transient mean-square properties of stochastic systems arising in ecology, fluid dynamics, and system control. *SIAM Journal on Applied Mathematics*, 74(2):411–433, 2014.

[81] Stuart Townley, David Carslake, OWEN KELLIE-SMITH, Dominic McCarthy, and David Hodgson. Predicting transient amplification in perturbed ecological systems. *Journal of Applied Ecology*, 44(6):1243–1251, 2007.

[82] Alan Hastings. Transients: the key to long-term ecological understanding? *Trends in Ecology & Evolution*, 19(1):39–45, 2004.

[83] Andrzej M Kierzek, Jolanta Zaim, and Piotr Zielenkiewicz. The effect of transcription and translation initiation frequencies on the stochastic fluctuations in prokaryotic gene expression. *Journal of Biological Chemistry*, 276(11):8165–8172, 2001.

[84] Andrew J Black and Alan J McKane. Stochastic formulation of ecological models and their applications. *Trends in ecology & evolution*, 27(6):337–345, 2012.

[85] Thomas Butler and Nigel Goldenfeld. Robust ecological pattern formation induced by demographic noise. *Phys. Rev. E*, 80(3):030902, 2009.

[86] Tommaso Biancalani, Duccio Fanelli, and Francesca Di Patti. Stochastic turing patterns in the brusselator model. *Phys. Rev. E*, 81(4):046215, 2010.

[87] Thomas Butler and Nigel Goldenfeld. Fluctuation-driven turing patterns. *Physical Review E*, 84(1):011112, 2011.

[88] William G Wilson, Susan P Harrison, Alan Hastings, and Kevin McCann. Exploring stable pattern formation in models of tussock moth populations. *Journal of animal ecology*, 68(1):94–107, 1999.

[89] M Mimura and JD Murray. On a diffusive prey-predator model which exhibits patchiness. *Journal of Theoretical Biology*, 75(3):249–262, 1978.

[90] Alan Mathison Turing. The chemical basis of morphogenesis. *Philosophical Transactions of the Royal Society of London. Series B, Biological Sciences*, 237(641):37–72, 1952.

[91] AJ Koch and Hans Meinhardt. Biological pattern formation: from basic mechanisms to complex structures. *Reviews of Modern Physics*, 66(4):1481, 1994.

[92] James Dickson Murray. *Mathematical Biology. II Spatial Models and Biomedical Applications {Interdisciplinary Applied Mathematics V. 18}*. Springer-Verlag New York Incorporated, 2001.

[93] Vincent Castets, Etiennette Dulos, Jacques Boissonade, and Patrick De Kepper. Experimental evidence of a sustained standing turing-type nonequilibrium chemical pattern. *Physical Review Letters*, 64(24):2953, 1990.

[94] Qi Ouyang and Harry L Swinney. Transition from a uniform state to hexagonal and striped turing patterns. *Nature*, 352(6336):610–612, 1991.

[95] Philip K Maini, Thomas E Woolley, Ruth E Baker, Eamonn A Gaffney, and S Seirin Lee. Turing's model for biological pattern formation and the robustness problem. *Interface focus*, page rsfs20110113, 2012.

[96] Samik Datta, Gustav W Delius, Richard Law, and Michael J Plank. A stability analysis of the power-law steady state of marine size spectra. *Journal of mathematical biology*, 63(4):779–799, 2011.

[97] Juan A Bonachela, Miguel A Muñoz, and Simon A Levin. Patchiness and demographic noise in three ecological examples. *Journal of Statistical Physics*, 148(4):724–740, 2012.

[98] Thomas Charles Butler, Marc Benayoun, Edward Wallace, Wim van Drongelen, Nigel Goldenfeld, and Jack Cowan. Evolutionary constraints on visual cortex architecture from the dynamics of hallucinations. *Proceedings of the National Academy of Sciences*, 109(2):606–609, 2012.

[99] Michael G Neubert, Hal Caswell, and JD Murray. Transient dynamics and pattern formation: reactivity is necessary for turing instabilities. *Mathematical biosciences*, 175(1):1–11, 2002.

[100] J. Weiss and D. Marsan. Three-dimensional mapping of dislocation avalanches: clustering and space/time coupling. *Science*, 299(5603):89–92, 2003.

[101] M.C. Miguel, A. Vespignani, M. Zaiser, and S. Zapperi. Dislocation jamming and andrade creep. *Physical Review Letters*, 89(16):165501, 2002.

[102] G Tsekenis, JT Uhl, N Goldenfeld, and KA Dahmen. Determination of the universality class of crystal plasticity. *EPL (Europhysics Letters)*, 101(3):36003, 2013.

[103] J.P. Hirth and J. Lothe. *Theory of dislocations.* Krieger, Malabar, 1992.

[104] M Miguel, Alessandro Vespignani, Stefano Zapperi, Jérôme Weiss, Jean-Robert Grasso, et al. Complexity in dislocation dynamics: model. *Materials Science and Engineering: A*, 309:324–327, 2001.

[105] M.C. Miguel, L. Laurson, and MJ Alava. Material yielding and irreversible deformation mediated by dislocation motion. *Eur. Phys. J. B.*, 64(3-4):443–450, 2008.

[106] Péter Dusán Ispánovity, István Groma, Géza Györgyi, Péter Szabó, and Wolfgang Hoffelner. Criticality of relaxation in dislocation systems. *Physical Review Letters*, 107(8):085506, 2011.

[107] Ferenc F Csikor and István Groma. Probability distribution of internal stress in relaxed dislocation systems. *Phys. Rev. B*, 70:64106–64106, 2004.

[108] I. Groma and B. Bakó. Probability distribution of internal stresses in parallel straight dislocation systems. *Phys. Rev. B*, 58(6):2969, 1998.

[109] Andrea J Liu and Sidney R Nagel. Jamming is not just cool any more. *Nature*, 396(6706):21–22, 1998.

[110] P Hähner. On the foundations of stochastic dislocation dynamics. *Applied Physics A*, 62(5):473–481, 1996.

[111] P Hähner. Stochastic dislocation patterning during cyclic plastic deformation. *Applied Physics A*, 63(1):45–55, 1996.

[112] H. Schulz. Pairing transition of a one-dimensional classical plasma. *J. Phys. A*, 14:3277, 1981.

[113] C.W.J. Beenakker. Random-matrix theory of quantum transport. *Rev. Mod. Phys.*, 69(3):731, 1997.

[114] T. Tao. *Topics in random matrix theory*, volume 132. Amer Mathematical Society, 2012.

[115] W. König. Orthogonal polynomial ensembles in probability theory. *Probab. Surv*, 2:385–447, 2005.

[116] W. König, N. OConnell, and S. Roch. Non-colliding random walks, tandem queues, and discrete orthogonal polynomial ensembles. *Electron. J. Probab*, 7(5), 2002.

[117] Y.V. Nazarov. Fluctuations of transmission distribution in disordered conductors. *Physical Review Letters*, 76(12):2129–2132, 1996.

[118] PJ Forrester. Solvable isotherms for a two-component system of charged rods on a line. *J. Stat. Phys.*, 51(3):457–479, 1988.

[119] Maria Adam and Michael J Tsatsomeros. An eigenvalue inequality and spectrum localization for complex matrices. *Electron. J. Linear Algebra*, 15:239–250, 2006.